Polyarene-Based π-Conjugated Systems: Synthesis, Characterization, and Mechanistic Studies

by

© Cheng Wang

A thesis submitted to the School of Graduate Studies in partial fulfilment of the requirements for the degree of

Ph.D.

Department of Chemistry

Memorial University of Newfoundland

August 2019

St. John's Newfoundland

Abstract

This thesis mainly deals with the synthesis and characterization of arene-based π-conjugated systems. The content can be divided into three major parts. In the first section, a series of tetraaryl-anthraquinodimethane derivatives (Ar_4-AQs) was synthesized via Suzuki coupling reactions, and these compounds were subjected to intramolecular cyclization reactions under chemical and photochemical conditions with the aim of making highly π-delocalized polycyclic aromatic hydrocarbons (PAHs). The Ar_4-AQs and their cyclized products were investigated by various spectroscopic analyses, including NMR, UV-Vis absorption spectroscopy, and X-ray crystallography to understand their structural, electronic, and photochemical properties. In the second part, microporous organic cross-linked polymer networks were successfully prepared from Schiff base condensation of a tetrabis(carboxaldehyde)-substituted Ar_4-AQ and *para*-phenylenediamine. Under optimized conditions, the resulting microporous organic materials showed good microporosity and crystallinity. In the third section, the detailed reaction mechanisms of intramolecular alkyne-dithiolium [3+2] cycloaddition reactions were investigated by a joint experimental and theoretical approach. A number of alkynyl-subsituted phenyldithiafulvenes was prepared as model compounds. Density functional theory (DFT) calculations were performed to reveal the effects of pH and degree of π-conjugation on reactivity.

Acknowledgements

First of all, I would like to express my sincere thanks to my supervisor Dr. Yuming Zhao for his guidance and support during my research work and thesis writing. Yuming is really kind and always helpful all the time. I have learned so much from him and this is such a great research experience to me. I would also like to thank to my co-supervisor, Dr. Yan Zhang, and supervisory committee member, Dr. Christopher Flinn, for their help throughout my program. I would also like to thank to Dr. Micheal Katz and Dr. Kelly Hawboldt for allowing me to have access to their instruments for surface area analysis.

I would also like to thank my parents for their encouragement and support.

I would also like to thank my colleagues in my research group as well as other research groups in the Chemistry Department. They helped me a lot during my program. I would also like to thank to Dr. Celine Schneider, Ms. Linda Winsor, and other C-CART staff for their kind help and guidance in all the instrumental analyses. I would also like to thank to Drs. Wanda Aylward (CREAIT) and Bob McDonald (University of Alberta) for their assistance in powder and single-crystal X-ray analyses. Dr. David Grant is acknowledged for help in SEM imaging. Mason Lawrence and Hanieh Bamdad offered valuable assistance in BET analysis.

Last but not the least, I would also like thank all the faculty members and staff of the Chemistry Department and Memorial University for creating such a great and friendly environment for students. I sincerely thank Memorial University and NSERC for funding support.

Contents

List of Figures

List of Schemes

List of Tables

List of Abbreviations and Symbols

APPI	atmospheric pressure photo ionization
aq	aqueous
ca.	circa
calcd	calculated
cm	centimeter(s)
CV	cyclic voltammetry
d	doublet
MOF	metal organic framework
COF	covalent organic framework
DTF	dithiafulvene or dithiafulvenyl
Et	ethyl
exTTF	π-extended tetrathiafulvalene
FTIR	Fourier transform infrared

g	gram(s)
h	hour(s)
HRMS	high resolution mass spectrometry
Hz	hertz
IR	infrared
J	coupling constant
m	multiplet
m/z	mass to charge ratio
MALDI-TOF	matrix assisted laser desorption/ionization-time of flight
Me	methyl
mg	milligram(s)
MHz	megahertz
min	minute(s)
mL	milliliter(s)
mmol	millimole(s)
mol	mole(s)
m.p.	melting point

MS	mass spectrometry
mV	millivolt(s)
mW	milliwatt(s)
nm	nanometer(s)
NMR	nuclear magnetic resonance
ppm	parts per million
PXRD	powder X-ray diffraction
s	singlet
t	triplet
TFA	trifluoroacetic acid
THF	tetrahydrofuran
TLC	thin-layer chromatography
DMF	dimethylformamide
SEM	scanning electron microscope
DLS	dynamic light scattering
TTF	tetrathiafulvalene
TTFAQ	anthraquinone-type π-extended tetrathiafulvalene

TTFV	tetrathiafulvalene vinylogue
UV-Vis	ultraviolet-visible
V	volt(s)
XRD	X-ray diffraction
δ	chemical shift
ϵ	molar attenuation coefficient
λ_{max}	maximum absorption wavelength
FET	field effect transistors
HBC	hexa-*peri*-hexabenzocoronene
HOPG	highly ordered pyrolitic graphite
c-OBCB	contorted octabenzocircumbiphenyl
CDHC	photochemical cyclodehydrochlorination

Chapter 1

Introduction

1.1 From Polycyclic Aromatic Hydrocarbons (PAHs) to Graphene

1.1.1 Introduction to PAHs

Polycyclic aromatic hydrocarbons (PAHs) can be viewed as segments of graphene, which is an intriguing two-dimensional carbon allotrope composed of a single-layer of sp^2 carbon atoms. PAHs can be widely found in the residues of incomplete combustion of coal, oil, petrol, wood, and other organic materials, and even in interstellar space.[1] They are harmful persistent organic pollutants and in some cases even carcinogenic, and can be accumulated in nature and humans.[2,3] Synthesis and purification of functionalized PAHs with high molecular weights are challenging. The seminal research on the synthesis and characterization of PAHs was done by R. Scholl and E. Clar in the first half of the 20th century.[1,4–8] More recently, the progress in

modern synthetic methods and analytical techniques has made it possible to efficiently synthesize various PAHs under mild conditions. PAHs contain two or more fused benzene rings; the systems made up of four or less than four fused rings are referred to as light PAHs, while those have more than four rings are heavy PAHs. Structurally, the benzenoid ring arrangements in PAHs have a wide diversity of physical, chemical, and toxicological properties. The hydrophobicity and electrochemical stability of PAHs increase as the size and angularity of PAHs increase.[9] The thermal and chemical stabilities of PAHs depend both on their size and the topological arrangement of the benzenoid rings. Figure 1.1 shows a group of commonly seen PAHs. According to Clar's aromatic sextet rule, the most significant resonance structure of a PAH has the largest number of disjoint aromatic π-sextets.[10] Generally speaking, the greater the number of aromatic π-sextets the more stability a PAH system possesses.

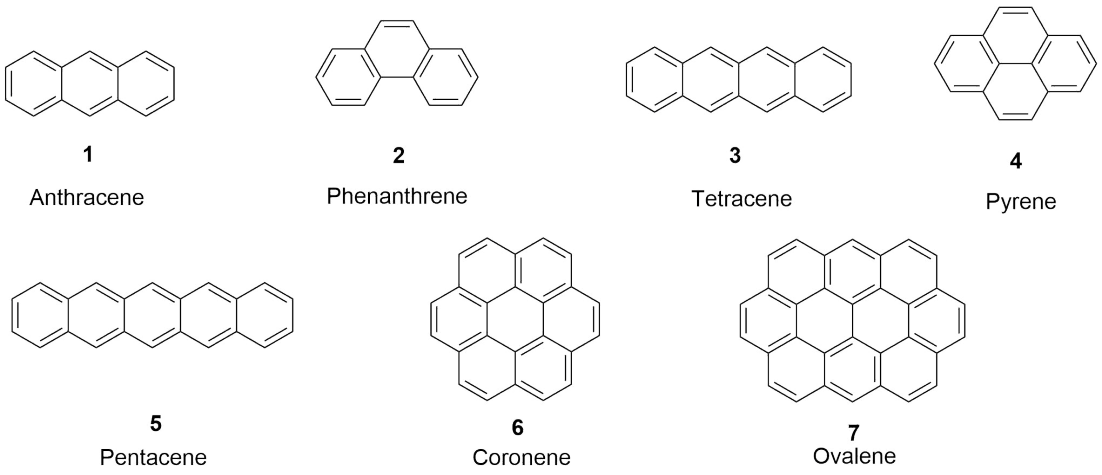

Figure 1.1: Chemical structures of representative PAHs.

1.1.2 Graphene and Nanographene

Graphene can be regarded as a PAH -+consisting of an infinite number of benzene rings fused together. Since the first successful isolation by Andre Geim and Konstantin Novoselov in 2004, graphene has attracted intensive research interest due to its special chemical structure and properties.[11] Graphene is a zero bandgap semiconductor with bipolar electrical properties. It exhibits excellent mechanical properties with high Young's modulus, high thermal conductivity, and a very large specific surface area. Graphene also exhibits remarkable optical properties, high transparency, and excellent electrical properties.[11] All these properties have made graphene a popular electronic material in various fields, ranging from solar cells, light-emitting diodes (LED), touch panels, to smart window or cell phones.[12] It can be also used in other electronic devices, such as capacitors and field effect transistors (FETs).[11] Key physical processes involved in the operation of these electronic devices include the formation, transport, and recombination of electrical charges. One of the most important parameters for solid-state electronic materials is the mobility of charge carriers. In the field of organic electronics, various PAH compounds have been designed and tested. Usually, organic materials with high crystallinity show good charge carrier mobility, but their processability tends to decrease with increased crystallinity.[13] Liquid-crystalline materials with good solubility can improve solution processability and facilitate the fabrication of high-quality thin film devices.[14] Conjugated oligomers and polymers are also widely used as active materials for organic electronics. However, the one-dimensional structure of a polymer/oligomer has a serious limitation, which is low conductivity in the solid state.[15,16] In addition to

the above organic materials, disc-like PAHs with extended two dimensional structures and high purity are growing in interest. Figure 1.2 illustrates typical examples of such disc-like PAHs, including triphenylene, coronene and hexa-*peri*-hexabenzocoronene (HBC). These PAHs were termed "nanographenes" in recent literature because they are small segments of graphene on the nanometer scale.

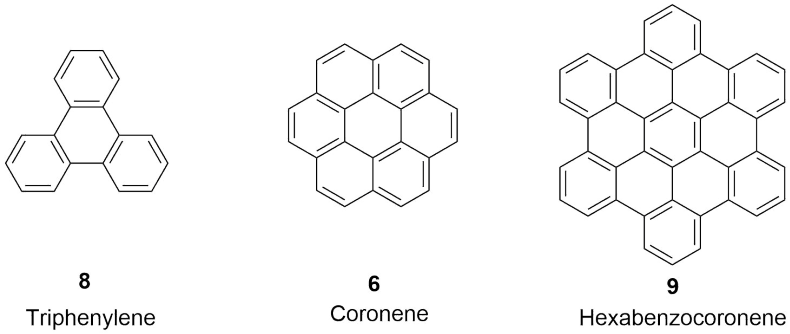

Figure 1.2: Typical examples of disc-like PAHs.

Large PAHs or nanographenes usually possess very poor solubility in various solvents, owing to the strong π-stacking of these planar molecules.[11] Attachment of flexible aliphatic chains to the edges of PAHs can significantly increase their solubility and alter their thermal behaviour. The disc-like aromatic cores of PAHs can stack on one another to form highly ordered columnar assemblies, with their disordered alkyl chains filling the periphery.[17] Such structures favor the overlap of π-orbitals and significantly increases the charge carrier mobility of the solid materials. Furthermore, charge transport can be enhanced by shortening the distance between adjacent molecular building blocks using non-covalent forces such as hydrogen bonding interactions.[18–20] Charge carrier transport occurs along the stacks of PAHs due to intra-columnar packing, but is limited by the surrounding insulating

aliphatic chains.[21] Because of these properties, disc-like PAHs or nanographenes have been identified as promising organic semiconductors in the application of FETs and photovoltaic devices. Increasing the size of the aromatic core of this kind of materials could improve the order of columnar superstructures and overlap of π-orbitals, which in turn enhance the charge carrier mobility.[22] But the synthesis of relatively large PAHs (i.e., nanographenes) becomes more and more challenging as molecular size increases.

1.1.3 Synthesis of Nanographenes

1.1.3.1 Coronene and Hexa-*peri*-hexabenzocoronene

Large graphenes can be prepared by exfoliation of highly ordered pyrolitic graphite (HOPG); however, the exfoliated graphenes are not well defined in structure and may contain many defects which affect their electronic properties considerably.[11] Nanographenes, on the other hand, provide a solution to this problem, since they can be readily prepared with well-defined and defect-free structures. For example, coronene and HBC are D_{6h}-nanographenes with very promising applications. The aromatic core of coronene is relatively small, which leads to better solubility in organic solvents compared with the relatively large HBC. Practically, coronene can be produced during the petroleum-refining process of hydrocarbon cracking, in the form of needle-like crystals with a monoclinic, herringbone-like solid packing structure.[23–25] The application of unfunctionalized coronene is however limited by its low solubility. Functionalized coronenes can solve the solubility problems but there are only a few examples existing in the literature.[23–25] Shen and coworkers used

$TpRuPPh_3(CH_3CN)_2PF_6$ as catalyst to prepare substituted coronene derivatives by four-fold benzannulations with yields of 53% to 86% (Scheme 1.1). The use of an expensive catalyst, however, makes this method impractical for scaled-up synthesis.

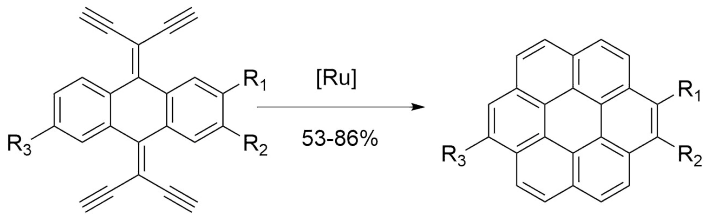

10 **11**

[Ru]=$TpRuPPh_3(CH_3CN)_2PF_6$

R_1=R_2=R_3=H,	5% [Ru]	86%
R_1=Me, R_2=R_3=H,	10% [Ru]	75%
R_1=Cl, R_2=R_3=H,	10% [Ru]	53%
R_1=R_3=Ph, R_2=H,	10% [Ru]	63%

Scheme 1.1: Synthesis of functionalized coronenes through $TpRuPPh_3(CH_3CN)_2PF_6$ catalyzed benzannulation reactions.

Another approach for coronene synthesis was reported by the Müllen group in 2008.[25] The key step of the synthesis is the generation of a [2,2,2]paracyclophane through a sequence of a doubly *Z*-selective Wittig reaction and a McMurry reaction under pseudo-dilution conditions (Scheme 1.2). This paracyclophane precursor **15** was then subjected to photoirradiation (λ = 300 nm) in the presence of an oxidant such as iodine to produce coronene product **16** in a yield of 80%. Compared with Shen's method, Müllen's synthesis avoided the use of expensive catalysts. However, the double Wittig reaction only gave a moderate yield of 46% and the McMurry reaction gave a 48% yield. Thus the total yield of the synthesis was low. In Müllen's work, the methoxy-substituted coronene was found to show very good solubility in CH_2Cl_2, which is a significant improvement compared to unsubstituted coronene. The

presence of methoxy groups increases the intermolecular π–π stacking distance and decreases intermolecular attraction (aggregation).

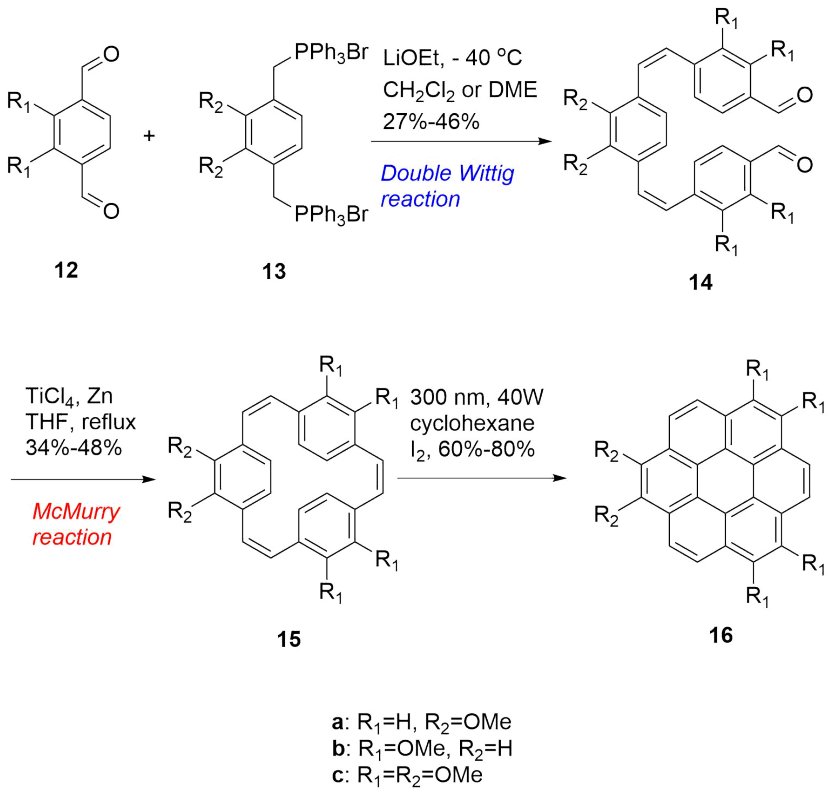

Scheme 1.2: Sythesis of substituted coronenes reported by Müllen's group in 2008.

Compared with coronene, there have been more synthetic methods developed for the preparation of HBC. Among them, the Scholl reaction is probably the most famous and popularly adopted method. Scholl, Clar, and Zander were the main contributors to the synthesis and characterization of various PAHs in the first half of the 20th century, and the first synthesis of HBC was reported by Clar's group in 1958.[26,27]

In Clar's work (Scheme 1.3), the bromination of 2:3-7:8-dibenzo-*peri*-naphthalene **17** in benzene gave a deep brown precipitate, which was then treated with three equivalents of HBr. The precipitate was heated at 153 °C to give the

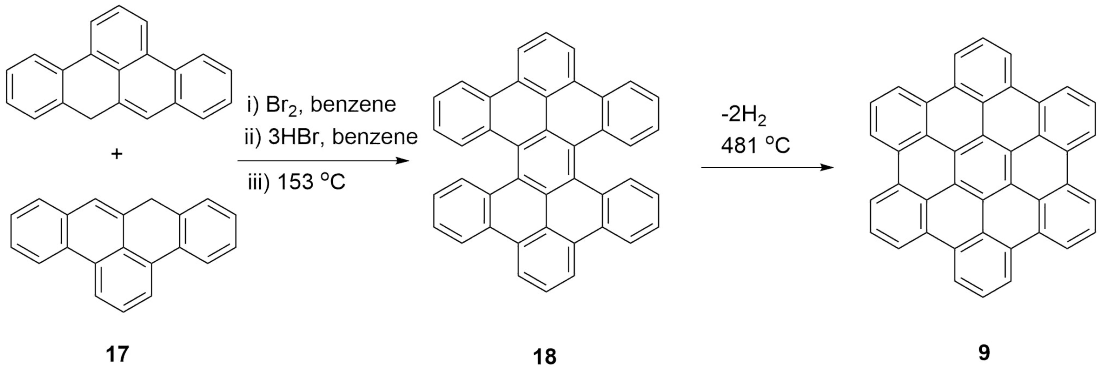

Scheme 1.3: Clar's route to prepare HBC.

tetrabenzoperipyrene **18**, which was subjected to heating at 481 °C to give HBC as a pale yellow solid.

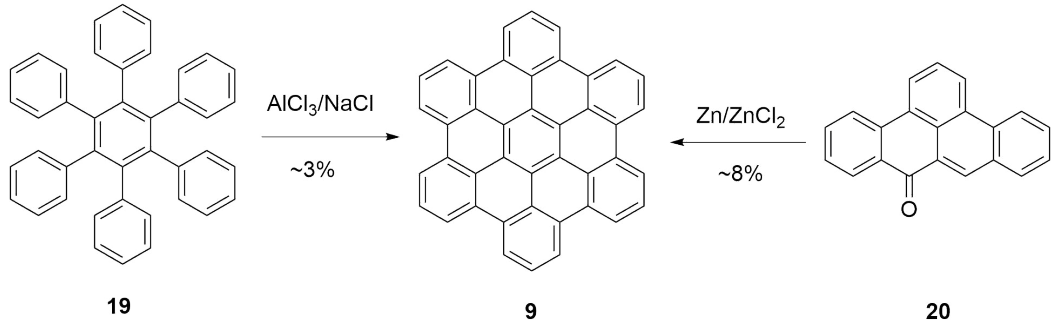

Scheme 1.4: Halleux's routes to prepare HBC.

Aside from Clar's HBC synthesis, Halleux's group in the same year reported the synthesis of HBC through two different one-step approaches. The first synthetic process was done through cyclodehydrogenation of hexaphenylbenzene by using molten $AlCl_3$/NaCl, and the second was by the reaction of dibenz-1,9;2,3-anthrone **20** with $Zn/ZnCl_2$ (Scheme 1.4). The yields of Halleux's two reactions were, however, extremely low, making them not applicable to large-scale synthesis.[28]

Later in 1986, Schmidt's group reported a method for preparing HBC as shown

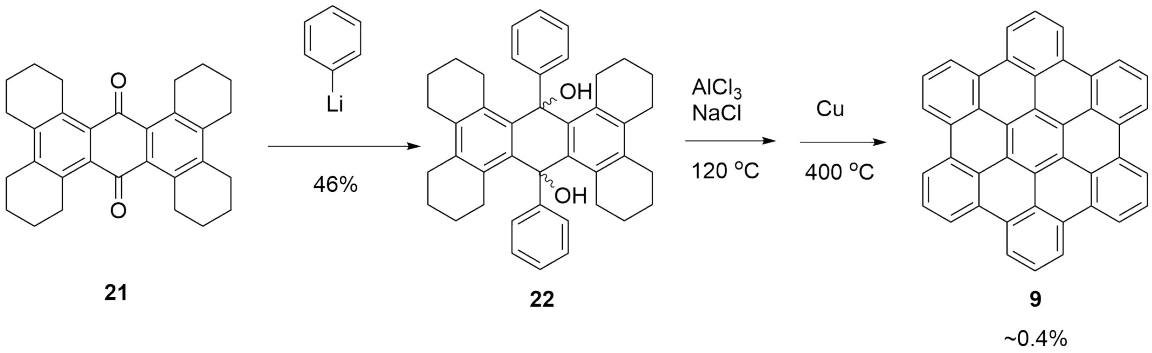

Scheme 1.5: Schmidt's route to prepare HBC.

in Scheme 1.5. A quinone compound **21** was treated by phenyllithium to give diol **22** with a moderate yield (from 29% to 46%). Diol **22** was subjected to a cyclization reaction under the conditions of molten $AlCl_3$/NaCl at 120 °C for 3 min, followed by aromatization promoted by Cu at 400 °C, to give HBC with a low yield of 0.4%.[29]

All the above synthetic methods required high temperature and harsh conditions, and the yields were very low. A truly efficient synthesis of HBC and related PAHs was achieved by Müllen's group using the Scholl reaction as a key step.

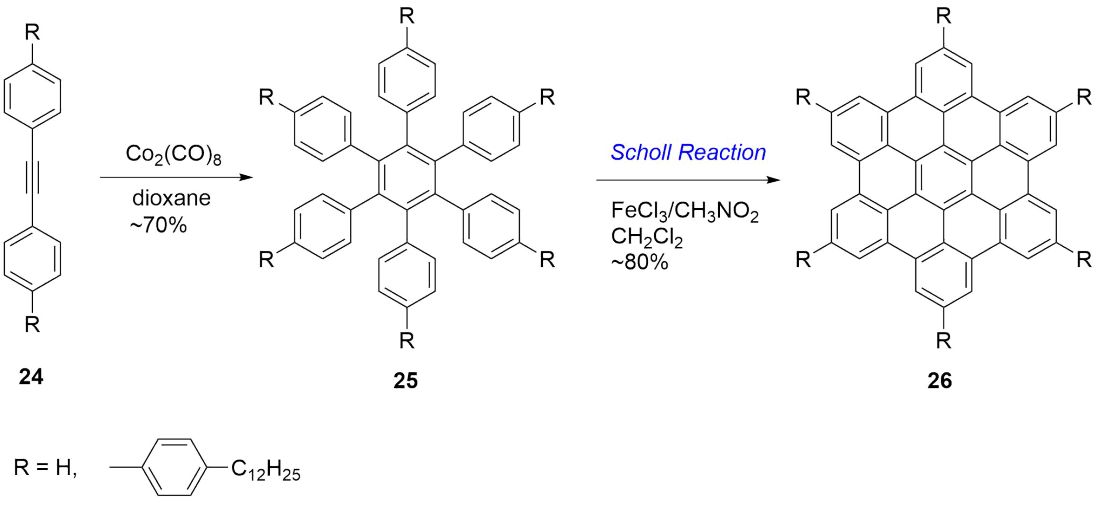

Scheme 1.6: Synthetic route to sixfold symmetric HBCs via the Scholl reactions.

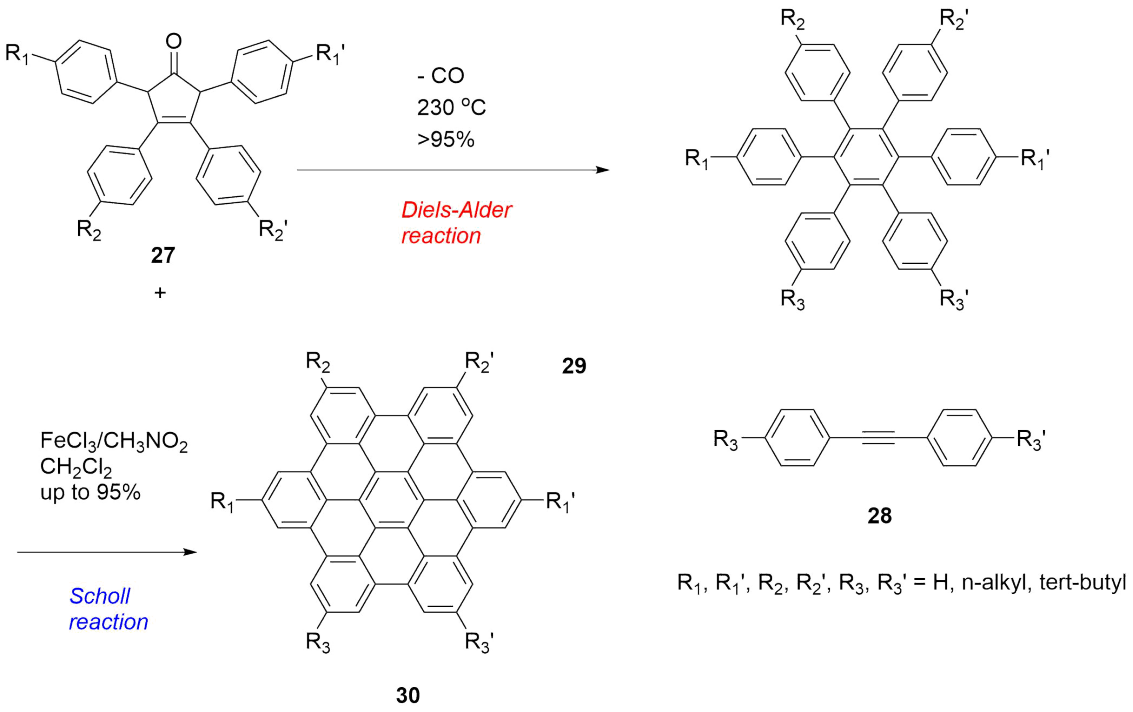

Scheme 1.7: Synthetic route to HBCs with low symmetry by the Scholl reactions.

As shown in Scheme 1.6, hexaphenylbenzenes **25** were first synthesized by cyclotrimerization of substituted diphenylacetylenes using $Co_2(CO)_8$ as the catalyst. The hexaphenylbenzene intermediates were then subjected to cyclodehydrogenation under different Scholl reaction conditions to afford HBC products with a sixfold symmetric structure. Typical Scholl reaction conditions involved Cu(II) salts (e.g., $CuCl_2$ and $Cu(OTf)_2$) and $AlCl_3$ as Lewis acid catalysts. Another commonly used Lewis acid catalyst for the Scholl reaction was $FeCl_3$. As shown in Scheme 1.6 the use of $FeCl_3$ in the Scholl reaction resulted in very good yields of HBCs (ca. 80%).

The synthesis of HBC derivatives with different substitutes can be achieved by the approach shown in Scheme 1.7. This method began with the Diels-Alder cycloadditions between tetraphenylcyclopentadienone derivatives **27** and substituted diphenylacetylenes **28**, which yielded hexaphenylbenzene derivatives **29** with different

substituent groups attached. Compounds **29** underwent Scholl reaction to afford corresponding HBC derivatives in the presence of $FeCl_3$ with high yields.[1] In Müllen's work, $FeCl_3$ or $Cu(OTf)_2/AlCl_3$ has often been used as the catalyst for Scholl reactions in the synthesis of larger graphene discs, but a large excess of oxidants and prolonged reaction times were required in order to obtain good yields.

1.1.3.2 Synthesis of Large Nanographenes

The methodologies for preparing small PAH molecules can be also applied to the synthesis of large nanographene molecules. Generally speaking, nanographene molecules have discotic molecular shapes that favor columnar stacking among the molecules. Increase in the size of the π-core should enhance the interactions between each layer of the columnar superstructure, resulting in better overlap of the π-surface and improved charge carrier mobilities.[30] On the other hand, increased intermolecular stacking would lead to reduced solubility and processibility in solution. Nevertheless, some of the very large PAHs synthesized by the Müllen group (e.g., **31a-c**, Figure 1.3) still show good solubility in normal organic solvents owing to the presence of long aliphatic side chains in their structures. Those large PAHs carrying relatively short aliphatic chains, such as compounds **31d-e**, show poor solubility. Similarly, compound **32** as shown in Figure 1.4 bears long flexible phytyl chains and shows good solubility.[31]

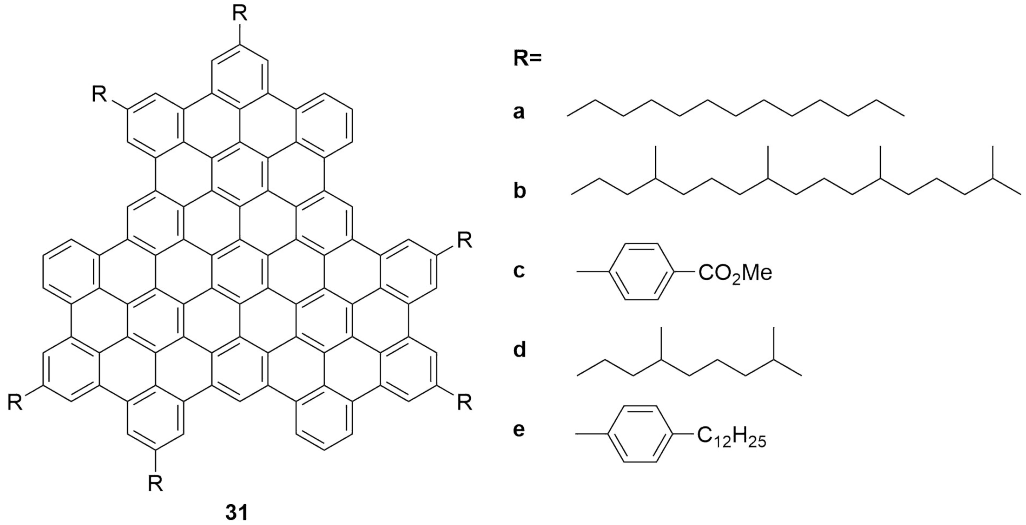

Figure 1.3: Super-phenylenes with different side groups.

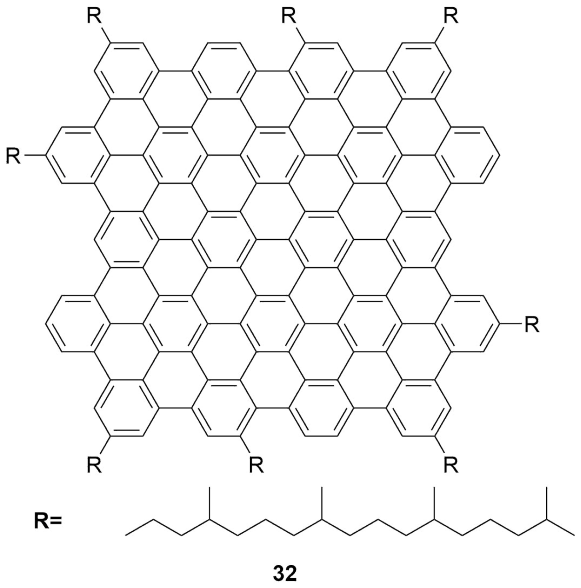

32

Figure 1.4: Structure of phytyl-substituted nanographene **32**.

Besides the solubility issues, the complete cyclodehydrogenation of large oligophenylene precursors has to be carefully controlled, since reaction time and amounts of reagents and oxidants would all affect the reaction outcomes significantly. When the branched oligophenylene becomes too large, the complete oxidative cyclodehydrogenation cannot happen. For example, in one of Müllen's papers, the cyclization of a giant oligophenylene dendrimer only yielded a partially closed three-dimensional graphitic propeller-shaped product.[31]

The synthesis of large nanographenes is very difficult, and characterization of their structures is even more challenging. The poor solubility of giant nanographenes is a key limiting factor for their characterization; in particular, the strong aggregation propensity of these type of molecules in solution prohibits meaningful NMR analysis. Other spectroscopic methods can be used for characterizing these compounds, includes MALDI-TOF mass spectrometry, solid-state UV-Vis absorption, and Raman

spectroscopy. Müllen's group also reported the optical absorption properties of these molecules, in which the maximum absorption wavelength of the lowest energy band (α-band) was found to redshift and broaden with increasing number of six-membered rings.[32,33] Such behavior is very similar to that of linear π-conjugated oligomers, the maximum absorption bands of redshift as the chain length increases within the effective conjugation length (ECL).[16] Novel 2D and 3D graphitic materials show excellent charge storage capacity upon alkali metal reduction, which suggests potential application to battery technology.[34]

Further extension of HBC in one direction can yield the ribbon-like graphene structure. A series of well-defined graphene ribbons was reported by Müllen's group as shown in Figure 1.5. Similar to the case of effective conjugation lengths in linear π-conjugated polymers, the maximum electronic absorption peaks of these ribbon-like products show a redshift trend as the number of six-membered rings increases.[30,35]

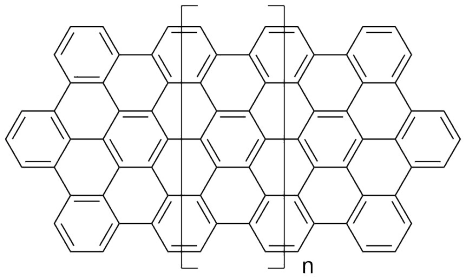

33a, n=0, C60;
33b, n=1, C78;
33c, n=3, C114

Figure 1.5: Well-defined nanographene ribbons synthesized by the Müllen group.

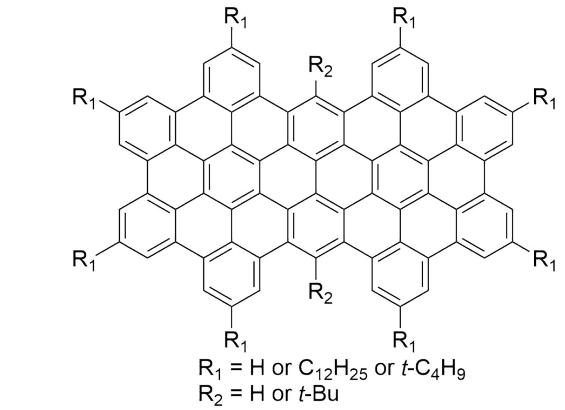

34

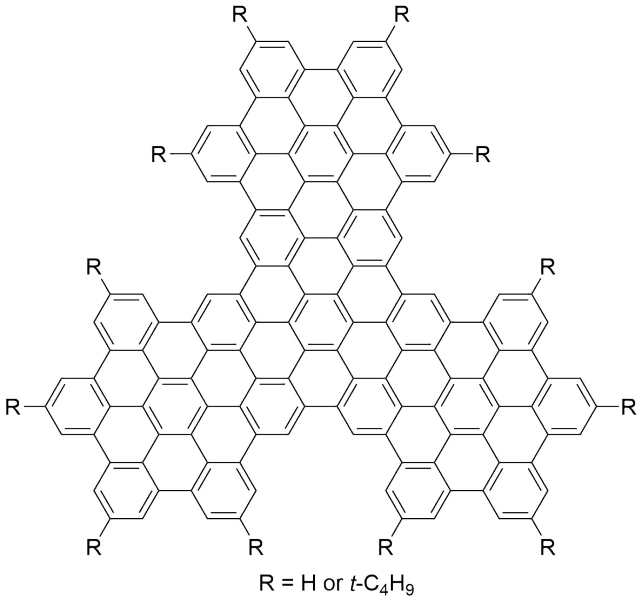

35

Figure 1.6: HBC "naphthalene" and "triphenylene".

In addition to nanographene ribbons, extension of HBC can also lead to other types of nanographenes. As shown in Figure 1.6, the HBC "naphthalene" **34** and "triphenylene" **35** were also prepared by Müllen's group. These large PAHs were substituted by flexible alkyl chains on the peripheral positions, allowing them to form an ordered columnar liquid crystalline phase.[35,36] For HBC "naphthalene" **34** with

two t-butyl substituents, the compound showed a high solubility in organic solvents as a result of the effective suppression of aggregation by bulky t-butyl groups. Because of this, it became possible to purify compound **34** with standard laboratory techniques and a resolved ^{1}H NMR spectrum was obtained. When the t-butyl substituents were removed, the compound showed lower solubility. The aromatic signals in the ^{1}H NMR spectrum could not be resolved any more due to the effect of strong self-aggregation.

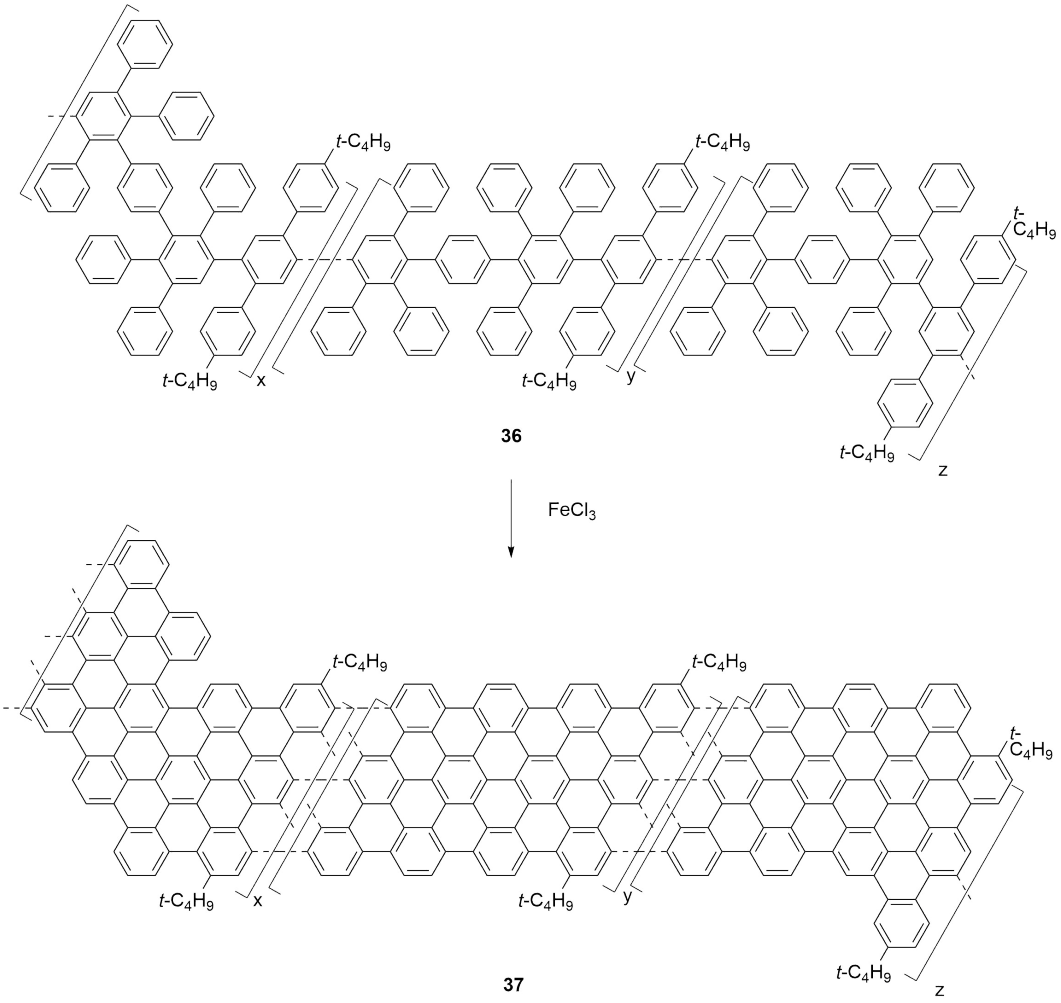

Scheme 1.8: Synthesis of one dimensional extended graphene ribbons by intramolecular oxidative cyclodehydrogenation.

Scheme 1.8 illustrates the synthesis of another one dimensional polymeric graphite ribbons by Müllen's group.[33] Different from the above examples, these graphite ribbons were prepared by intramolecular oxidative cyclodehydrogenation reactions. The products are insoluble, and were only characterized by solid-state UV-Vis, Raman, and IR spectroscopy. In their UV-Vis spectrum, a broad and structureless absorption band around 800 nm was observed, indicating the presence of highly extended π-conjugated frameworks. In the Raman analysis, two strong vibrational bands appeared at 1603 and 1322 cm^{-1}, which correspond to the G and D bands of graphite. TEM imaging, however, showed that their structures are partially ordered. This may be due to the non-linear structures and random stacking of these nanographenes in the solid state.

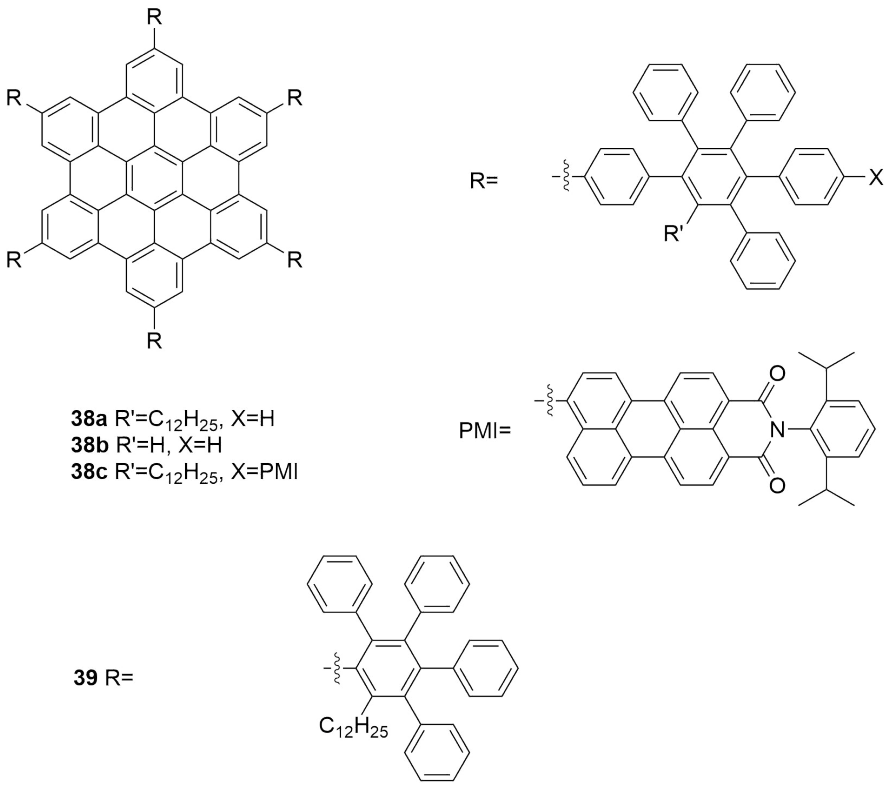

Figure 1.7: Structures of dendronized HBC molecules.

The aggregation of graphitic compounds has a strong effect on the order and structures of their thin films, as well as their photophysical and electronic properties.[37–39] To control the self-assembling behaviour of HBC in solution, bulky substitutes were attached to the HBC core. One example contributed by Müllen's group utilized rigid oligophenylene end groups (Figure 1.7). The rigid end groups in **38a** weaken the π-stacking among the HBC cores. NMR analysis showed a slow monomer–dimer equilibrium.[40] This equilibrium could be controlled by temperature, concentration, and solvent effects. As a result, pure monomer or dimer could be obtained respectively with careful control and separation. A stable dimer of compound **38b** was obtained after further structural modifications. The non-aggregated monomer could be obtained by moving the aryl arms more closely to the HBC core such as in compound **39**. With or without π-stacking occurring among these compounds, the UV-Vis absorption and fluorescence spectral properties showed significant differences. Compound **38c** was reported to show efficient intramolecular energy transfer from the HBC core to perylene monoimide (PMI) upon photoexcitation. In this process, the PMI group acted as a typical electron acceptor and the HBC an electron donor.[40]

1.1.3.3 Contorted Polycyclic Aromatics

Besides the strategy of using side groups, distortion of the planar aromatic core of PAHs presents another way to control their self aggregation. Such a concept was first introduced by Nuckolls and co-workers, and they termed this class of PAHs "contorted polycyclic aromatics".[41] Adding strain to a PAH would force its aromatic core to adopt a twisted structure instead of being planar. The twisted shape can lead to

several advantageous consequences for materials applications. This type of molecules can form unique π–π contacts in thin films and crystals.[42–46] Another interesting property is that these curved, twisted, or bowl-like structures are complementary to fullerenes in shape and size. Such supramolecular interactions can be utilized in the fabrication of efficient photovoltaic cells.[47–50]

Over the past few years, the Nuckolls group has prepared and investigated a series of contorted HBC molecules.[42–45,51] Contorted HBC (c-HBC) and its derivatives are very efficient materials used in solar cells; however, their applications are somewhat limited by the poor overlap of the absorption profiles with the solar spectrum.[51] Recently, efforts were made to expand the aromatic core of c-HBC to overcome this barrier. For example, compounds **41**, namely contorted octabenzocircumbiphenyl (c-OBCBs), were prepared and their structures feature eight aromatic rings appended around a circumbiphenyl core as shown in Figure 1.9.[41]

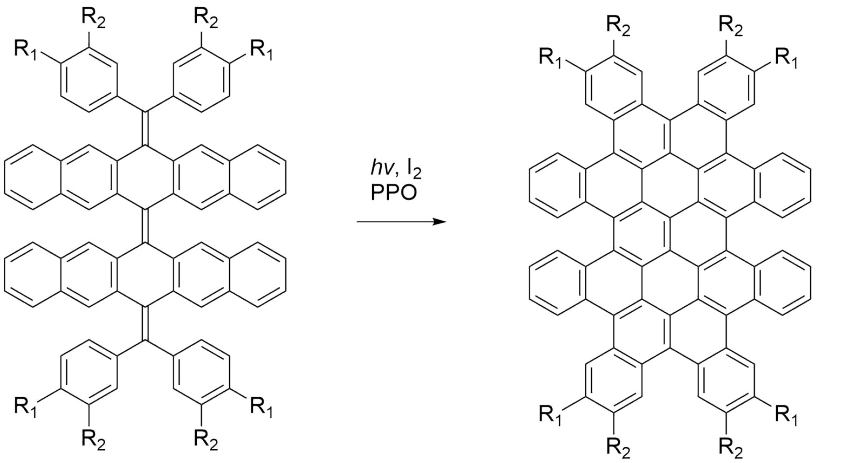

Scheme 1.9: Preparation of c-OBCBs by photocyclodehydrogenation (Mallory reaction).

The c-OBCB compounds **41** were prepared from tris-olefins **40** through photocyclodehydrogenation in the presence of I_2 and propylene oxide (PPO) in dry benzene. The reaction is generally referred to as the Mallory reaction. The conformation of **41a** was studied by single crystal X-Ray diffraction analysis. The data show that two pentacene-like substructures along the short axis of the molecule are bent into opposite directions and the three double bonds along the long axis of the molecule adopt a "zig–zag" orientation. The unsubstituted c-OBCB **41a** is a red powder and has low solubility in common organic solvents, while **41b** and **41c** show much better solubility due to the presence of side chains. Compared with c-HBC, the maximum absorption band of c-OBCB is redshifted. c-OBCB is an electron donor and can self-assemble into columnar superstructures like other planar PAH molecules. The columnar packing motif makes the compound photoconductive exhibiting p-type, hole transporting properties FET devices.

1.1.4 Introduction to the Scholl Reaction

As discussed above, the Scholl reaction has played a key role in the synthesis of PAH molecules. This type of reaction was first reported by Roland Scholl, a Swiss chemist, in 1910.[52] In Scholl's work, quinone **43** and perylene **45** were prepared from naphthalene using $AlCl_3$ as catalyst (Scheme 1.10).

As shown in Scheme 1.10, the π-extended quinone **43** was prepared by treatment with an excess of neat anhydrous $AlCl_3$ for 45 min at 140–145 °C, and the yield of this reaction was not given. In a subsequent publication, this reaction was used to prepare perylene from 1,1'-binaphthalene with a yield of 15%. Perylene **45**can

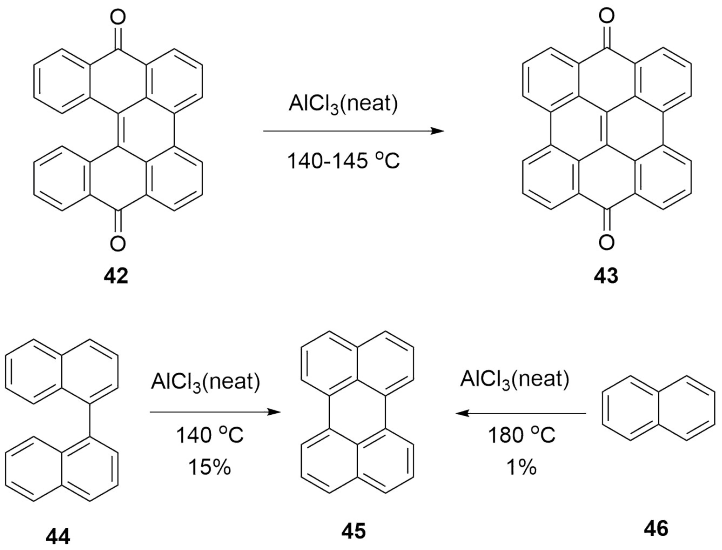

Scheme 1.10: The first reported Scholl reactions in 1910.

be also obtained from naphthalene under higher temperature without isolation of the intermediate binaphthalene; however, the yield of this reaction was much lower due to decomposition. The same reaction was also applied to the synthesis of benzanthrone **48** and compound **49** as shown in Scheme 1.11. Other examples were also published by Scholl in the following years.[53,54] The mechanism of the Scholl reaction is still not clear. There were several reports discussing its possible mechanism. One possible mechanism was proposed as dehydrogenative coupling of aromatic compounds upon treatment by anhydrous $AlCl_3$, based on the similarity to the Friedel-Crafts reaction.[54]

The original procedures of the Scholl reaction required harsh conditions. Later, Kranzlein and Vollmann modified the reaction by using an equimolar mixture of $AlCl_3$ and NaCl. The mixture is liquid above 100 °C at a low vapor pressure. In 1971, Wick found that in the cyclization of bis(1-anthraquinonyl)amine to form 1,2;7,8-diphthaloylcarbazole, the $AlCl_3$/pyridine complex worked as a better catalyst than

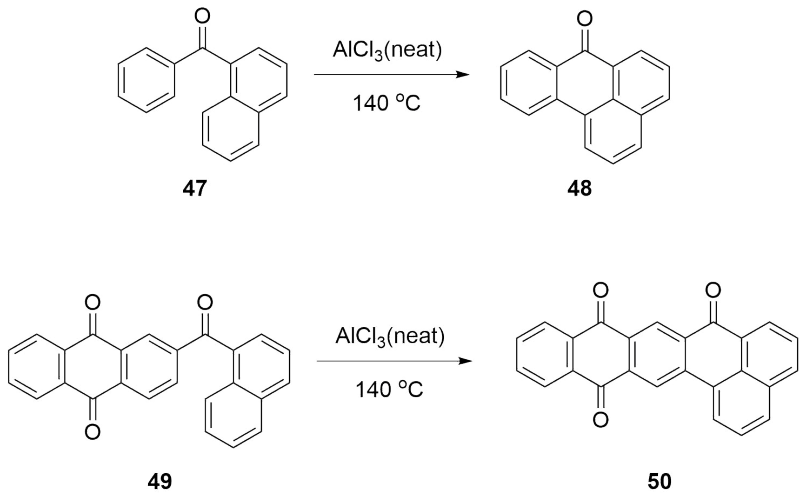

Scheme 1.11: Preparation of benzanthrone compound **48** and compound **50** by the Scholl reactions.

the melted mixture of $AlCl_3$ and NaCl.[54] Other modifications include the use of $AlCl_3$ in a high boiling solvent such as dichlorobenzene or trichlorobenzene, the low-melting complex $AlCl_3/SO_3$, or $ZrCl_4$. The reaction conditions modified by Müllen's group were based on the work of Kovacic and Kyriakis, who used mixed $AlCl_3/CuCl_2$/neat conditions. Müllen's group used $AlCl_3/CuCl_2/CS_2$ and $AlCl_3/Cu(OTf)_2/CS_2$ instead, which allowed the reaction to happen at room temperature.[55–57]

The Scholl reaction needs a strong acid, often a Lewis acid, together with an oxidant to promote the reaction. A single reagent can serve both roles. Brønsted acids, which usually appear as common impurities in Lewis acids, also are formed as byproducts of the Scholl reaction, and they can accelerate the reaction as well.[58] The following lists all the conditions reported in the literature: $FeCl_3$ in CH_2Cl_2,[59] $CuCl_2$,[60] $Cu(OSO_2CF_3)_2$ with $AlCl_3$ in CS_2,[61] $MoCl_5$ with or without $TiCl_4$ in CH_2Cl_2,[55,62–64] $(CF_3COO)_2I^{III}C_6H_5$ (PIFA) with BF_3Et_2O in CH_2Cl_2,[65,66] $Pb(OAc)_4$ with $BF_3\,Et_2O$ in MeCN,[67,68] $Tl(O_2CCF_3)_3$ in CF_3CO_2H,[68] and $Tl(O_2CCF_3)_3$ with

$BF_3\,Et_2O$ in organic solvents.[68]

In early years the Scholl reaction was mainly used to prepare large polyaromatic ketones and quinones. The first example of a multiple dehydrogenative coupling reaction was reported by Scholl's group in 1913 (Scheme 1.12).[69,70] In this reaction, 4,4'-dibenzoyl-1,1'-binaphthyl **51** was treated by $AlCl_3$(neat) for 8.5 h at 95–100 °C to give the multiple dehydrogenation product **52**.

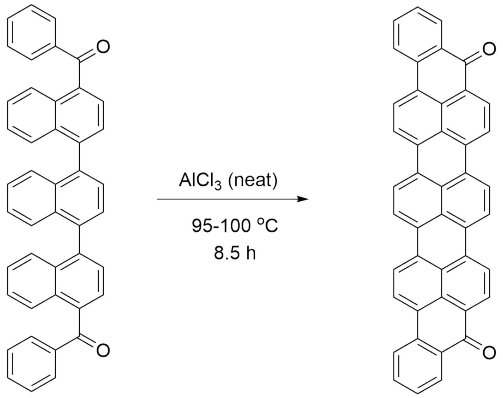

51 **52**

Scheme 1.12: The first reported multiple Scholl reaction.

Müllen's group has been using the Scholl reaction to create large, interesting PAH molecules. In 2006, they reported that 3-(1-naphthyl)perylene **54** could form six membered ring product **53** by oxidative coupling with $AlCl_3$ as the catalyst (Scheme 1.13). When the catalyst was switched to $FeCl_3$, however, a five membered ring product **55** was produced. The reaction outcomes could be controlled by varying the reaction conditions.[71] Compared with $FeCl_3$, $AlCl_3$ is a non-oxidizing Lewis acid. The different regioselectivities indicate that the cyclization of aromatic hydrocarbons proceeds by different mechanisms. Which type of Lewis acid was used, oxidizing or non-oxidizing, plays a key role.

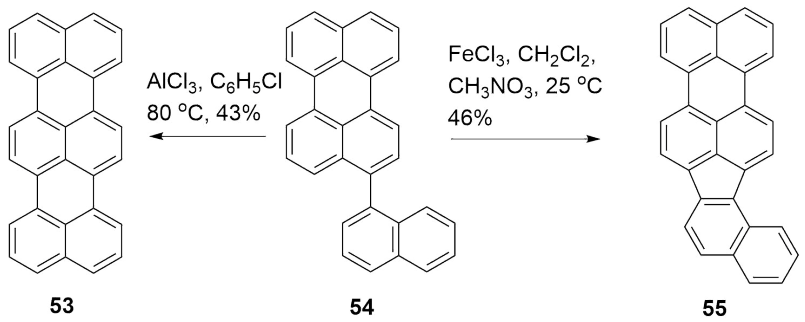

Scheme 1.13: Different cyclization routes of 3-(1-naphthyl)perylene under the catalysis of different Lewis acids.

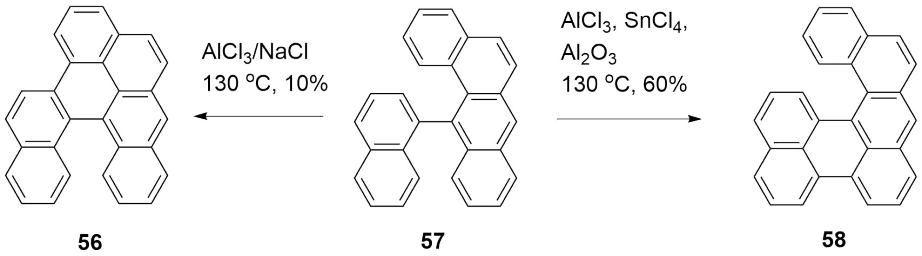

Scheme 1.14: Different cyclization routes of 1,2-(1-naphthyl)benz[a]anthracene under controlled reaction conditions.

Scheme 1.14 shows the cyclization reactions of 1,2-(1-naphthyl)benz[a]anthracene (**57**) through the Scholl reaction with different catalysts.[72] The cyclization afforded benzo[d,e,f]naphtha[1,2-p]chrysene **56** as the major cyclization product with a low yield of 10%, when $AlCl_3$/NaCl was used as the catalyst. Under the catalysis of $AlCl_3/SnCl_4$, naphtho[1,2-a]perylene **58** was formed as the major product with a yield of 60% . The results testify to the importance of reaction conditions to the regioselectivity of Scholl reactions.

Despite the complex outcomes, the Scholl reaction is still a very useful and popular synthetic method. Müllen's group demonstrated that the Scholl reaction was capable

of making 126 C–C bonds in a single synthetic step.[61] Limitations of the Scholl reaction, on the other hand, have also been recognized. As discussed above, products of the Scholl reaction were greatly affected by reaction conditions. In certain cases, the Scholl reaction was found to result in completely unexpected products. Scheme 1.15 illustrates an example of such cases.

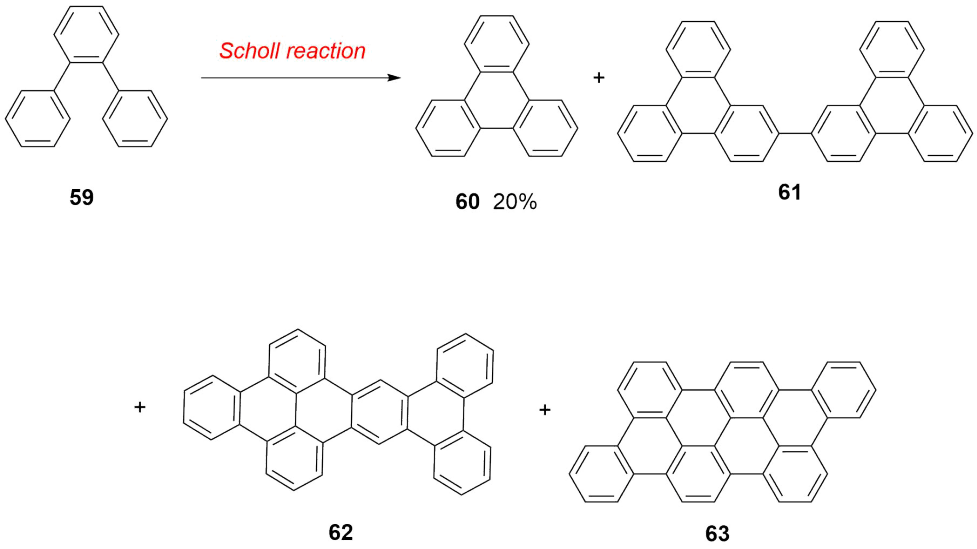

Scheme 1.15: Different products resulting from the Scholl reaction of *o*-terphenyl.

Herein, unfunctionalized *o*-terphenyl **59** was subjected to the Scholl reaction and it was expected to give compound **60** as the major product under typical Scholl reaction conditions. The optimized yield, however, was low (20%). The use of chlorinated solvents ($CH_2Cl_2, CHCl_3, CCl_4, CH_2ClCH_2Cl$) led to faster reaction rates compared with CH_3NO_2 or hexanes. When $MoCl_5$ was used as the catalyst and CH_2Cl_2 as the solvent, the yield was still around 20%.[62,63,73] The crude product of the reaction was identified as a mixture of triphenylene, unreacted *o*-terphenyl, and other insoluble byproducts. MALDI-MS analysis detected two compounds with molecular masses 2

or 4 amu less than that of **60**. Since the Scholl reaction is likely to give fully fused products,[74,75] compounds **61** and **62** were proposed to be the possible structures of these two products. Attempts to run the Scholl reaction at low concentrations did not help to improve the reaction results.

An interesting ^{13}C-labeled experiment was conducted to study the formation of dimeric products in the Scholl reaction of *o*-terphenyl **59**. The 1:1 mixture of ^{13}C-labeled *o*-terphenyl (C_6H_5-C_6H_4-$^{13}C_6H_5$) **59** and unlabeled triphenylene **8** was treated by sub-stoichiometric oxidant (10 mol% with respect to both reactants). MALDI-TOF MS showed that the mass of the dimeric product **60** is unlabelled. This experiment revealed that the formation of the dimeric product is much faster than the formation of the cyclized product, which may explain why this type of reaction always has a much lower yield than expected.

The attempted cyclization of terphenyl homologues suffered similar problems (Scheme 1.16). Both *o*-quaterphenyl **63** and 1,2,3-triphenylbenzene **64** failed to yield the expected cyclized product **65** under Scholl reaction conditions, using either $MoCl_5$ or PIFA/BF_3 Et_2O as the catalyst. Also the *o*-quinquephenyl compound **66** failed to give cyclized product **67** under the same Scholl reaction conditions.[74,75]

To avoid the formation of unexpected side products, a strategy of introducing blocking groups was devised. For example, a bulky *t*-Bu group was chosen to be the blocking group to inhibit the dimerization reaction (Scheme 1.17).

The oxidation of 4,3',4"-tri(*t*-butyl)-*o*-terphenyl compound **68** successfully gave the cyclized product **69** with an excellent yield of 86% under the conditions of PIFA/BF_3 Et_2O. However, the oxidation of 4,4"-di-*t*-butylterphenyl compound **70**, gave a mixture of the cyclized product and dimer with an almost 1:1 ratio under

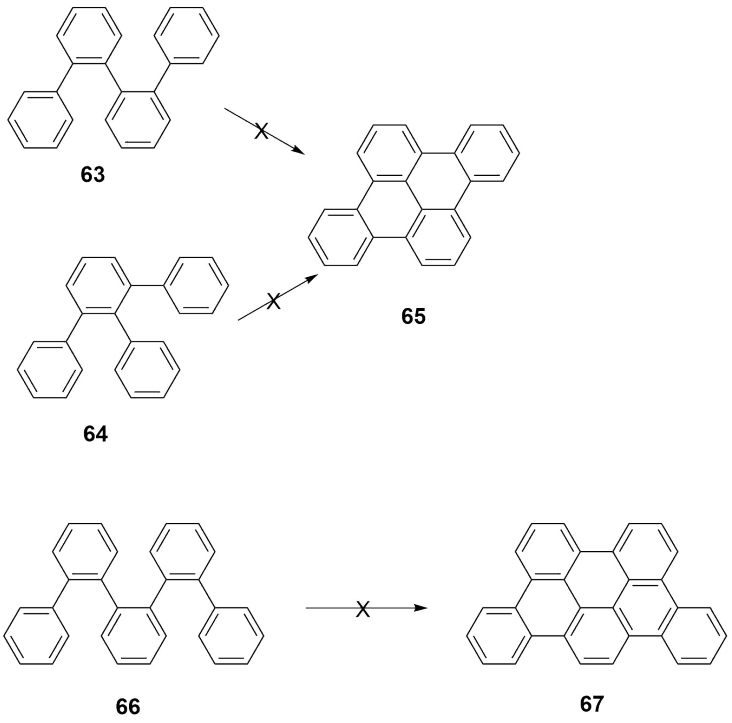

Scheme 1.16: Failed Scholl reactions of terphenyl homologues.

the same conditions. Comparing compounds **68** and **70**, one can clearly see that in compound **70**, one of the three benzene rings is less hindered by the bulky *t*-Bu group.

A common substituent used in the Scholl reaction is the methoxy group, since it is an effective *o*/*p*-director and can help improve the regioselectivity of the Scholl reaction. Scheme 1.18 shows several reactions, in which methoxy groups were used to affect the Scholl reaction.

Treatment of 3,3"-dimethoxy-*o*-terphenyl **73** with $MoCl_5$ in CH_2Cl_2 gave cyclized product, dimethoxytriphenylene **74**, with a yield of 53%. Tetramethoxy derivative **75** was subjected to the same conditions, giving the expect cyclized product 1,3,10,12-tetramethoxytriphenylene **76** with a low yield of 30%. This may be because the methoxy groups cause the cyclized product to be nonplanar and hence reduce the

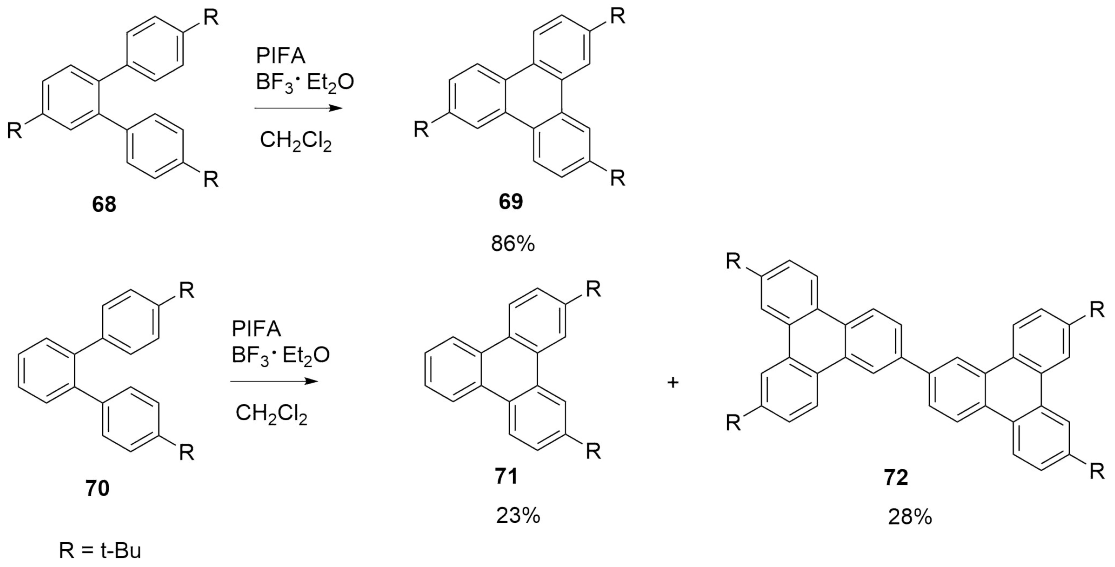

Scheme 1.17: Oxidation of *t*-butylated terphenyls.

aromaticity of the compound. Compared with **73**, the Scholl reaction of 3-methoxy-*o*-terphenyl **77** under the same conditions gave a mixture that was difficult to isolate. The mixed terphenyl/triphenylene dimer **78** was obtained when PIFA/$BF_3\,Et_2O$ was used as the catalyst at -78 °C. According to these examples, it is clear that the *ortho* and *para* positions are more reactive than the others. Interestingly, the oxidation of 2,2"-dimethoxy-*o*-terphenyl **79** did not give the expected cyclized product. Instead, the reaction gave a dimer of the starting material with a yield of 26%. The intermolecular coupling reaction appeared to be more efficient than the intramolecular oxidation.

Bromo is another popular substituent used in the Scholl reaction. For example, 3,3"-dibromo-*o*-terphenyl **81**, which is structurally similar to **73**, underwent the Scholl reaction to give a cyclized product, 2,7-dibromotriphenylene **82**, in the presence of $MoCl_5$ (Scheme 1.19). Bromine atom is also an *o*/*p*-director and influences the Scholl reaction in a way very similar to the methoxy group. In contrast to methoxy

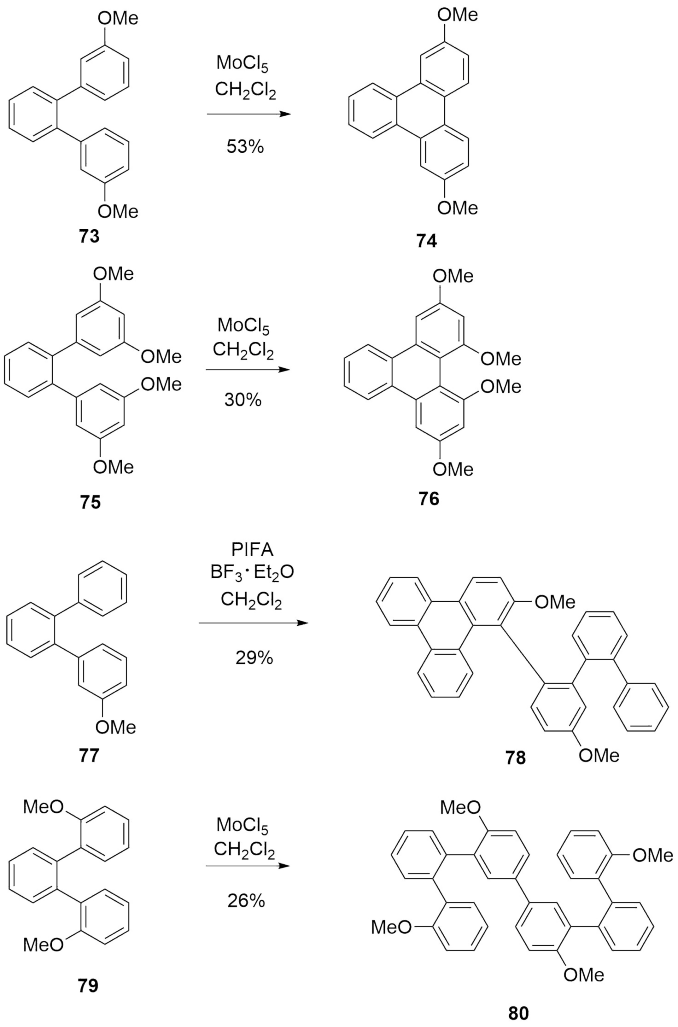

Scheme 1.18: Scholl reactions of methoxylated terphenyl derivatives.

group, bromide is a deactivating substituent. Hence the Scholl reactions of bromo-substituted substrates usually gave low yields. If the substrate is substituted with a nitro group(s), a much stronger deactivating group, the Scholl reaction will be completely inhibited.

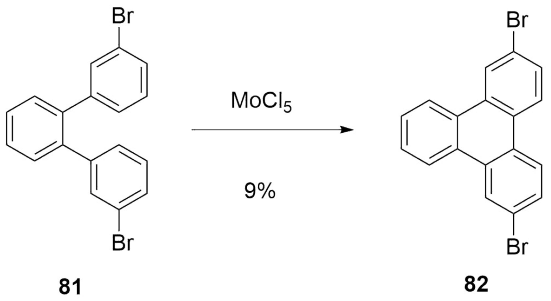

Scheme 1.19: Oxidation of brominated terphenyl derivatives.

1.1.5 Photochemical Cyclodehydrochlorination

Besides the Scholl reaction, which often suffers from poor regioselectivity, there are many other reactions that can be used to prepare PAH molecules, including palladium-catalyzed direct C-H arylation,[76] Al_2O_3-mediated HF elimination,[77,78] Yamamoto cyclotrimerization,[79] palladium-catalyzed [2+2+2] cycloaddition,[80] Mizoroki-Heck coupling,[81,82] and the Katz-modified Mallory reaction.[42,45] Among these reactions, photochemical cyclodehydrochlorination (CDHC) reaction shows outstanding regioselectivity.

The application of the cyclodehydrochlorination reaction in preparation of PAH molecules was first investigated as early as the 1970s,[83] and was further explored by several groups.[84–86] In 2016, Morin's group reported a regioselective synthesis of nanographenes by photochemical cyclodehydrochlorination (CDHC) (Scheme 1.21).[87] Compared with the Scholl reaction, the CDHC reaction is more regioselective, which is quite useful in defining the required structure of the PAH molecules. Morin's group also mentioned that the CDHC can provide better control over the edge configuration of the nanographenes, which significantly influences the properties of the molecule. Moreover, the CDHC reaction does not require metal catalysts, and

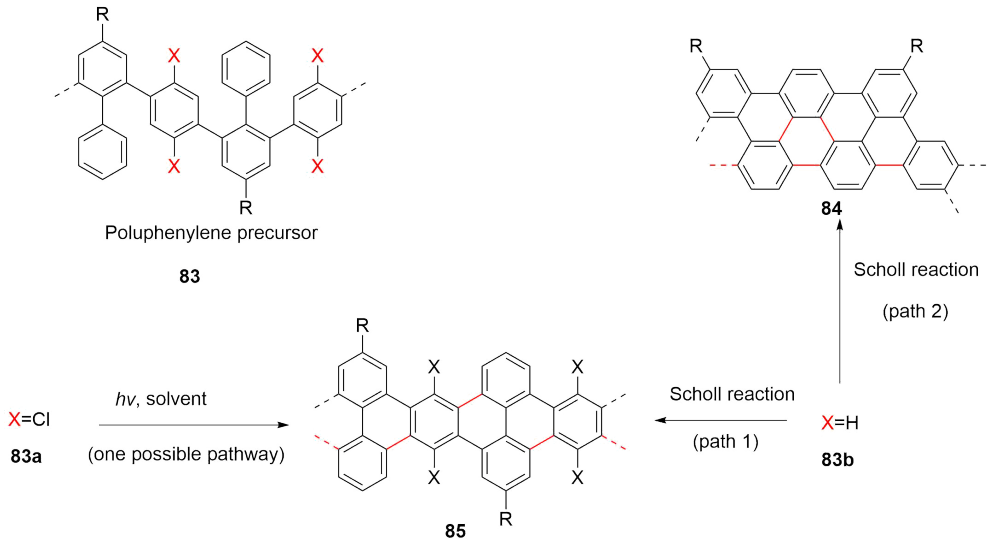

Scheme 1.20: Different reaction paths for the CDHC (X = Cl) and Scholl (X = H) reactions.

it is not likely to form rearranged side products. Chlorine atoms can be introduced into the precursors by careful design, fallowed by CDHC reaction to produce the PAH molecules with desired structures. The CDHC reaction always proceeds under mild conditions, making it possible to introduce different functional groups onto the nanographene products. As such, the properties of the nanograohene synthesized by the CDHC reaction can be controlled by carefully chosen functional groups attached to its precursor.

Compared with the Scholl reaction, the yield of the CDHC reaction can be significantly higher, even for those reactions with multiple cyclizations in one single step. For precursors with electron-rich thiophene or electron-poor pyridine groups, the CDHC reaction can still occur to give the corresponding cyclized product.

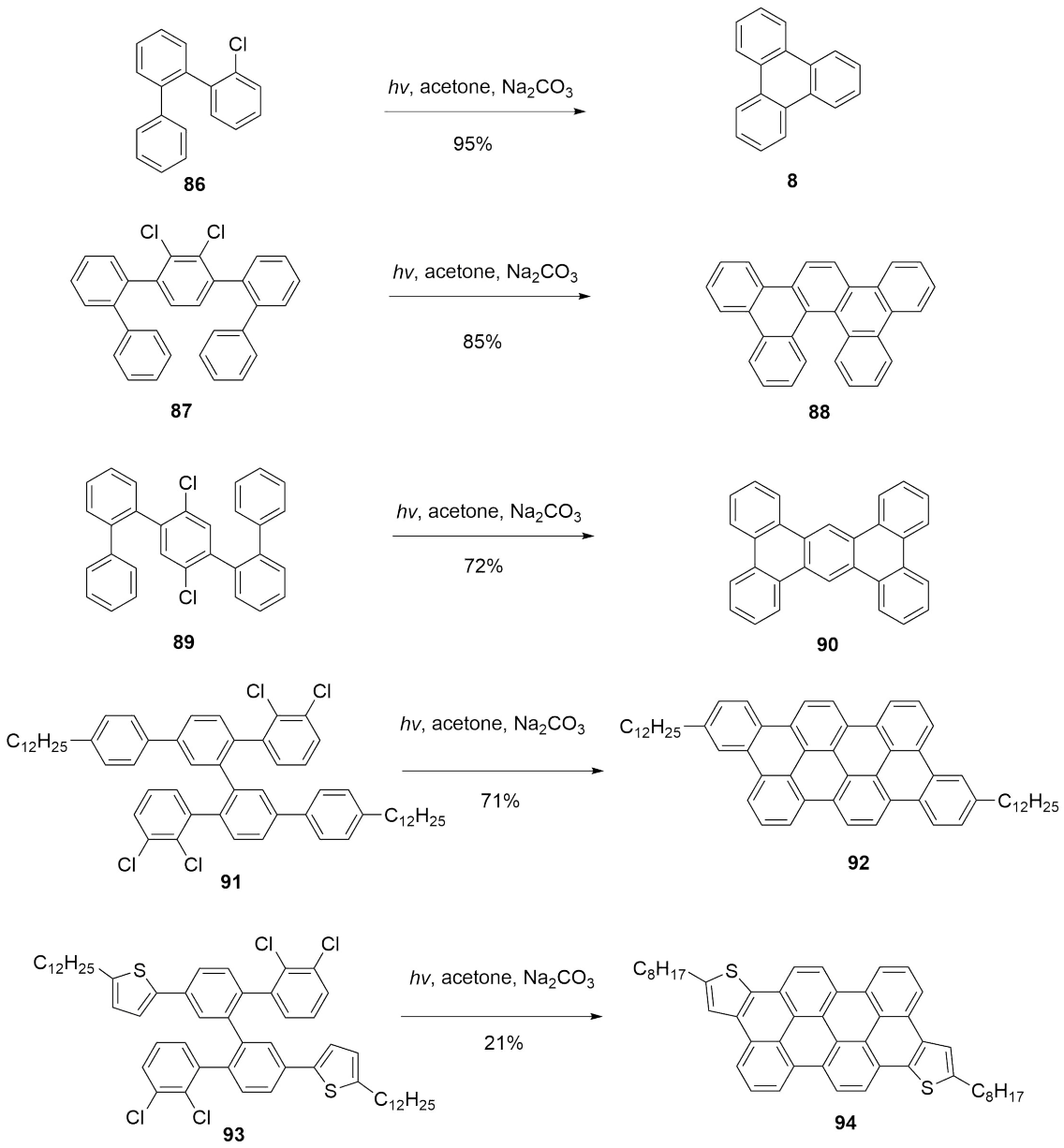

Scheme 1.21: Morin's synthesis of nanographenes through the CDHC reaction.

1.2 Porous Organic Frameworks

Porous materials have attracted more and more research interest owing to their outstanding properties and broad application in many fields, such as gas storage, gas separation, superhydrophobic interfaces, drug delivery, catalysis, energy storage, and optoelectronics. A wide variety of porous materials has been synthesized so far, including metal-organic frameworks (MOFs), covalent organic frameworks (COFs), zeolites, and porous cross-linked polymers.[88]

After the seminal work of MOF (MOF-5) by the Yaghi group in 1999, thousands of papers relevant to the topic of MOFs have been published and new types of MOFs are continuously reported by researchers today.[88–91] MOFs are molecular frameworks in which metal atom or metal clusters are interconnected by organic linkage groups. MOFs possess enormous surface areas and channels or cavities with defined shapes and dimensions. Because of these, MOFs show very large storage capacities. Also, the size and shape of the channels or pores within MOFs can be controlled through design of different organic linkers. Despite these remarkable properties, MOFs still suffer from several weaknesses in material application. MOFs cannot tolerate very high temperature and strong acidic or basic conditions. This may be due to the main interactions between the metal clusters and organic linkers are coordination bonds. In 2005, Yaghi and co-workers demonstrated a new type of organic porous materials in which organic molecular building blocks are connected via covalent bonds, named covalent organic frameworks (COFs).[92]

Since COFs are composed of light-weight elements (mostly C, H, B, O, and N), they have pretty low mass densities. Compared with MOFs, COFs possess

much higher thermal stability due to the strong covalent bonds in their frameworks. COFs can be divided into two classes, two- (2D) and three-dimensional (3D) COFs, depending on the dimensions of the building blocks. The structures of 2D COFs are typically planar 2D sheets, since most of the carbon atoms in the building blocks are sp^2 hybridization. The sheets will further stack to form a layered eclipsed structure that presents periodically aligned columns, which is quite similar to that of PAH molecules. Just like the PAH disc columns, the ordered 2D COF columns can also facilitate charge carrier transport in the stacking direction. Thus 2D COFs have the potential in new types of π-electronic and photo-functional materials for optoelectronic and photovoltaic devices. In contrast to 2D COFs, 3D COFs have sp^3 carbons in their building blocks, which lead to the formation of frameworks in three dimension. The surface areas of 2D COFs are much smaller than those of 3D COFs. Some 3D COFs have surface areas lager than 4,000 m^2g^{-1}, and thus have application in gas storage and gas separation.

1.2.1 Design and Synthesis of COFs

The synthesis of COFs is challenging and needs to be carefully controlled. The preparation of polymeric materials are generally dominated by kinetically controlled (i.e., irreversible) reactions. This type of reaction is not suitable for growing crystalline and ordered organic polymers. Dynamic covalent chemistry (DCC), which leads to the reversible formation of covalent bonds, is an ideal choice for preparation of COFs.[93] DCC is thermodynamically controlled and provides a reversible reaction system that can achieve the so called error checking and proof-reading steps. As

such, DCC results in the most thermodynamically stable structure. By applying DCC to the preparation of COFs, the polymer skeleton formation occurs together with the crystallization process. In the mean time, the product continues to undergo the self-healing process that fixes the incidence of structural defects. Eventually, an ordered polymeric structure is formed. Given a long enough reaction time, the final COF product can attain an ordered crystalline structure with high thermodynamic stability. The design and synthesis of COFs need to consider two important issues. The first one is the structure of the building block, which will affect the size, shape and properties of the final product. The second one is the synthetic method. The reaction must be reversible. The chosen reaction determines the reaction media and conditions.

The structures of building blocks are critical to the synthesis of COFs, and they must meet two requirements. (i) The formation of COFs is a reversible reaction. Thus the building blocks should contain reactive groups that allow the reversible reaction to happen without any irreversible side reactions. (ii) Since the geometry of building blocks will dominate the final structures of the COFs, the building blocks adopted should be conformationally rigid, and the bond formation direction must be discrete. Scheme 1.22 summarizes the reversible reactions commonly used in the synthesis of COFs.

A majority of the reported COFs were synthesized based on boron chemistry, since boronic acids can be either self-condensed or co-condensed with diols to obtain six-membered boroxine and five-membered boronate ester linkages.[92] Acetonide-protected catechols, instead of reactive diols, can also be used to react with boronic acids in the presence of a Lewis acid catalyst (e.g., $BF_3\,OEt_2$) to form COFs.[94] This

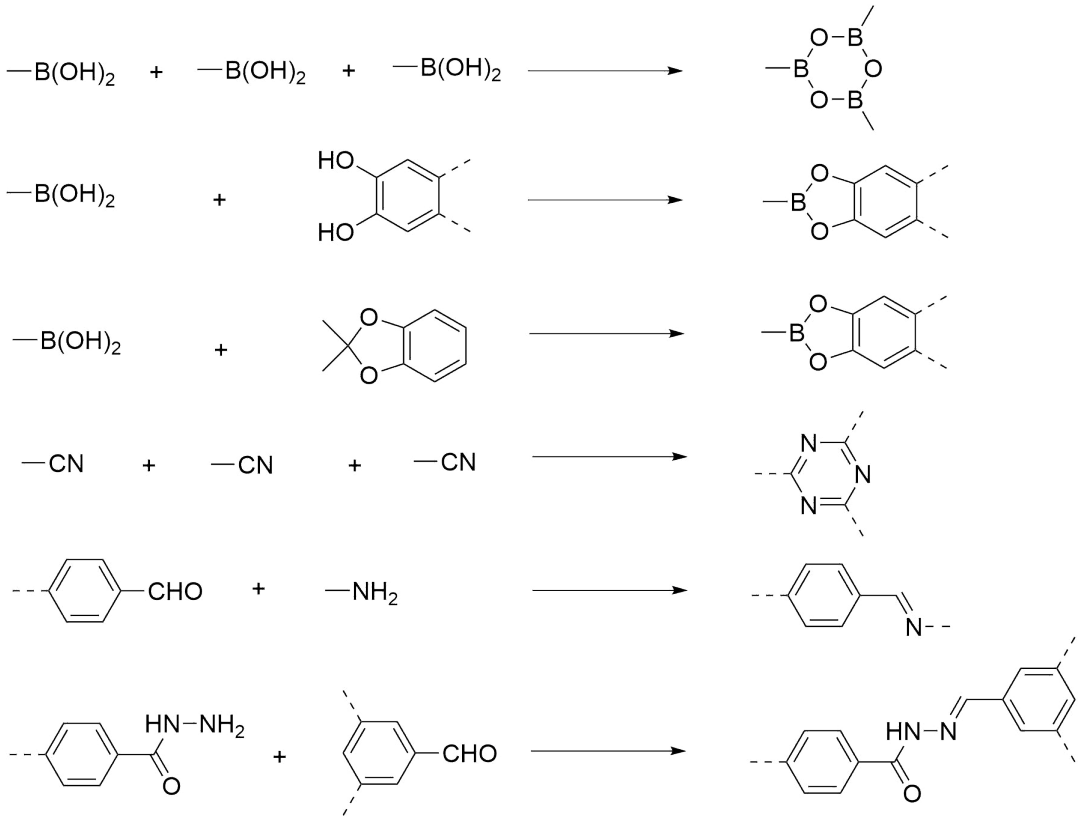

Scheme 1.22: Reversible reactions applied in synthesis of COFs.

modification helps to solve both the oxidation and solubility issues with the diol building blocks, especially for large, poorly soluble aromatic diols. Besides carbon functional groups, borosilicate linkages have been also used to prepare COFs by condensation of tetraboronic acid with *t*-butylsilanetriol in a way similar to boroxines or boronate esters.[95]

Boron-based COFs have outstanding thermal stability; however, they cannot tolerate water. It has been reported that boron-based COFs can be decomposed by water vapor in the air.[96] To overcome this hurdle, Yaghi's group investigated a new reaction for preparing COFs, Schiff base condensation, which can form imine or hydrazone linkages.[97–99] The cyclical trimerization of cyano groups under ionothermal

conditions was also used in preparing COFs with triazine linkages.[100,101] However, the formation of triazine is not as reversible as other linkages. Therefore, the triazine COFs tend to show low crystallinity, even though they can achieve high thermal, chemical, and mechanical stability, as well as high degrees of π-conjugation.

The rigid conformation of building blocks will determine the structures of COFs. These building blocks can be classified as either 2D or 3D based on simplified symmetry notation, referred to as the directional symmetry of the functional group where the reversible reaction happens. 2D building blocks always contain sp and sp^2 carbons, and 3D building blocks contain at least one sp^3 carbon or silicon. The combination of 2D building blocks leads to the formation of 2D COFs, while the combination of 3D building blocks or 3D and 2D building blocks leads to the formation of 3D COFs. The rigid nature and discrete bonding direction of arenes make aromatic compounds suitable building blocks for making COFs. The diversity of aromatic molecules allows researchers to design and create numerous COFs with high flexibility.

The preparation process for COFs needs to be carried out under thermodynamic equilibrium. Thus, the reaction media and conditions, such as temperature, pressure, catalyst, and presence or absence of templates, need to be carefully controlled. Both mixed solvent systems and molten metal salts have been used to prepare COFs. Similar to the preparation of MOFs, the solvothermal method is the most classic and popular method for making COFs. A typical solvothermal method always starts by adding the building block and other required reagents (such as the catalyst or template) to the solvent (mostly mixed solvent), no matter if they dissolve completed or not. Degassing is usually performed by several freeze-pump-

thaw cycles. Then the reaction tube is sealed and heated to a designated temperature for a certain period of time and then slowly cooled down to room temperature. After the reaction, COFs are collected as precipitates, washed with suitable solvents and dried under vacuum to yield the desired COFs. There are a lot of factors that need to be considered in this process, which makes preparation of COFs really challenging. The formation of COFs and the crystallization process need to be balanced when choosing the solvent combinations with suitable ratios. For boronate ester and boroxine linked COFs, the most common solvent combinations are dioxane/mesitylene,[92] DMAc/o-dichlorobenzene,[102] and THF/methanol.[103] For the imine-linked COFs, the most commonly used solvent system is dioxane/aqueous acetic acid.[98] Mesitylene/dioxane/aqueous acetic acid has been often used for making hydrazone linked COFs.[97] The concentrations of building blocks in the solvent system are also important. In the solvothermal method, another dominate factor is reaction temperature. Generally speaking, COFs are usually prepared at temperatures between 85—120 °C depending on the chemical reactivity of the building blocks. A closed reaction environment is necessary, since it can provide suitable pressure inside the reaction tube and avoid losing water, which is required for keeping the reaction system reversible.

Other methods for preparing COFs include microwave synthesis, ionothermal synthesis, and monolayers on surfaces such as a metal surface,[104] a highly ordered pyrolytic graphite (HOPG) surface,[105] or a graphene surface.[106–108] The microwave synthetic method was developed by Cooper's group and it can rapidly synthesize boronate ester linked COFs.[109,110] Microwave synthesis has been reported to prepare COFs 200 times faster than the solvothermal method, and it does not require

a sealed vessel. The frameworks produced have physical properties that are comparable to materials prepared by solvothermal synthesis. The microwave solvent extraction process can remove residues and impurities trapped in the frameworks more efficiently. Thus the frameworks produced by microwave synthesis usually give much larger surface areas and better porosity. The microwave synthesis seems to be a promising method to replace the slow solvothermal method to make COFs; however, publications on COFs prepared by this method are still rare in the current literature.

The ionothermal synthetic method was used by Thomas' group in making triazine COFs.[100,101] The cyclotrimerized aromatic nitrile building units such as 1,4-dicyanobenzene were treated by molten $ZnCl_2$ at 400 °C to give crystalline conjugated triazine COFs. The molten $ZnCl_2$ acted as both solvent and catalyst in this trimerization reaction. However, the reaction temperature required by this method was high, which poses a significant limitation since most organic building blocks would decompose at such a high temperature.

COFs are highly crystalline polymers, but single crystals of COFs have not been obtained so far. Both 2D and 3D COFs have distinct X-ray diffraction (XRD) patterns. The crystalline structures of COFs can be deduced from their PXRD data. Structural simulation of COFs is another useful tool for structural characterization of COFs, especially 2D COFs. Simulation of 3D COFs is much more difficult than 2D COFs. Other methods to study the structures of COFs include infrared spectroscopy, solid-state NMR spectroscopy, elemental analysis, and X-ray photoelectron spectroscopy.

1.3 Introduction to Tetrathiafulvalene and Tetrathiafulvalene Vinylogues

The discovery of tetrathiafulvalene (TTF) as the first organic conductor was published by Fred Wudl and co-workers in 1970.[76] Even though Hünig[111] and Coffen[112] also studied similar sulfur-based π-conjugated heterocycles at the same time, Wudl was the first to demonstrate that high electrical conductivity could be achieved from TTF radicals. TTFs are remarkable organic electron donors and have been widely used as redox-active building blocks in the preparation of organic electronic materials and devices.[113–120]

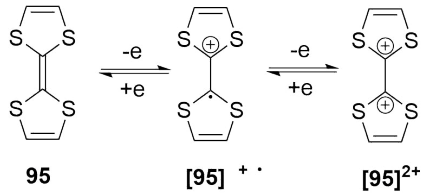

Scheme 1.23: The unique aromaticity-stabilized cationic states of TTF.

In the gas phase, based on density functional theory (DFT) studies, the TTF molecule takes a non-planar, boat-like molecular shape with a C_{2v} symmetry.[118,121] In the solid state, however, TTF is known to adopt a planar geometry with either an orange monoclinic α form[122,123] or a yellow triclinic β form depending on different crystallization conditions.[124,125] As shown in Scheme 1.23, the electron-donating properties of TTF come from the transformation from its non-aromatic dithiole units **95** to aromatic dithiolium cations after releasing one and/or two electrons. In the dicationic state of TTF, the two dithiolium moieties are perpendicular to each other

to minimize disfavored charge repulsion.

After Wudl's paper on TTF, researchers soon became more and more interested in preparing new TTF derivatives, including the so-called π-extended TTF analogues (exTTFs). Attachment or introduction of π-conjugated groups to the two dithiole rings can retain the redox-activity of pristine TTF, reduce the charge repulsion by enhancing the delocalization of the positive charges, and thus lower the oxidation potentials and facilitate intermolecular interactions. These properties have made exTTFs widely used molecular building blocks in many organic electronic devices, such as molecular switches, molecular shuttles, molecular tweezers, chemosensors, molecular wires, and molecular logic gates.[113–120]

In the family of exTTFs, tetrathiafulvalene vinylogues (TTFVs) have received considerable attention over the past decade. TTFVs are π-extended analogues of TTF with the vinyl groups located between the two dithiole rings of TTF. Like TTF, TTFVs are also excellent electron donors and can undergo reversible electron transfers under mild redox conditions.[126–130] Among the TTFVs, the class of aryl-substituted TTFVs show very interesting conformational switching properties together with a dramatic color change when undergoing oxidation or reduction. The structure of an aryl-substituted TTFV can be transformed from a pseudo *cis* (yellow color) to a complete *trans* conformation (green color) upon oxidation.

As shown in Scheme 1.25, in general, an aryl-substituted TTFV can be prepared from the dimerization of a corresponding dithiafulvene (DTF) precursor, which is readily accessible through olefination between an aldehyde precursor and a thione precursor. The aldehyde precursor determines the skeleton of the resulting TTFV molecule. The synthesis of some TTFVs may be hampered by their poor solubility.

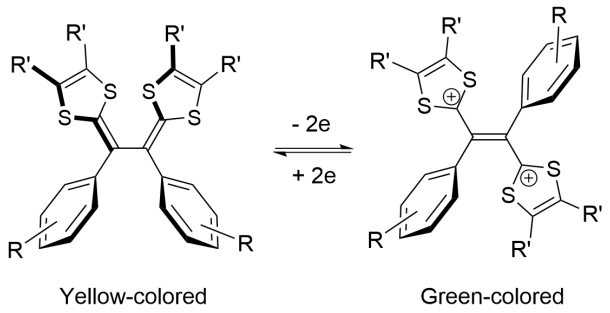

Scheme 1.24: Reversible electron transfers of ary-substituted TTFVs and associated color changes.

One way to circumvent this problem is to incorporate long alkyl chains into the dithiole groups.[131,132]

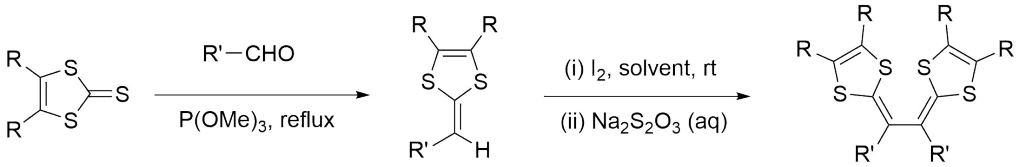

Scheme 1.25: A general synthetic route for TTFVs.

The preparation method for thione precursors was first developed by Hoyer's group in 1979.[133] As shown in Scheme 1.26, CS_2 **128** and sodium metal were mixed in DMF, and the reaction was heated at reflux for a few hours depending on the scale of the reaction. The mixture was then cooled down to room temperature, and the excess sodium was carefully quenched by adding MeOH at 0 °C. The resulting dithiolate intermediate was stabilized by complexation with Zn(II) ion. The zinc complex **129** was later reacted with an electrophile to generate the thione product **130**, while the substituents attached to the dithiole ring in the product could be readily modified by the electrophile chosen for the reaction.

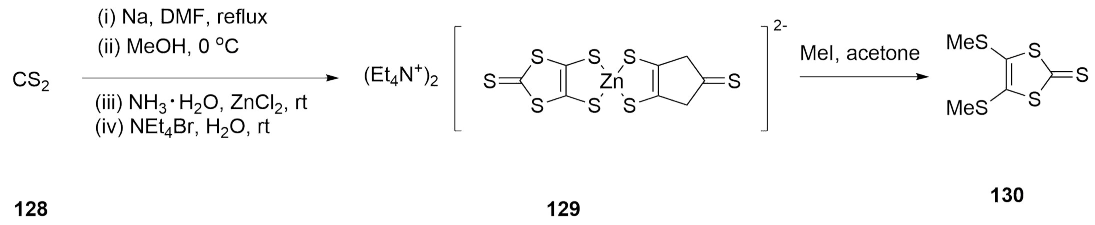

Scheme 1.26: An example of synthesis of thione precursor.

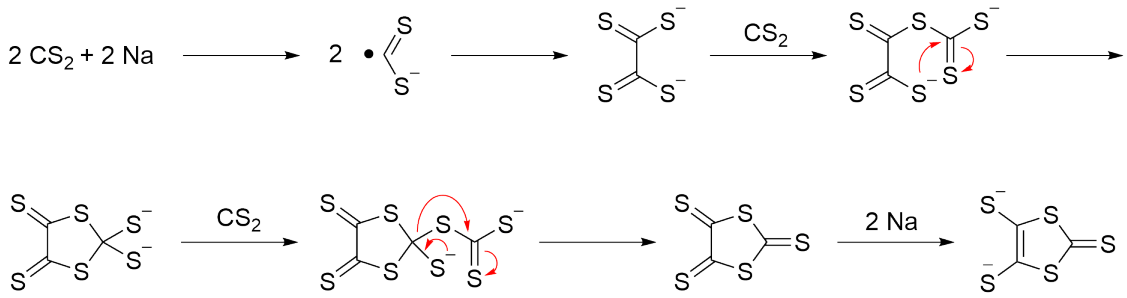

Scheme 1.27: Mechanism of the formation of the dithiolate compound.

The detailed mechanism for the formation of the dithiolate intermediate is outlined in Scheme 1.27. The reduction of CS_2 by sodium leads to the formation of a radical species that quickly dimerizes. The dimer intermediate continues to react with another two moles of CS_2 to produce the dithiolate compound after a rearrangement process. The five-membered ring dithiolate anion is formed after an elimination step. The anion can coordinate with Zn(II) to yield a stable complex as a red-colored solid.

The mechanism of the DTF oxidative dimerization reaction begins with a single-electron transfer from DTF to the oxidant, forming the corresponding DTF radical cation. The DTF radical cation will then undergo a quick dimerization to form a new carbon-carbon bond. The TTFV compound can be achieved after deprotonation and reductive workup as shown in Scheme 1.28

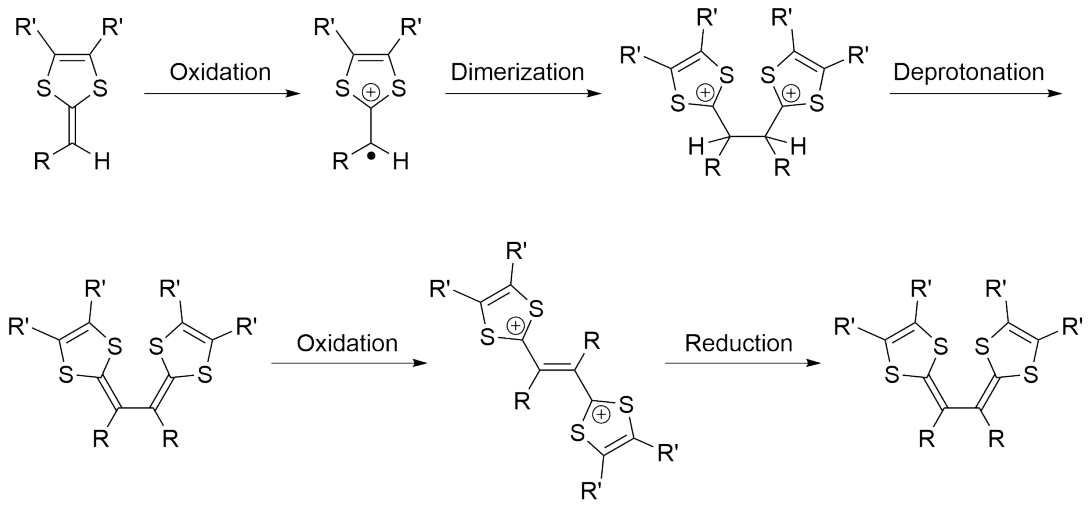

Scheme 1.28: Mechanism of the DTF oxidative dimerization reaction.

1.4 Motivations of This Thesis Work

Graphene is a very popular carbon material for preparing solar cells, light-emitting diodes (LEDs), touch panels, and smart windows and phones, due to its unique electronic properties. While large graphenes always suffer from preparation and solubility issues, small-size graphenes (nanographene) can be a better choice. Recently, tetraarylanthraquinodimethanes (Ar4-AQs) were used as the precursors for preparation of disc-like PAHs or nanographenes. The most common method for synthesizing disc-like PAHs is the Scholl reaction. However, the Scholl reaction requires harsh conditions and suffers from poor yields due to side reactions. In this thesis work, photocyclization was utilized in the attempted synthesis of tetrabenzocoronene (TBC) and related structures. The mechanism of this type of reaction was also studied in Chapter 2.

In our previous study, we generated a butterfly-shaped DHA-tetraaldehyde **98** with four formyl groups functionalzed at its end positions.[134,135] It can also be

potentially used in preparing covalent organic frameworks (COFs), a very promising porous material. In contrast to the commonly used planar organic building blocks for COFs, the non-planar shape of compound **98** presents a challenge as well as some opportunities to construct new kinds of polymeric frameworks. In Chapter 3, we report a new class of cross-linked polymer networks which was prepared from compound **98** and *p*-phenylenediamine though Schiff base condensation.

DTFs can be readily converted into TTFVs through a straightforward oxidative dimerization reaction.[128,136–143] However, in the study by Yunfei Wang, a former member of the Zhao group, an unexpected reaction outcome was observed. When a bis(DTF)-endcapped diphenylbutadiyne **117** was subjected to oxidative treatment with iodine.[144], the oxidation of **117** ended up with the formation of compound **118** as the major product. In Chapter 4, a series of experiments was designed and conducted, while computational density functional theory (DFT) calculations were also performed to investigate the detailed reaction mechanisms of this type of intramolecular alkyne-dithiolium cycloaddition reactions.

Chapter 2

Photocyclodehydrogenation of Tetraarylanthraquinodimethanes

2.1 Introduction

Tetraarylanthraquinodimethanes (Ar_4-AQs) are a class of highly π-conjugated organic materials with interesting structural, electronic, and electrochemical redox properties.[134,145,146] Synthetically, Ar_4-AQs can serve as the precursors for the preparation of highly π-delocalized PAHs through intramolecular cyclization approaches. For example, tetraphenylanthraquinodimethane (Ph_4-AQ) can undergo a four-fold cyclodehydrogenation to yield tetrabenzocoronene (TBC), which features a coronene central segment (see Figure 2.1). In recent years, TBC-based conjugated systems have captured considerable research interest owing to their applications as novel organic semiconductors. This chapter describes a systematic study of Ar_4-AQs in terms of synthesis, structural properties, and photocyclization reactivity.[41,147]

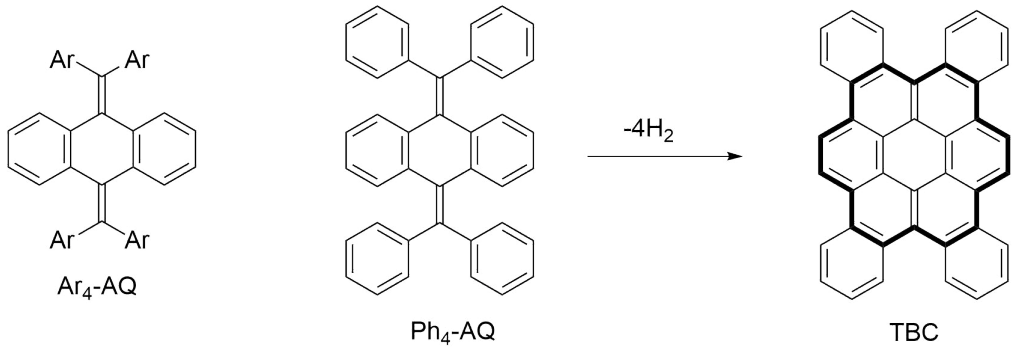

Figure 2.1: General structure of Ar_4-AQs and the formation of TBC from Ph_4-AQ through a four-fold cyclodehydrogenation process.

As introduced in Chapter 1, one of the popular methodologies for synthesizing TBC derivatives is the Scholl reaction.[1,4–8,26,27] However, the harsh conditions required by the Scholl reaction, such as high temperature and the presence of strong oxidants and Lewis acids, impose a barrier to its wide application in preparing various PAH derivatives. For example, the Scholl reaction may produce complex products which are difficult to purify, or ends up with poor yields due to significant side reactions such as oxidation and polymerization. In the literature, the Scholl reaction has only been successfully used in the synthesis of TBC derivatives carrying non-oxidizable functional groups (e.g., alkyl and halo groups). The synthesis of substituted TBCs with oxidizable groups (e.g., hydroxy, aldehyde, and amino) is thus very challenging.[148,149]

In addition to the Scholl reaction, photocyclization has been utilized in the synthesis of TBC related structures.[31–33] One popular photocyclization method is the so-called Mallory reaction, the mechanism of which involves a two steps–photochemically induced pericyclic reaction and oxidative dehydrogenation (e.g., using iodine as oxidant). Typical Mallory reactions suffer from a number of

drawbacks, including low yield, poor controllability, and multiple side products. Improvement on the Mallory reaction can be made by applying the called Katz's conditions or Katz's modification, in which propylene oxide (PPO) is added to quench the hydrogen iodide formed in the reaction, which tends to react with the carbon-carbon double bounds in the starting material.[42,45]

In contrast to the Scholl reaction, the Mallory reaction does not need very harsh conditions (e.g., heat, strong Lewis acids, and/or strong oxidants). In the literature, Ar_4-AQs derivatives have been reported to undergo cyclodehydrogenation reactions under the Katz's conditions.[42,45] However, most of these cases ended up with partially cyclized products. In these cases, the photocyclization yielded a mixture of multiple products which were not separated or specifically characterized. Instead, the mixture of products was immediately subjected to another step of cyclization under the Scholl conditions to yield fully cyclized products.[1,31–33] Indeed, the Mallory-Scholl reaction sequence has been so far a favored synthetic route for the preparation of TBC-based PAHs using corresponding Ar_4-AQs derivatives as starting materials.

Despite the fact that many Ar_4-AQs photocyclization reactions have been already explored and reported in the literature, the scope and mechanism of these types of reactions are still not well understood. To address these issues, studies on the photocyclodehydrogenation of Ar_4-AQs derivatives were conducted and detailed results are reported in this chapter.

2.2 Results and Discussion

2.2.1 Synthesis of Ar_4-AQs via Suzuki Coupling Reactions

Suzuki coupling, Suzuki reaction, or Suzuki-Miyaura coupling is a powerful C–C bond forming method which couples organoborons and organic halides under Pd catalysis. Since the first report in 1979 by Akira Suzuki, this cross-coupling reaction has been widely used in the preparation of conjugated materials such as polyolefins, styrenes, and substituted biphenyls.[150] A variety of organoboron compounds can be used in the Suzuki-Miyaura coupling. Among them organic boronic acids are commonly used owing to their simple synthesis, high stability to water and air, and easy purification. As such, Suzuki coupling is largely unaffected by the presence of water and can tolerate a broad range of functional groups. Another advantage of Suzuki coupling reactions is that they can achieve good regio- and stereo-selectivity. The inorganic boron-containing by-products of Suzuki reactions can be dissolved in water and are generally non-toxic (environmentally friendly). Because of these, Suzuki coupling is useful both in laboratorial research and large-scale industrial synthesis.[151–155]

The commonly used experimental conditions for Suzuki coupling reactions are described as follows. First, reactants, Pd catalyst, and base are mixed in a solvent(s). The reaction is usually conducted at elevated temperature (e.g., refluxing) for a reasonable period of time. Depending on the reactivity, a Suzuki coupling reaction can be accomplished within a couple of hours to a few days. The reaction typically needs to be kept in an oxygen-free environment to achieve a good yield.

In the reaction mechanism, oxidative addition in which the Pd(0) species reacts with a halogenated aromatic hydrocarbon substrate to form a complex of Pd(II)

is considered to be a critical step. The classic catalyst used in the Suzuki reaction is $Pd(PPh_3)_4$, while other catalysts such as $PdCl_2$,[156], $PdCl_2$ (dppf)[157,158] $Pd(OAc)_2$,[159–161] $Pd(PPh_3)_2Cl_2$,[162] and $NiCl_2$(dppf)[163] have also been reported. In addition to high catalytic efficacy, the catalysts should allow easy post treatment and exhibit low air sensitivity. Some reactions also require the participation of other highly catalytically active ligands, which have the commonality of strong electronegativity and large steric hindrance. This is because ligands with stronger electronegativity can accelerate the oxidative addition step, while large steric hindrance is beneficial for the reductive elimination. The Suzuki coupling also needs a base to be present. The most commonly used bases are K_2CO_3, K_3PO_4, Na_2CO_3, CsF, and Cs_2CO_3. Weak bases such as $NaHCO_3$ are rarely used. However, the reaction can be relatively clean when a weak base is used. The general solvent system used for the Suzuki coupling is a mixture of an organic solvent with other polar solvents; for example, toluene mixed with EtOH and H_2O, or THF and H_2O, or CH_3CN and H_2O, or dioxane and H_2O.[150–163]

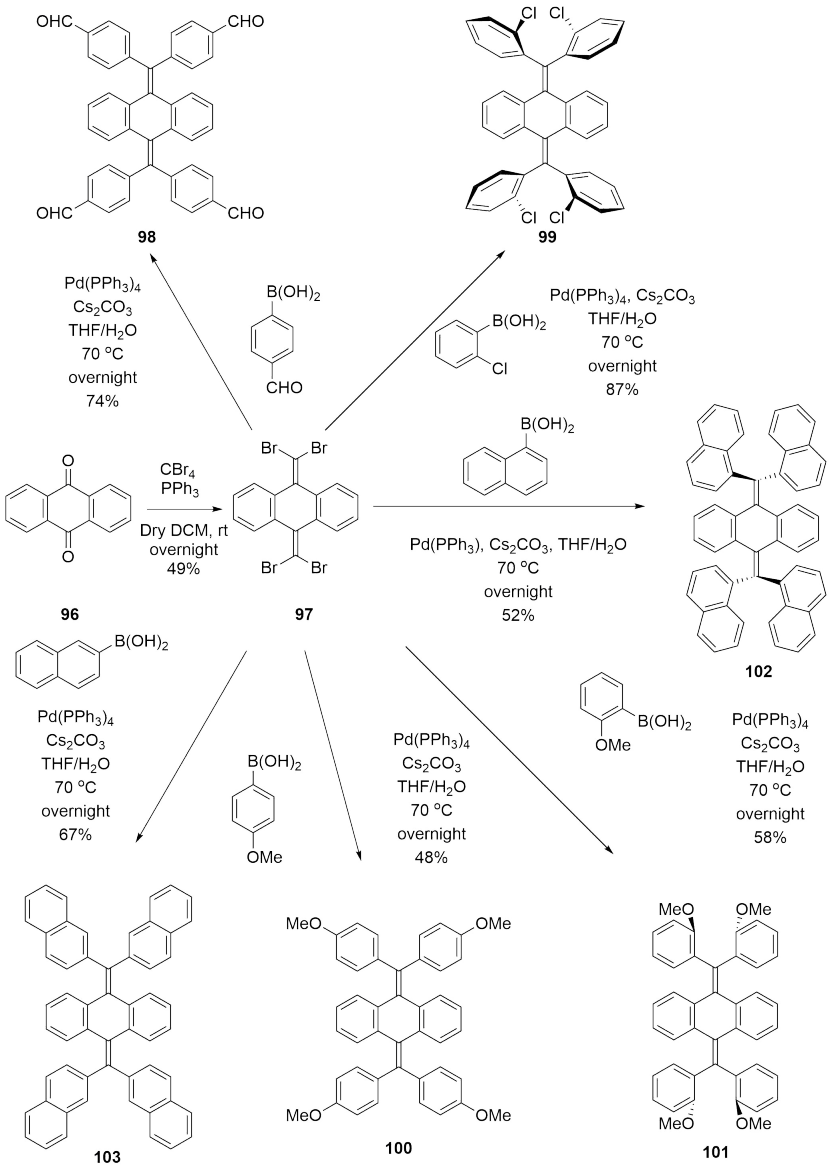

Scheme 2.1: Synthesis of Ar_4-AQs via Suzuki Coupling reactions.

Given the numerous advantages of the Suzuki-Miyamura coupling, this reaction was chosen as the synthetic method for the target Ar_4-AQs derivatives in this thesis work. Tetrabromo-AQ **97** was employed as a key starting material to undergo cross coupling with various aryl-boronic acids to generate Ar_4-AQs as shown in Scheme 2.1. Compound **97** was prepared from 9,10-anthraquinone through a dibromoolefination

reaction with CBr_4 and PPh_3. Compound **98** was obtained from compound **97** through Suzuki coupling reaction. Herein a mixture of THF and water was used as the solvent system. K_2CO_3 was first chosen as the base in the reaction, but the reaction efficient is low due to the low solubility of the base. Then Cs_2CO_3 was used to give a much better yield of 74%. The observation that Cs_2CO_3 worked as a better base than K_2CO_3 in this reaction can be attributed to the better solubility of Cs_2CO_3 in THF/water. Compound **98** was characterized by NMR, FTIR, MS analysis, as well as single crystal X-ray diffraction analysis (see Figure 2.2).

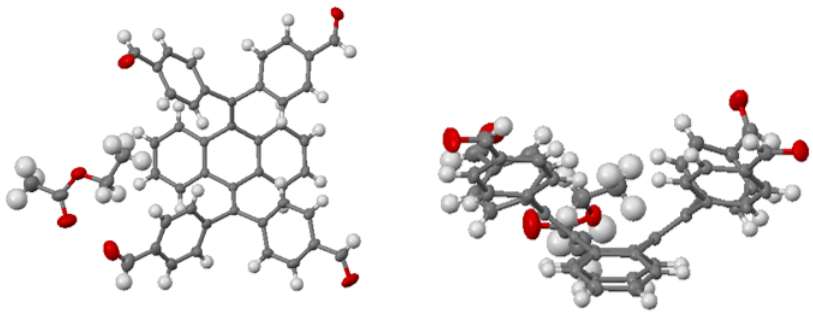

Figure 2.2: X-ray crystal structure of compound **98** (co-crystalized with ethyl acetate) viewed from different sides.

In a similar way, compounds **99**, **100**, **101**, **102** and **103** were prepared and purified by routine silica column chromatographic separation. Their molecular structures were characterized by routine spectroscopic analysis. Single crystals of **99** and **103** were successfully obtained and their detailed structures were elucidated by X-ray analysis. It is worth noting that compounds **102** and **103** were observed to be relatively stable in solution, but when their solutions were subjected to rotary evaporation, they quickly turned from colorless to red. TLC analysis indicated that

some reactions occurred during the fast solvent evaporation. Pure products could only be obtained by slow evaporation of the solvents at room temperature. In this way, pure products were formed at the bottom of the flask and then collected as needle-like white crystals.

2.2.2 Photocyclodehydrogenation of Ar_4-AQs Compound 98

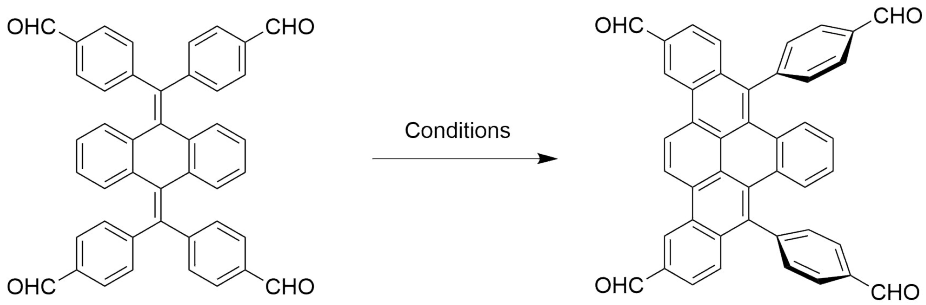

98 **104**

Scheme 2.2: Photocyclodehydrogenation of compound **98** under various reaction conditions.

During the fluorescence spectroscopic analysis of the sample solution of compound **98**, the solution was observed to become more emissive after the measurement. The results suggest that compound **98** is highly photoreactive, and very likely underwent a photocycylization reaction(s) when it was being irradiated. To unravel its photoreactivity, compound **98** was subjected to various photochemical conditions. Scheme 2.2 and Table 2.1 outline the different conditions and outcomes of photocyclodehydrogenation of compound **98**. First, the classic Mallory reaction conditions were applied. Compound **98** was dissolved in CH_2Cl_2 in a 25 mL round-bottom flask, and 4 equiv of I_2 was added as oxidant. A 100 W halogen lamp was

Entry	Reagent*	Solvent	Light Source	Time(d)	Yield(%)**
1	I_2	CH_2Cl_2	halogen lamp	0.5	trace
2	I_2, PPO	benzene	halogen lamp	0.5	37
3	air	CH_2Cl_2	302-312 nm	5	85
4	DDQ	benzene	302-312 nm	2	87
5	DDQ	toluene	302-312 nm	2	89
6	DDQ	chlorobenzene	302-312 nm	2	84
7	DDQ	CH_2Cl_2	302-312 nm	2	91

Table 2.1: Summary of reaction outcomes for the photocyclodehydrogenation of compound **98** under various conditions.*Amounts of reagents: I_2 (4 equiv); PPO (302 equiv); DDQ(5 equiv). ** Isolated yields.

used as the light source. Under these conditions, the photocyclodehydrogenation was sluggish. Only a trace amount of the cyclized product were detected by TLC analysis after 12 hours of reaction (see entry 1 of Table 2.1). The reaction was then improved by using the Katz-modified conditions,[42,45] where PPO was used to remove the unwanted HI byproduct. An increased yield of 37% was obtained after 12 hours of reaction (entry 2 of Table 2.1), but the reaction yield would not go higher when the reaction time was prolonged.

The relatively low yields could be due to several reasons. First, the 100 W halogen lamp seemed to be an ineffective light source to induce photo-excitation of compound **98**, considering the poor short-wavelength absorption of compound **98** in its UV-Vis absorption spectrum. Second, the glass wall of the round bottom flask could block

the UV light for photoreaction, since glass has a strong UV absorption in the spectral range of 200 nm to 400 nm, which overlaps with the main UV absorption bands of compound **98**. Thus the photocyclodehydrogenation reaction was undertaken in a quartz tube reactor, and a photochemical reaction chamber equipped with eight UV lamps (64 W in total) at the wavelength of 302 to 312 nm was used as the light source. In the experiments, compound **98** was dissolved in CH_2Cl_2 (10 mL) in a quartz tube capped with a rubber stopper, and the quartz tube was placed in the photochemical reaction chamber. The reaction was accomplished in 5 days as monitored by ^{1}H NMR and TLC analyses. Compound **104** was obtained as the major product in 85% yield after purification by column chromatography (entry 3 of Table 2.1).

With the use of a UV reactor and a quartz tube, the yield of photocyclization was increased significantly. However, the reaction rate was still very slow. The relatively slow reaction rate may be due to the lack of an effective oxidant in the reaction system to accelerate the dehydrogenation step. To increase the dehydrogenation rate, 5 equiv of DDQ was added to the reaction mixture, acting as the oxidant (entry 4 of Table 2.1). With DDQ, the reaction time was considerably shortened from 5 days to 2 days, and the yield was further improved to 91%. After the reaction, excess DDQ and byproducts could be easily removed by washing the organic layer with water. The resulting product had very good purity as evidenced by NMR analysis; therefore, further column chromatographic purification could be avoided, which presents a significant advantage for large-scale synthesis.

As shown in entries 4-7 of Table 2.1, four organic solvents were examined for the photocyclodehydrogenation. However, in contrast to CH_2Cl_2, the photocyclodehydrogenation in benzene, toluene, and chlorobenzene showed the

formation of side products according to TLC analysis. The isolated yields of the reaction in these three solvents were therefore slightly lower then in CH_2Cl_2 after column chromatographic purification.

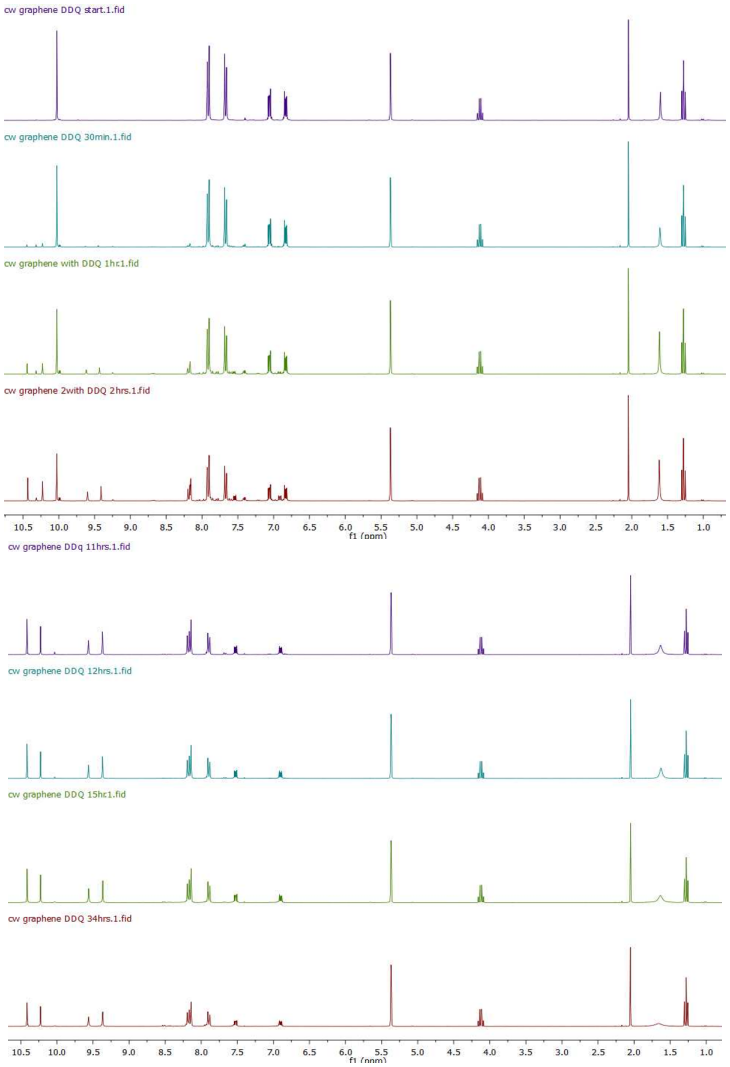

Figure 2.3: ^{1}H NMR (300 MHz, CD_2Cl_2) spectra monitoring the photocyclodehydrogenation of compound **98** in the presence of DDQ (5 equiv) at various reaction times.

To gain insight into the kinetic properties, the photocyclization of compound **98**

in CD_2Cl_2 under UV irradiation (302-312 nm) was monitored by ^1H NMR analysis versus time. In this experiment, compound **98** and 5 equiv of DDQ were dissolved in CD_2Cl_2 in an NMR tube. The NMR tube was put into the photochemical reaction chamber under UV irradiation. The recorded ^1H NMR spectra are shown in Figure 2.3.

The NMR monitoring data show complete conversion of **98** into the cyclized product **104** after 34 hours of UV irradiation. It is noteworthy that there are two new signals at 10.43 and 10.23 ppm growing as the reaction time increases. These two peaks come from the two sets of aldehyde protons of product **104**. In the meantime, a number of relatively weak signals can be observed; especially, the signals at 10.31, 10.00 and 9.98 ppm, which were only observed in the first few hours of the reaction. They can be reasonably assigned to three of the four different aldehyde protons of the monocyclized intermediate as shown in Figure 2.4 below, while the fourth aldehyde signal of this intermediate may coincidentally overlap with an NMR peak of either compound **98** or compound **104**. These three peaks become weaker and weaker as the reaction time increases, and hardly can be seen at the end of the reaction.

The distinctly separated aldehyde peaks in the ^1H NMR spectra allowed quantitative determination of the mole fractions of starting material, intermediate and the final product in the reaction mixture. Based on these peaks, kinetic profiles of the photocyclization reaction can be generated as shown in Figure 2.4.

In Figure 2.4, the black curve illustrates the variation of the starting material as a function of reaction time. The blue curve shows change of the final product and the red curve represents the intermediate. The mole fraction of the intermediate increases in the first hour and then declines as the reaction time extends. The

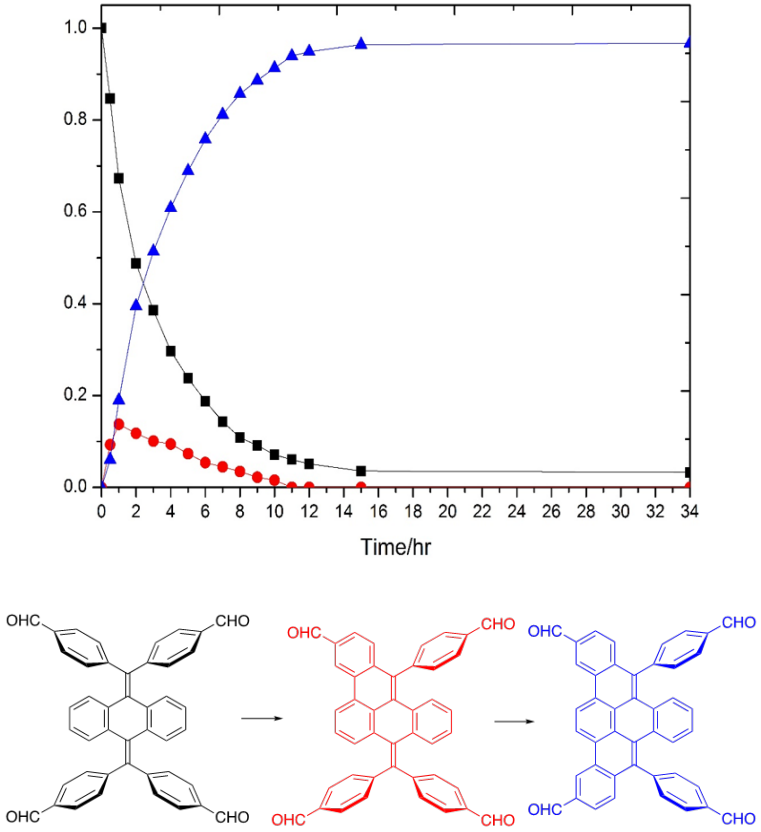

Figure 2.4: Kinetic profiles of the photocyclodehydrogenation of compound **98** as determined from NMR analysis.

kinetic plots match two possible reaction pathways. The first reaction pathway is a concerted double cyclization, and the second is a two-step cyclization mechanism with the second cyclization step being much faster than the first one.

To further evaluate the plausibility of the two mechanisms, density functional theory (DFT) calculations (B3LYP/6-31G(d) level) were performed. To reduce computational cost, unsubstituted 9,10-bis(diphenylmethylene)-9,10-dihydroanthracene (DHA) was used as the model compound in the computational study.

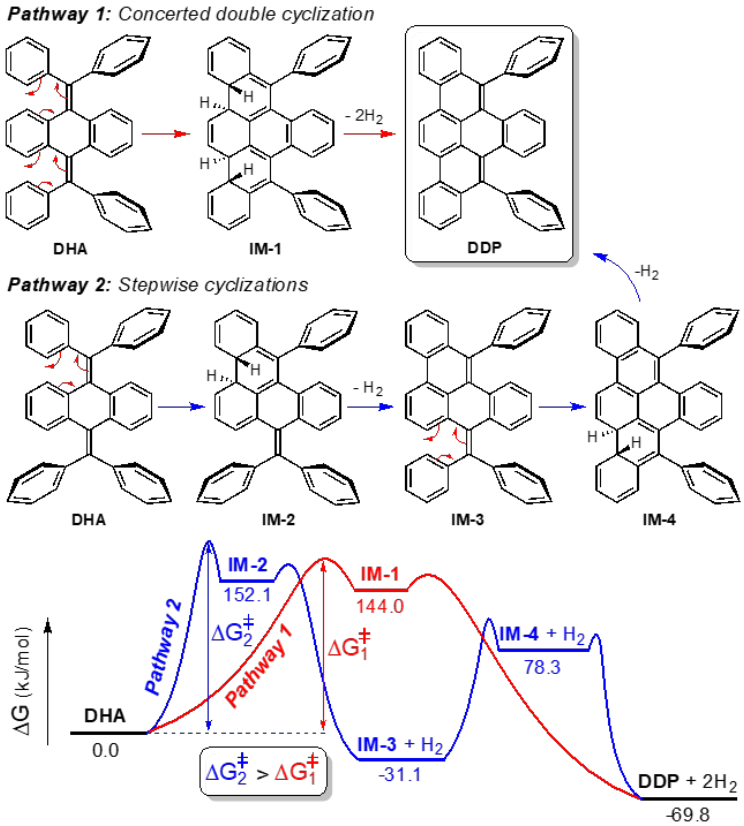

Figure 2.5: DFT calculated energetics for cyclodehydrogenation of compound **98**.

In theory, each stilbene segment in DHA should undergo a conrotatory ring closure under photochemical conditions. Figure 2.5 shows the detailed steps and intermediates involved in the two mechanistic pathways. The relative Gibbs free energies of starting material, intermediates, and the doubly cyclized product, diphenyldibenzopentaphene (DDP) were calculated to qualitatively assess the reactivities of the two reaction pathways based on the Bell-Evans-Polanyi principle.

As shown in Figure 2.5, the doubly cyclized intermediate **IM-1** of pathway 1 is about 8.1 kJ/mol lower in energy than the monocyclized **IM-2** in pathway 2, hence suggesting that the concerted double cyclization has a lower energy barrier to overcome than the stepwise approach. This offers a reasonable theoretical explanation

for the experimental outcomes, the photocyclodehydrogenation of compound **98** yielded the doubly cyclized product compound **104**, with little monocyclized intermediate formed at the intermediary stages. Moreover, the energy profiles for the cyclization of DDP into tetrabenzocoronene (TBC) were mapped out by DFT calculations as well. The results show that the cyclization pathway, either concerted or stepwise, would invariably encounter a much higher energy barrier than the cyclization of DHA. The substantially increased torsional energies in the cyclized intermediates between DDP and TBC could be the key reason for DDP not being able to further cyclize.

2.2.3 Photocyclodehydrochlorination of Compound 99

The synthesis of TBC molecules from Ar_4–AQs through photocyclodehydrogenation is difficult to achieve. The search for other photochemically-induced cyclization strategies was therefore carried out. Recently, photocyclodehydrochlorination (PCDHC) was utilized by the Morin group to prepare various large PAHs.[87] Compared with photocyclodehydrogenation, PCDHC is much more efficient, faster and regioselective. In view of these advantages, tetrachloro-substituted Ar_4–AQs **99** was synthesized and tested as a substrate for the PCDHC reaction with an aim of directly making TBC derivatives through photocyclization.

The first attempt of PCDHC reaction of compound **99** was conducted in CH_2Cl_2. In contrast to photocyclodehydrogenation, this reaction did not need an oxidant. Under UV irradiation, the PCDHC reaction was observed to be very slow. TLC analysis showed that there was no significant conversion of **99** into cyclized product(s)

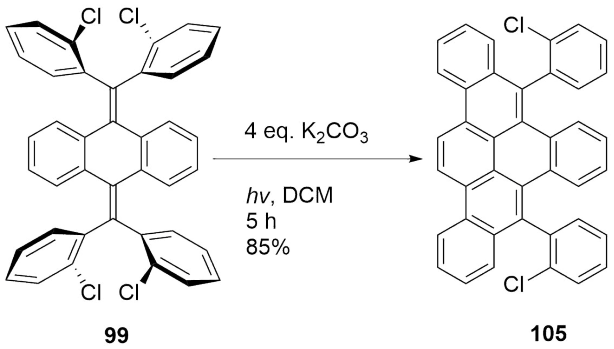

Scheme 2.3: PCDHC reaction of compound **99**.

in the first 2 hours of reaction. After 30 hours of UV irradiation (64 W, 302–312 nm), only a trace amount of product was observed by TLC analysis, while most of compound **99** remained unreacted.

Considering the side product of PCDHC reaction is HCl, the addition of base was expected to accelerate the reaction. To optimize the reaction conditions, 4 equiv of K_2CO_3 was added and the reaction mixture was then subjected to UV irradiation (Scheme 2.3). Under these conditions, the photocyclization became much faster. TLC analysis showed that the reaction started within 5 min and was complete in 5 hours. The reaction produced compound **105** as a yellow solution. The organic solution was washed with water to remove the excess amount of K_2CO_3 and then purified through silica column to **105** in a yield of 85%.

The reaction conditions were further modified by using acetone as the solvent. Again, the reaction was accomplished in 5 hours, affording the cyclized product **105** with an improved yield of 91%. Compared with the reaction in CH_2Cl_2, the reaction in acetone was much cleaner. TLC analysis showed there were no detectable side products formed when acetone was used as the solvent. One possible reason is that the quenching of HCl with K_2CO_3 occurs more efficiently in acetone. Additionally,

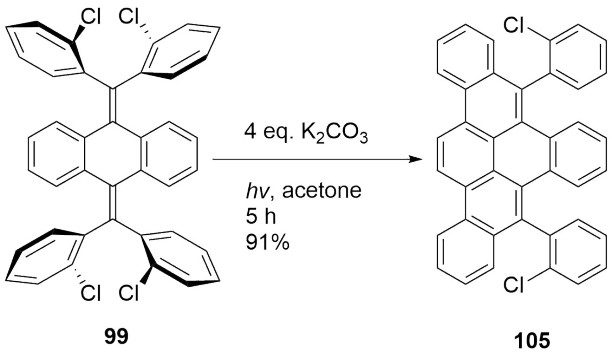

Scheme 2.4: PCDHC reaction of compound **99** in acetone.

acetone is known as a photosensitizer used in photochemical reactions. In this respect, acetone can facilitate the photoexcitation of **99** to improve the reaction efficiency.

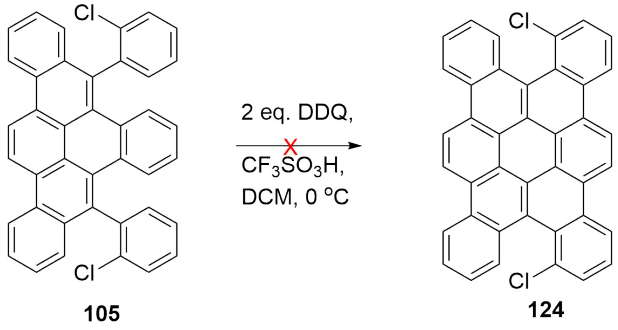

Scheme 2.5: Attempted synthesis of TBC from half-cyclized product via the Scholl reaction.

Similar to the photocyclodehydrogenation of compound **98**, PCDHC of **99** also gave the half cyclized product. Given that **105** is compatible with oxidative conditions, a classic Scholl reaction was then conducted in order to prepare the fully cyclized TBC product. As shown in Scheme 2.6, compound **105** and 2 equiv of DDQ were mixed in CH_2Cl_2 at 0 °C in an N_2 atmosphere. Then 1 equiv of CF_3SO_3H was slowly added. TLC analysis showed that the reaction started immediately after CF_3SO_3H was added. After 8 hours, TLC showed that most of compound **105** was

consumed, but no major product could be detected. Very likely, the Scholl reaction ended with the formation of decomposed products rather than the expected TBC. The reaction was then conducted at -20 °C but still gave the same results. Moreover, $FeCl_3$ was used in the Scholl reaction, acting as Lewis acid and oxidant. As shown in Scheme 2.6, the attempt of an $FeCl_3$ promoted Scholl reaction did not yield the desired product either.

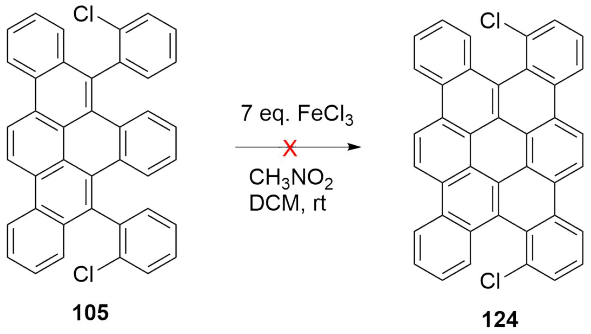

Scheme 2.6: Attempted synthesis of TBC from **105** via $FeCl_3$ promoted Scholl reaction.

The PCDHC reaction of **99** was also monitored by ^{1}H NMR analysis with time. As shown in Figure 2.6, the two weak signals at 8.43 and 8.45 ppm are due to the protons of compound **99**, while the signals at 9.40, 9.42, 9.22 and 9.25 ppm are from the protons of compound **105**. The signals of the possible intermediates are rather weak, so that the integration of these signals is not very accurate. Nevertheless, meaningful kinetic profiles could still be obtained based on the NMR data.

Figure 2.7 shows the detailed kinetic profiles, where the green curve is the relative mole ratio of compound **99** as a function of reaction time, the black curve is the relative mole ratio of compound **105**, and the red curve is the relative mole ratio of

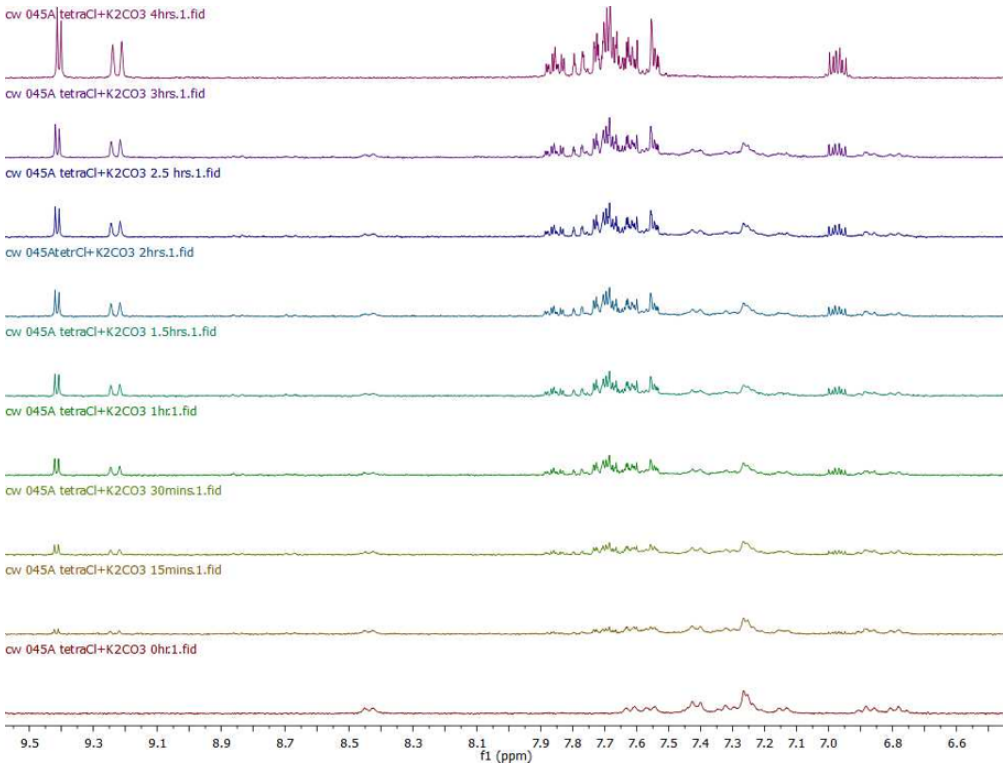

Figure 2.6: ^{1}H NMR spectra monitoring the PCDHC reaction of compound **99**.

possible intermediates. The irregular behavior of the red curve is possibly due to the weak signal intensity. The kinetic plots of the PCDHC reaction of compound **99** show similar patterns to those of the previous photocyclodehydrogenation reaction. The results indicate that the PCDHC reaction can only accomplish half cyclization. More likely the double ring closure process goes through a concerted mechanism rather than a stepwise mechanism.

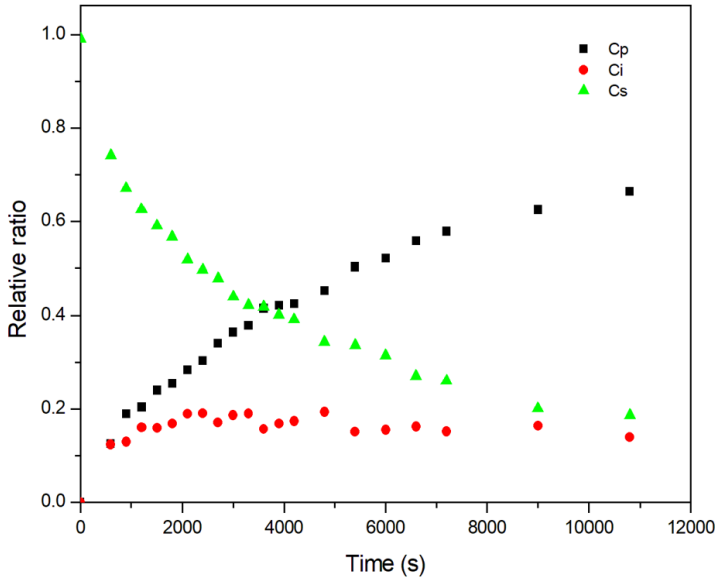

Figure 2.7: Kinetic profiles of PCDHC of compound **99** based on NMR analysis.

2.2.4 Photocyclodehydrogenation of Compounds 100 and 101

Compared with photocyclodehydrogenation, the PCDHC reaction of Ar_4–AQs **99** is indeed much faster. However, the reaction only led to double ring closure, whereas direct formation of TBC via photocyclization is still impossible. To address this issue, another strategy was attempted, in which electron-donating groups (OMe) were attached to Ar_4–AQs in order to activate the system to be more reactive toward photocyclization.

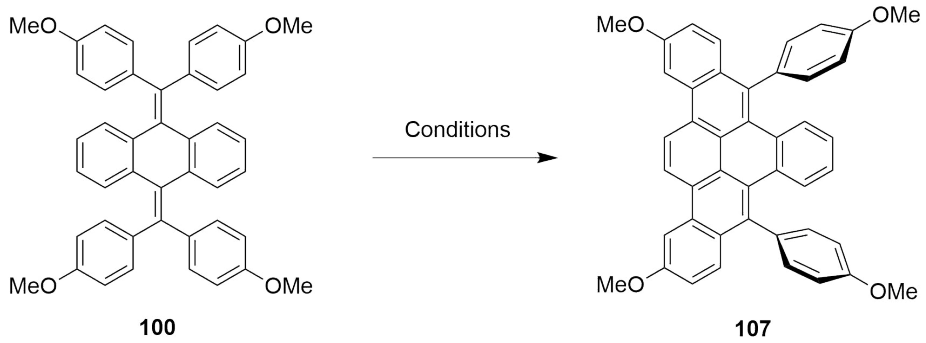

100 **107**

Scheme 2.7: Photocyclodehydrogenation of OMe-substituted Ar_4–AQs **100**.

The first attempted substrate was compound **100** (Scheme 2.7), in which OMe groups are substituted at the *para*-positions of the phenyl rings. Compound **100** in CH_2Cl_2 was subjected to UV irradiation in the presence of DDQ as the oxidant. Unfortunately, as soon as DDQ was added, the color of the reaction solution immediately turned from colorless to purple. UV-Vis analysis showed that there was a new charge-transfer band formed when **100** and DDQ were mixed, indicating the occurrence of a rapid electron transfer reaction **100** (donor) to DDQ (acceptor). The formation of such a charge-transfer complex prevented the

photocyclodehydrogenation from happening and resulted in slow decomposition of compound **100**, possibly oxidation of **100** to form other unwanted products. Lowering the reaction temperature to -20 °C did not cause any changes in the reaction outcomes. It was clear that addition of an oxidant such as DDQ proved to be harmful to the photocyclization of OMe-activated systems.

The second attempt to photocyclize compound **100** was made by using mixed solvents, CH_2Cl_2/acetone, without any oxidant. Under these conditions, the photocyclodehydrogenation reaction was observed to occur smoothly. Traced by NMR analysis, the reaction was done after 38 hours of UV irradiation, giving product **107** with a 38% yield after column chromatographic purification. Again, the photocyclization only afforded the half-cyclized product, while the formation of TBC remained unattainable.

Another OMe-substituted Ar_4–AQs **101** was also prepared and tested (Scheme 2.8). Compound **101** is a regioisomer of **100**, in which the OMe groups are attached to the *ortho*-positions of the phenyl groups. The molecular structural design here was aimed at inducing an efficient photocyclodemethoxylation reaction, considering that OMe itself is a reasonable leaving group in addition to being an activating group. Preliminary results showed that the photocyclodemethoxylation of **101** was kind of slow and required a long reaction time to accomplish. NMR analysis showed that the photocyclization in the NMR tube took almost a week to finish (see Figure 2.8, data acquired by another group member, Maryam Abdollahi). Addition of DDQ only resulted in decomposition of the starting material.

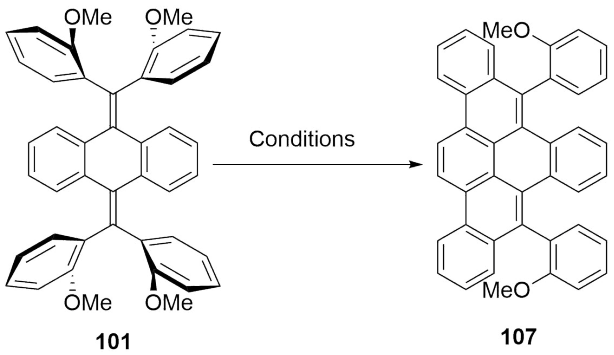

Scheme 2.8: Photocyclodemethoxylation of compound **101**.

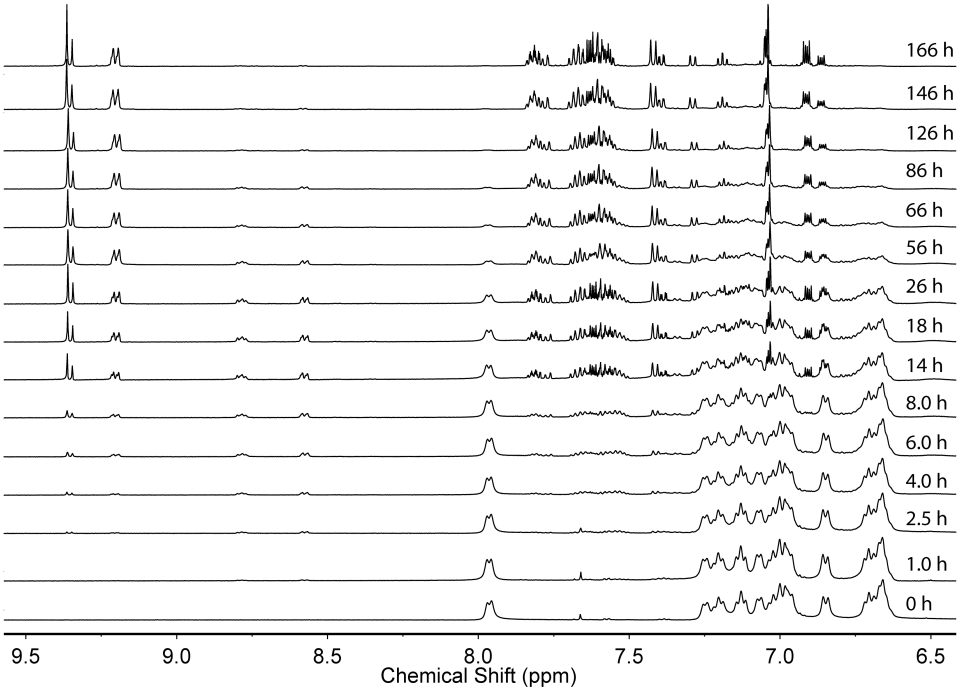

Figure 2.8: ^{1}H NMR (300 MHz, CD_2Cl_2) spectra monitoring the photocyclization of compound **101**.

2.2.5 Photocyclodehydrogenation of Compounds 102 and 103

In addition to the tetraphenyl-AQ systems investigated above, two tetranaphthyl-substituted AQs, **102** and **103**, were prepared and examined.

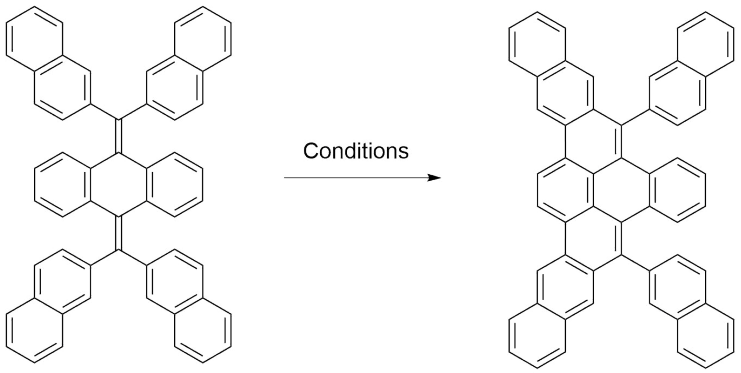

Scheme 2.9: Photocyclodehydrogenation of compound **103**.

As shown in Scheme 2.9, the structure of **103** contains four 2-naphthyl groups connected to an AQ core. Ideally, full cyclization of **103** should furnish a tetranaphthocoronene (TNC). In the experiment, **103** was dissolved in CH_2Cl_2 in an NMR tube and DDQ was added as the oxidant. After 1 hour of exposure to UV irradiation, the color of the reaction mixture changed from pale orange to pale yellow. The reaction was monitored by TLC analysis to show that the reaction completed after 5 hours. A dark red crude product was obtained with a yield of 39% after workup and silica column separation. Extending the reaction time led to the formation of more byproducts and the decomposition of the desired product. However, the product was characterized as the half-cyclized structure **109**, based on NMR, MS, and UV-

Vis data. Thorough purification of the product by column chromatography, however, turned out to be extremely difficult, due to the presence of some byproducts with very similar elution behavior.

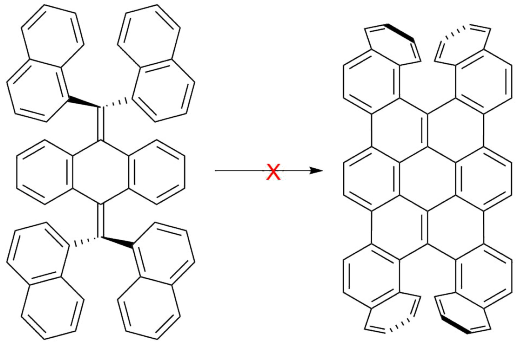

Scheme 2.10: Attempted PCDH reaction of compound **102**.

Compound **102**, in which 1-naphthyl groups are attached to the central AQ group, was then investigated. This compound did not show any photocyclization reactivity after more than 7 days of UV irradiation. Unlike compound **103**, this compound exhibits a considerable degree of steric hindrance due to the orientation of the 1-naphthyl groups. Single crystal X-ray analysis indicated that the molecular structure of **102** is highly twisted (see the following section). For this reason, PCDH reaction of **102** would need to overcome a very high energy barrier, which essentially makes it unreactive toward photocyclization.

2.3 Electronic and Structural Properties of Ar_4-AQs and Related Cyclized Products

2.3.1 UV-Vis Spectroscopic Properties

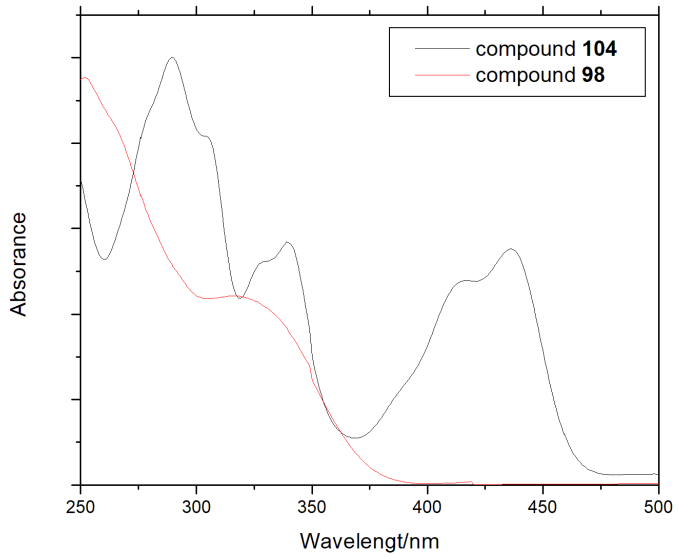

Figure 2.9: UV-Vis absorption spectra of compounds **98** and **104** measured in CH_2Cl_2.

The electronic absorption properties of compounds **98** and its photocyclized product **104** were investigated by UV-Vis analysis. As shown in Figure 2.9, the spectrum of compound **98** shows a broad maximum absorption peak around 300 to 325 nm, which is due to the $\pi \rightarrow \pi^*$ electronic transition. After photocyclization, the increased π-conjugation in **104** makes the absorption band substantially redshifted. As can be seen from the spectrum, the maximum absorb peak for compound **104**

moves to 440 nm.

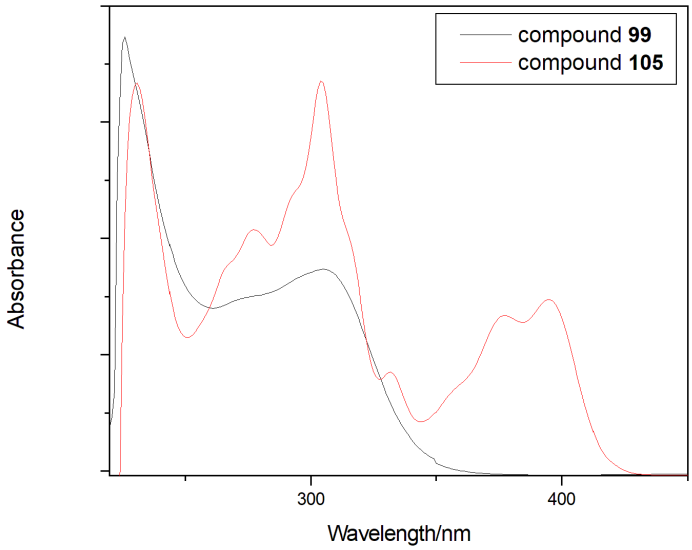

Figure 2.10: UV-Vis absorption spetra of compound **99** and its photocyclized product **105**.

In a similar way, the UV-Vis absorption band of compound **99** also shows a great redshift of $\pi \rightarrow \pi^*$ after PCDHC reaction. As shown in Figure 2.10, the maximum absorb peak for compound **99** is around 310 nm, and the maximum absorb peak for compound **109** moves to around 400 nm. Similar spectral patterns were observed in the UV-Vis analysis of compounds **100** and **102** as well.

The UV-vis spectra of MeO-substituted Ar_4-AQs **100** and **101** are shown in Figure 2.11. As can be seen, the UV-Vis trace for the mixture of **100** and DDQ shows a new low-energy peak around 540 nm, which is characteristic of the charge-transfer (C-T) absorption band. However, the C-T band was not observed when DDQ was added to a solution of compound **101**. The different spectroscopic behavior

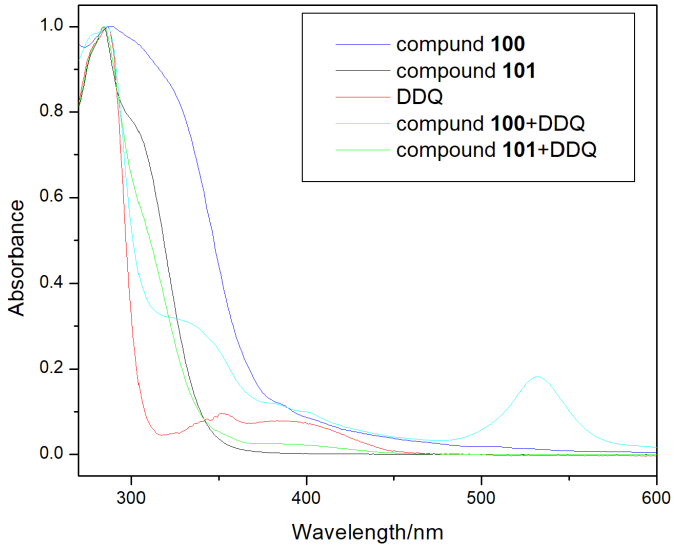

Figure 2.11: UV-Vis absorption spectra comparing compounds **100**, **101**, and their mixtures with DDQ.

can be explained because compound **100** is a much better π-electron donor than its regioisomer **101**. In the structure of **100**, OMe groups are attached to the *para* positions of the phenyl rings, allowing the molecule to adopt a more flexible and planar conformation than that of its isomer **101**. This effect enables compound **100** to more readily release electron(s) to its counterpart electron acceptor, DDQ.

2.3.2 X-Ray Structural Analysis

Single crystals of some Ar_4-AQs and related photocyclized products were successfully grown and their molecular structures were elucidated by X-ray single crystallographic analysis.

Figure 2.12 illustrates the X-ray structure of **99**, which shows a highly twisted

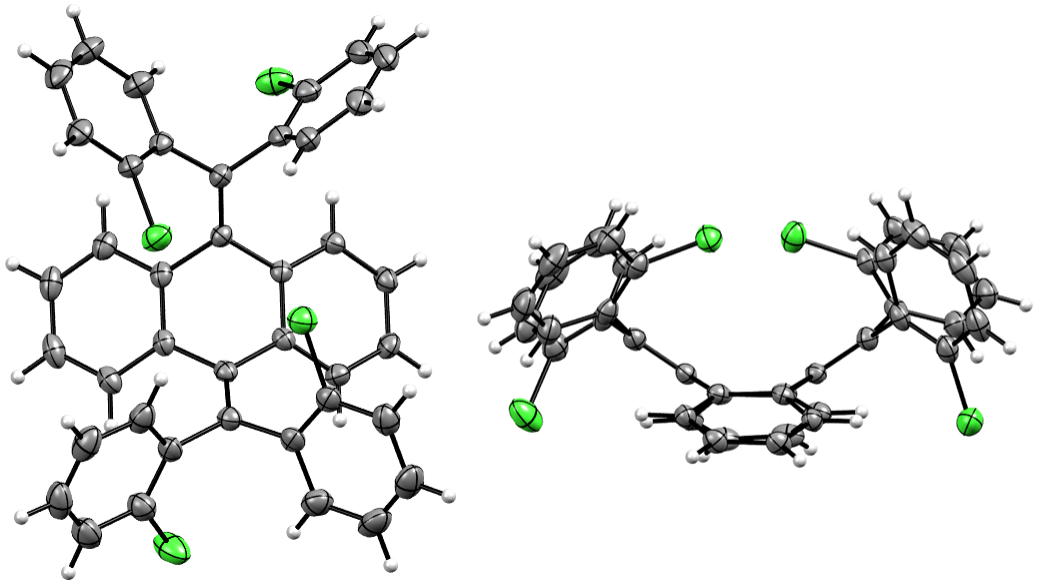

Figure 2.12: ORTEP drawing of compound **99** at 50% probability viewed from different perspectives.

conformation due to the steric crowding imposed by the *ortho*-chlorophenyl groups. It is worth noting that the chloro groups are arranged in the opposite directions on each side of the molecule to avoid steric interactions as well as to minimize the dipole moment. The X-ray structure of **99** also suggests that the molecule needs to undergo a certain degree of conformational change (e.g., rotation of one of the *ortho*-chlorophenyl rings) to achieve the PCDHC reaction.

Figure 2.13 shows the X-ray structure of PCDHC product **105**. As can be seen, the π-conjugated framework of this molecule becomes significantly more planar compared with its precursor **99**. The extended π-delocalization thus lowers the HOMO–LUMO gap of the compound and causes a substantial degree of redshift in the low-energy $\pi \rightarrow \pi^*$ transition band.

Figures 2.14 and 2.15 show the X-ray structures of OMe-substituted Ar_4–AQs

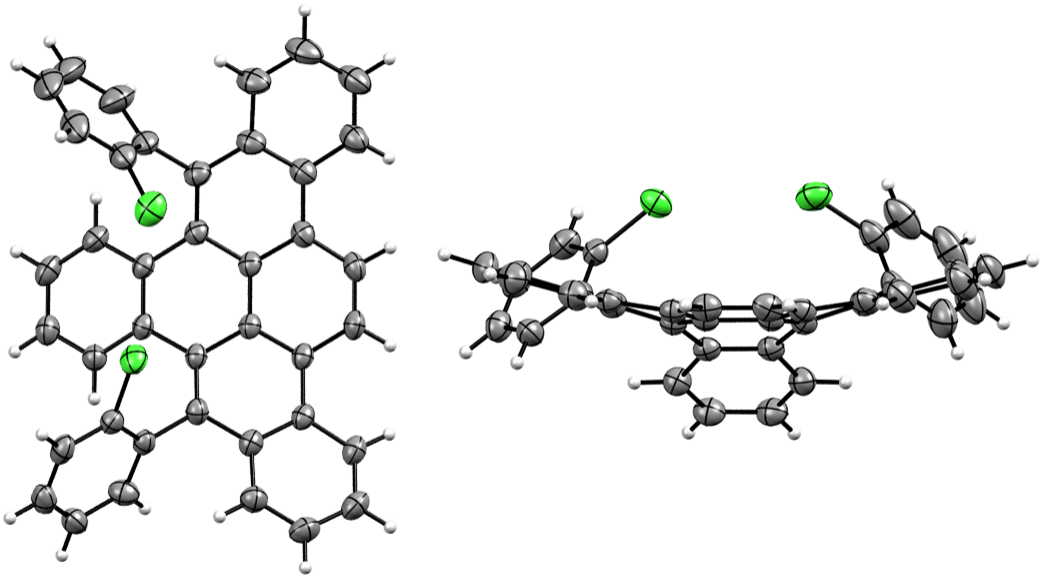

Figure 2.13: ORTEP drawing of compound **105** at 50% probability viewed from different perspectives.

100 and 2-napthyl-substituted **102**. Like the other Ar_4-AQs, the conformations of these two compounds are also highly twisted with the central AQ unit taking a saddle-like shape. The relatively large size of the 2-naphthyl groups in **102** make the four naphthyl groups adopt a *trans* like orientation on each side of the molecule. As such, steric crowding around the AQ center can be mitigated. This conformation also suggests that cyclization of **102** would encounter more significant steric hindrance and hence would be more difficult than for tetraphenyl-substituted AQs.

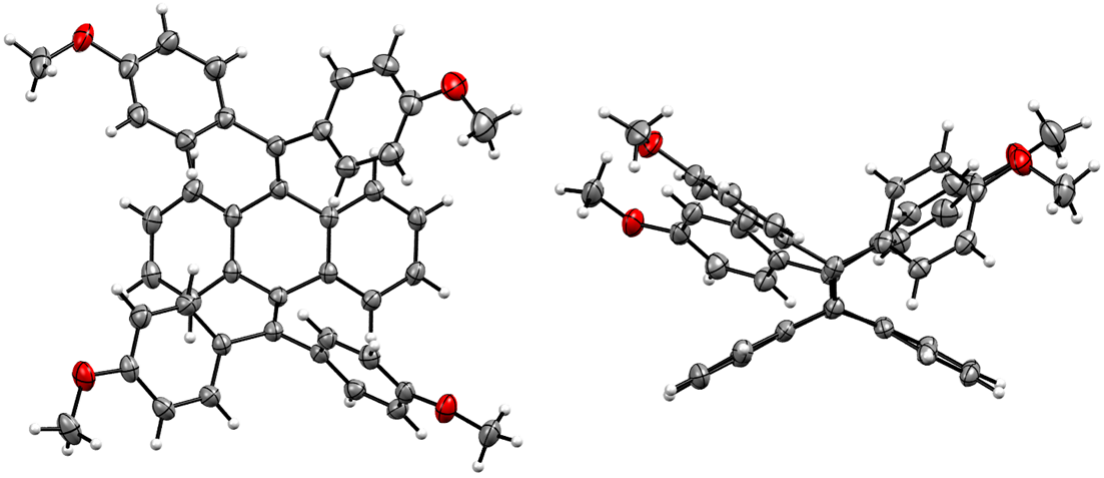

Figure 2.14: ORTEP drawing of compound **100** at 50% probability viewed from different perspectives.

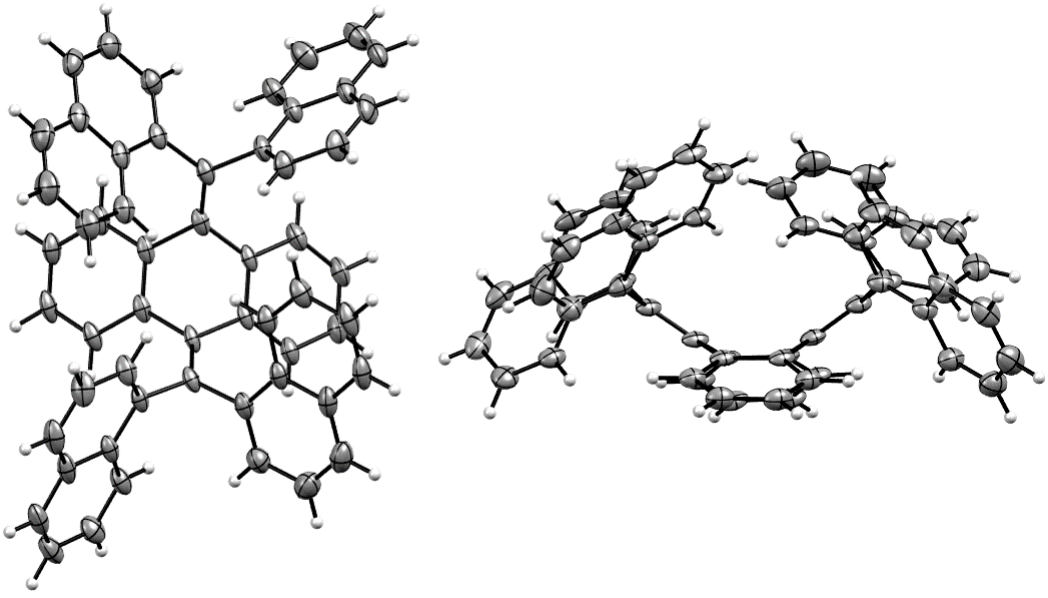

Figure 2.15: ORTEP drawing of compound **102** at 50% probability viewed from different perspectives.

2.4 Photocyclization of Ar_4-AQs in the Solid State

So far, the photocyclization reactivity of various Ar_4-AQs has been demonstrated only in the solution phase. The photochemical reactivity of Ar_4-AQs in the solid state has not been clearly demonstrated in the literature. To address this issue, a cross-linked polymer network **P1** was prepared through the Schiff base condensation reaction of **98** and *p*-phenylenediamine in the presence of acetic acid. As shown in Scheme 2.11, the condensation reaction was done in 1,4-dioxane with heating, resulting in cross-linked polymer **P1** as an insoluble solid.

Polymer **P1** was then subjected to UV irradiation (302–312 nm) at room temperature for 7 days. Presumably, the Ph_4-AQ units in the structure of **P1** would undergo photocyclodehydrogenation reaction under these conditions. For comparison purposes, another cross-linked polymer **P2** was prepared through the Schiff base condensation of compound **104** and *p*-phenylenediamine under the same conditions as the synthesis of **P1** (see Scheme 2.11). In the structure of **P2**, the Ph_4-AQ unit is half-cyclized prior to polymerization. Comparison of the structures of UV-irradiated **P1** and **P2** was then carried out by IR analysis.

As shown in Figure 2.16, the IR spectrum of precursor **98** (Figure 2.16A) shows characteristic vibrational peaks at 1732 cm^{-1} (C=O stretching), 1690 cm^{-1} (C=C stretching), and 1596 cm^{-1} (aromatic C=C). After condensation with *p*-phenylenediamine, the C=O peak disappears in the spectrum of **P1** indicating the consumption of the C=O group. In the meantime, a new peak at 1619 cm^{-1} shows up, indicating the formation of C=N groups (Figure 2.16B). Upon UV irradiation,

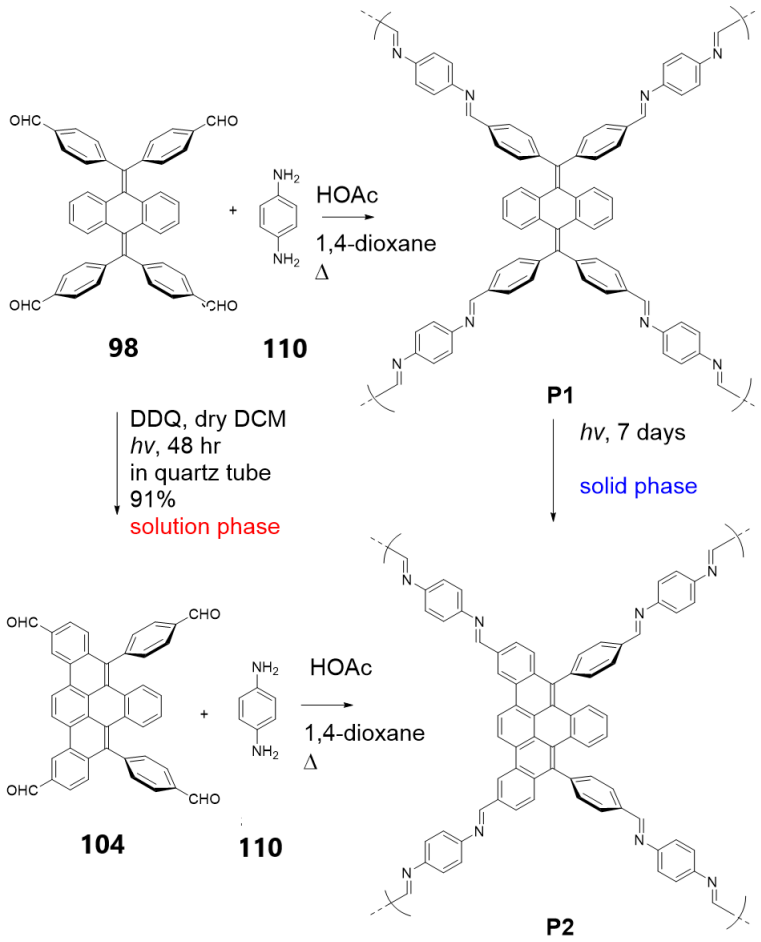

Scheme 2.11: Photoreactivity of Ph_4–AQ units embedded in the framework of a cross-linked polymer **P1** in the solid state.

the IR spectrum shows a dramatic change in the C=C stretching region. As can be seen in Figure 2.16C, the 1690 cm^{-1} peak (C=C stretching) is substantially weakened, while a new peak at 1672 cm^{-1} emerges. This vibrational peak resembles that in the IR spectrum of **P2** (Figure 2.16D), suggesting that the structures of **P1** after UV irradiation and **P2** are similar. The IR data offer evidence for the occurrence of photocyclodehydrogenation of Ph_4–AQ in polymer **P1**. It seems that the photocyclization reactivity in the solid state is the same as that in the solution

phase; that is, only the half-cyclized structure can be formed under UV irradiation.

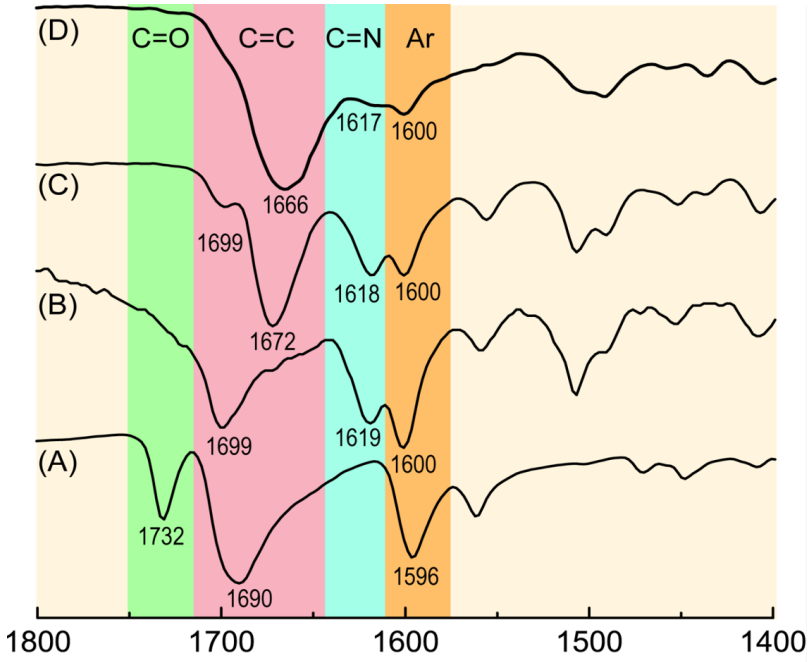

Figure 2.16: IR spectra of (A) compound **98**, (B) cross-linked polymer **P1** before UV irradiation, (C) cross-linked polymer **P1** after UV irradiation, and (D) cross-linked polymer **P2**.

2.5 Conclusions

In summary, a series of Ar_4-AQs has been synthesized and characterized. Their photocyclization reactivity was investigated by NMR analysis. It was found that photocyclodehydrogenation can be accelerated significantly by oxidants such as DDQ. However, for electron-donor substituted Ar_4-AQs, they may undergo intramolecular charge transfer reactions with DDQ, which hinder the photocyclization pathway. PCDHC was observed to be much faster than photocyclodehydrogenation,

particularly in the presence of base. So far, all the Ar_4-AQs investigated in this work ended up with half-cyclized products under photochemical conditions. The goal of forming TBCs directly from Ar_4-AQ precursors via photocyclization still remains a challenge and awaits further exploration. Finally, this work for the first time demonstrates that photocyclodehydrogenation of Ar_4-AQs units embedded in solid-state polymer networks is possible. This finding offers opportunities for the design and development of photo-responsive solid materials in our future work.

2.6 Experimental Section

Chemicals were purchased from commercial suppliers and used directly without purification. Photocyclization reactions were performed in a quartz NMR tube or custom-made a quartz glass tube according to the scale of reaction. The reactions were conducted under the irradiation of a halogen lamp (100 W) or in a Rayonet photochemical reactor equipped with eight UV lamps (64 W in total). Evaporation and concentration were carried out with a water-aspirator. Flash column chromatography was performed with silica gel 60 (240-400 mesh). Thin-layer chromatography (TLC) was done with silica gel F254 coated on plastic sheets and visualized by UV light. Melting points were measured on an MPA100 melting point apparatus (Stanford Research Systems). ^{1}H NMR spectra were measured on a Bruker Avance III 300 MHz multinuclear spectrometer. Chemical shifts are reported in ppm downfield relative to the signal of either the internal reference SiMe4 (0 ppm) or residual solvent $CHCl_3$ (7.26 ppm). Coupling constants (J) are given in Hz. Infrared spectra (IR) were recorded on a Bruker Alfa spectrometer. HRMS analyses

were performed on an Agilent 6230 TOF LC/MS instrument using an APPI ionizer and a QSTAR XL hybrid quadrupole/TOF mass spectrometer equipped with an o-MALDI ion source. UV-Vis-NIR absorption spectra were measured on a Cary 6000i spectrophotometer.

Density functional theory (DFT) calculations were performed at the B3LYP/6-31G(d) level of theory using the Gaussian 09 software. Visualization of the molecular structures and vibrational properties was performed using GaussView 5. Plotting of optimized molecular structures was done by CYLview.

Syntheis of compound 99

Compound **97** (0.50 g, 0.94 mmol), 2-chlorophenylboronic acid (0.89 g, 5.6 mmol) and Cs_2CO_3 (2.2 g, 6.6 mmol) were dissolved in THF/H_2O (45 ml/15 ml), purged with N_2 for 10 minutes to give a yellow suspension. $Pd(PPh_3)_4$ (0.11 g, 0.19 mmol) was added, the reaction was stirred at 70 °C overnight under N_2. The reaction mixture turned into a black cloudy solution by the next morning. Crude product was extracted by DCM and washed with water. The organic layer was dried with $MgSO_4$ and concentrated with rota-vapor. Silica column chromatography (CH_2Cl_2/hexane, 1:1) was used to purify the product to give compound **99** (0.53 g, 0.82 mmol, 87%) as a white crystalline solid. ^{1}H NMR (300 MHz, CD_2Cl_2) δ 8.38 (d, J = 7.7 Hz, 2H), 7.51 (dd, J = 7.6 Hz, 4H), 7.48-6.96 (m, 14H), 6.81 (dt, J = 7.2 Hz, 4H) ppm; ^{13}C (75 MHz, CD_2Cl_2) δ 142.1, 141.1, 139.0, 137.1, 136.6, 134.7, 132.6, 131.7, 131.5, 131.0, 130.4, 130.2, 129.2, 129.0, 128.2, 127.8, 127.0, 126.8, 125.6, 126.0 ppm; FTIR (neat) 3065, 3046, 2973, 2866, 1464, 1426, 1257, 1050, 1035 cm^{-1}; HRMS (APPI-TOF, positive) m/z calculated for $C_{40}H_{24}Cl_4$ 646.4306, found 647.0682 $[M + H]^+$. M.P. 306.4–308.4 °C.

Synthesis of compound 101

Compound **97** (0.50 g, 0.94 mmol), 2-methoxybenzeneboronic acid (0.85 g, 5.6 mmol) and Cs_2CO_3 (2.2 g, 6.6 mmol) were dissolved in THF/H_2O (45 ml/15 ml), purged with N_2 for 10 minutes. $Pd(PPh_3)_4$ (0.11 g, 0.19 mmol) was added, the reaction was stirred at 70 °C overnight under the protection of N_2. The reaction mixture turned into a black cloudy solution by the next morning. Crude product was extracted by DCM and washed with water. Silica column chromatography (CH_2Cl_2/hexane, 1:1) was used to purify the product to give compound **101** (0.35 g, 0.55 mmol, 58%) as a white needle like crystalline solid. ^{1}H NMR (300 MHz, CD_2Cl_2) δ 8.02 (s, 2H), 7.29-6.87 (m, 22H), 3.99 (s, 6H), 3.63 (s, 6H) ppm; ^{13}C (75 MHz, CD_2Cl_2) δ 137.9, 137.4, 132.1, 128.4, 127.5, 126.7, 125.3, 120.3, 111.2, 110.6 ppm; FTIR (neat) 3057, 3000, 2935, 2837, 1592, 1577, 1488, 1455, 1430, 1256, 1116, 1052, 1022 cm^{-1}; HRMS (APPI-TOF, positive) m/z calculated for $C_{44}H_{36}O_4$ 628.2613, found 629.1702 $[M + H]^+$.

Synthesis of compound 102

Compound **97** (0.10 g, 0.18 mmol), 1-naphthylboronic acid (0.19 g, 1.1 mmol) and Cs_2CO_3 (0.43 g, 1.26 mmol) were dissolved in THF/H_2O (30 ml/ 10 ml) mix solvent, then the mixture was bubbled with N_2 for 10 mins. $Pd(PPh_3)_4$ (0.043 g, 0.036 mmol) was carefully added and the reaction was kept stirring at 70 °C for overnight under the protection of N_2. Then the crude product was extracted with CH_2Cl_2 and washed with H_2O, the organic layer was dried using anhydrous $MgSO_4$ and concentrated by rotary evaporator. The crude product was then purified by silica column chromatography (ethyl acetate / hexane, 1:19). However, when the pure product solution was concentrated by rotary evaporator, the color of the solution

quickly turned from colorless to red, and TLC also showed a reaction may have happened. Thus pure product was obtained by crystallization. The purified product solution was collected in a beaker and the solvent was slowly evaporated under room temperature to give a needle-like white crystalline product, compound **102** (0.066 g, 0.094 mmol, 52%). ^{1}H NMR (300 MHz, CD_2Cl_2) δ 8.94 (dd, J = 16.2, 8.5 Hz, 4H), 8.16 (d, J = 7.2 Hz, 2H), 7.95 (d, J = 8.2 Hz, 2H), 7.87-7.62 (m, 15.4, 7.8 Hz, 14H), 7.51–7.14 (m, 8H), 7.00 (d, J = 7.9 Hz, 2H), 6.54–6.48 (m, 2H), 6.40-6.35 (m, 2H) ppm; FTIR (neat) 3057, 3040, 1592, 1569, 1505, 1393, 1021 cm^{-1}; HRMS (APPI-TOF, positive) m/z calculated for $C_{44}H_{36}O_4$ 708.2817, found 709.2013 $[M + H]^+$.

Synthesis of compound 103

Compound **97** (0.10 g, 0.18 mmol), 2-naphthylboronic acid (0.19 g, 1.1 mmol) and Cs_2CO_3 (0.43 g, 1.26 mmol) were dissolved in THF/H_2O (30 ml/ 10 ml) mix solvent, then the mixture was bubbled with N_2 for 10 min. $Pd(PPh_3)_4$ (0.043 g, 0.036 mmol) was carefully added and the reaction was kept stirring at 70 °C overnight under the protection of N_2. Then the crude product was extracted with CH_2Cl_2 and washed with H_2O, the organic layer was dried using anhydrous $MgSO_4$ and concentrated by rotary evaporator. The crude product was then purified by silica column chromatography (Ethyl acetate / Hexane, 1:19). However, similar as compound **102**, when the pure product solution was concentrated by rotary evaporator, the color of the solution quickly turned from colorless to red, and TLC also showed a reaction may happened. Thus pure product was obtained by crystallization. The purified product solution was collected in a beaker and the solvent was slowly evaporated under room temperature to give a needle-like white crystal product compound **103** (0.085 g, 0.12 mmol, 67%).

^{1}H NMR (300 MHz, CD_2Cl_2) δ 8.06 (d, J = 1.1 Hz, 4H), 7.89 – 7.80 (m, 12H), 7.71 (d, J = 1.7 Hz, 2H), 7.68 (d, J = 1.7 Hz, 2H), 7.56 – 7.42 (m, 8H), 7.15 (dd, J = 5.8, 3.3 Hz, 4H), 6.65 (dd, J = 5.8, 3.3 Hz, 4H) ppm; ^{13}C (75 MHz, CD_2Cl_2) δ 133.7, 132.3, 132.0, 131.9, 131.8, 129.1, 128.9, 128.6, 128.4 ppm; TIR (neat) 3050, 3018, 1593, 1498, 1451, 1272, 1189, 1140, 1021 cm^{-1}; HRMS (APPI-TOF, positive) m/z calculated for $C_{44}H_{36}O_4$ 708.2817, found 709.2254 $[M + H]^+$.

Synthesis of compound 104

Compound **98** (0.080 g, 0.13 mmol) and DDQ (0.12 mg, 0.53 mmol) were dissolved in CH_2Cl_2 (10 ml) in a quartz tube to form a pale orange solution. The solution was purged with N_2 for 10 minutes and sealed with a rubber stopper. The tube was kept in a photo reactor for 2 days; the wavelength of the light in this reaction ranges from 302 nm to 312 nm. The solution turns yellow after 2 days, and is then washed with saturated $NaHCO_3$ solution until the water layer is almost colorless. By this washing step, the excess DDQ and the byproduct formed during the reaction was removed. The organic layer was dried by rotary evaporator to give the pure compound **104**, which is yellow solid (0.073 g, 1.18 mmol, 91%). ^{1}H NMR (300 MHz, CD_2Cl_2) δ 10.32 (s, 2H), 10.11 (s, 2H), 9.50 (s, 2H), 9.32 (s, 2H), 8.06 (d, J = 8.2 Hz, 4H), 8.04 (s, 4H), 7.79 (d, J = 8.0 Hz, 4H), 7.43 (dd, J = 6.2, 3.4 Hz, 2H), 6.79 (dd, J = 6.2, 3.4 Hz, 2H) ppm; FTIR (neat) 2954, 2921, 2848, 2726, 1690, 1598, 1305, 1207, 1168 cm^{-1}; HRMS (APPI-TOF, positive) m/z calculated for $C_{44}H_{24}O_4$ 616.1675, found 617.1681 $[M + H]^+$.

Synthesis of compound 105

Compound **99** (0.050 g, 0.077 mmol) and K_2CO_3 (0.051g, 0.31 mmol) were dissolved in acetone (1.5 ml) in a quartz tube and then kept in a ultrasonic bath

for 5 minutes to create a colorless suspension. The reaction was subject to UV light (302 nm to 312 nm) in a reactor for 5 hours to give a yellow suspension. The reaction mixture was filtered to remove the excess base added in the reaction. Acetone was removed by rotary evaporator to give a yellow powder product. The crude product was dissolved in CH_2Cl_2 washed with water, then dried with anhydrous $MgSO_4$ and concentrated in a rotary evaporator. Thin layer chromatography showed that the product was pure and did not need further purification. The product **105** is a yellow cubic crystal (0.037g, 0.065 mmol, 85%). ^{1}H NMR (300 MHz, CD_2Cl_2) 9.23 (d, J = 4.2 Hz, 2H), 9.06 (d, J = 8.5 Hz, 2H), 7.87-7.39 (m, 16H), 6.94 (ddd, J = 7.2, 6.3, 3.4 Hz, 2H) ppm; ^{1}3C (75 MHz, CD_2Cl_2) 129.8, 129.6, 128.6, 128.7, 128.1, 127.6, 127.5, 127.2, 126.7, 123.4, 123.0, 122.9, 122.8, 122.53, 122.51 ppm; FTIR (neat) 3066, 2916, 2845, 1474, 1411, 1245, 1033 cm^{-1}; HRMS (APPI-TOF, positive) m/z calculated for $C_{40}H_{22}Cl_2$ 572.1091 found 573.1173 $[M + H]^+$. M.P. 290.8–292.6 °C.

Chapter 3

Synthesis of Cross-linked Polymers via Schiff Base Condensation

3.1 Introduction

Covalent organic frameworks (COFs) are very promising porous materials that have attracted enormous interest in recent years.[92] COFs are crystalline networks in which organic building blocks are connected with each other via strong covalent bonds. As such, COFs usually show much higher thermal stability compared with metal organic frameworks (MOFs).[88–91] The pore size, symmetry and geometry of COFs can be controlled at the molecular level, through careful design of organic building blocks. The defined channels and pores inside COFs make them potential materials for gas storage, release, and separation. COFs can also be potentially used in optoelectronics and electrochemical energy storage due to their remarkable charge carrier transport properties.

COFs can be assembled through reversible condensation reactions, which allow self error correction and rearrangement to occur, eventually giving highly regular crystalline structures rather than amorphous polymers.[92–95] The very first COFs were made by the condensation of boronic acids with catechols to form five-member boronic ester rings; however, this type of COFs is very sensitive to hydrolysis.[92,102,103] Another popular method is Schiff base condensation, which gives such linkages involving imines, hydrazones, azines, and imides.[97–101] The imine-linked COFs are much more stable than the boronic ester COFs. Furthermore, longer π-conjugation can be achieved by Schiff base condensation between aromatic amine with an aromatic aldehyde, making it possible to create fully π-conjugated systems throughout the entire sheet of a 2D COF.

The geometry of COFs is dominated by the shape and connectivity of the organic building blocks. For example, trigonal planar building blocks can form 2D sheets with hexagonal pores, and these 2D sheets further stack to generate superstructures with defined 1D channels. The 3D COFs are constructed from building blocks with defined 3D-shapes, such as tetrahedral geometry.

The tetraarylanthraquinodimethanes (Ar_4-AQs) and related derivatives are interesting precursors and building blocks for novel functional π-conjugated materials. In our previous study, we generated a butterfly-shaped Ar_4-AQ **98** with four formyl groups functionalzed at its end positions.[134,135] Unlike commonly used planar organic building blocks for COFs, the non-planar shape of compound **98** presents a challenge as well as some opportunities to construct new polymeric frameworks. Cross-linking reactions, such as Schiff base condensation, can be envisioned to take place between its four formyl groups and suitable amine counterparts to form cross-

linked molecular frameworks with nanoscale intrinsic porosity.[97–99] Herein, we are particularly interested in exploring the possibility of assembling functional porous polymeric networks (e.g., COFs or COF-like substances) using **98** as an organic linkage.

In contrast to other 3D building blocks, there is no sp^3 carbon in compound **98**. But the special butterfly molecular shape of **98** renders it an unusual 3D geometry that may lead to the formation microporous 3D frameworks. Another interesting property about the Ar_4-AQ is that it has the potential to be transformed into highly conjugated tetrabenzocoronenes (TBCs) via an oxidative cyclodehydrogenation reaction. TBCs are appealing polycyclic aromatic hydrocarbons (PAHs) with more planar and π-conjugated features. Polymeric networks embedded with TBC units have not been reported so far, but they are expected to possess novel electronic and photonic properties which should make them, if synthesized, widely applicable in advanced optoelectronic devices.

3.2 Results and Discussion

As discussed before, the four formyl groups in compound **98** offer the opportunity to construct polymeric frameworks via cross-linking reactions. Schiff base condensation polymerization between compound **98** and *p*-phenylenediamine (**110**) in the presence of acetic acid was first carried out. The reaction occurred smoothly in 1,4-dioxane in a Teflon-lined hydrothermal reactor upon heating at 105 °C by an oven. Polymeric product **P1a** was slowly formed as pale a brown precipitate after 3 days with a rather low yield of 7%. The reaction was modified by applying different temperatures

from 105 to 120 °C and extending the reaction time. The results showed that the quality of **P1** is dependent on the experimental conditions. The best reaction condition modified involved dissolving compound **98** and *p*-phenylenediamine with 1,4-dioxane in a Teflon-lined hydrothermal reactor in the presence of 3 M acetic acid. The reactor was first heated at 120 °C for 3 days and then at 110 °C for another 4 days in an oven. The resulting polymer **P1c** was obtained with a much higher yield of 45% and polymer **P1c** shows reasonably good crystallinity as evidenced by the distinctive diffraction peaks observed in its powder X-ray diffraction (PXRD) spectrum. However, polymers prepared at other temperatures showed no crystallinity in their PXRD spectrum, which means that in order to obtained the polymer with an ordered structure, the reaction temperature needs to be carefully controlled. SEM imaging of the polymer product also revealed the presence of microcrystals on the scale of hundreds of nanometers. The polymer was also prepared by using a sealed glass tube as the reactor, which was heated in an oil bath at 110 °C for 7 days. Polymer **P1e** was obtained under these conditions as a brownish solid. PXRD analysis showed that the diffraction patterns of polymer **P1c** and **P1e** are similar, but the diffraction patterns of polymer **P1e** are less distinctive. The results indicate that it is possible to generate relatively ordered cross-linked polymers by using an oil bath as the heating source other than the classic solvothermal method. Nevertheless, the polymer products obtained by the solvothermal method and the oil bath method give similar IR spectral data, suggesting that the chemical structures of polymers **P1c** and **P1e** are similar. In the IR spectrum, the characteristic C=N stretching band is observed at ca. 1619 cm^{-1}, and the C=O stretching band at 1732 cm^{-1} of the precursor compound **98** disappears completely. This result confirms the formation of

the Schiff base structure in the polymer. Compared with polymer **P1c**, the polymer obtained from the solvothermal method at other temperatures also give very similar IR spectral data. This indicates that Schiff base condensation still happened under these conditions; however, the resulting polymer is amorphous in micro-morphology. Furthermore, with the butterfly molecular shape of precursor compound **98**, polymer **P1c** was expected to possess ordered microstructures and microporosity. The BET surface area of **P1** acquired under hydrothermal conditions is determined to be 390.0 m^2 g^{-1}, and its BJH adsorption average pore width was 7.5 nm.[164] The polymer was also expected to show CO_2 gas capture due to the presence of Schiff base moieties and/or unreacted amino groups in the polymer. However, polymer **P1** did not show significant adsorption of CO_2 gas. The polymer **P1** was found to show very good thermal stability; in particular, TGA analysis indicated that **P1** retains fairly good thermal stability up to 500 °C.

Polymerization reactions of compound **98** with *o*-phenylenediamine or *m*-phenylenediamine were also conducted. In the synthesis, compound **98** and *o*-phenylenediamine were dissolved in 1,4-dioxane in a sealed glass tube. To this mixture was added 3 M acetic acid and the reaction was heated at 110 °C with an oil bath for 16 days to give the condensation product. PXRD analysis showed that the product is amorphous. When using *m*-phenylenediamine, the reaction was performed under the same conditions, but no precipitates formed after 16 days, suggesting that the polymerization degree was very limited. The poor polymerization degree may be explained as follows. The two amino groups in *o*- and *m*-phenylenediamines are much closer compared with those in *p*-phenylenediamine. The condensation of *o*-phenylenediamine with DHA compound **98** may favor the

formation of low-degree polymerized oligomers rather than ordered, extended cross-linked polymers. In contrast to *p*-phenylenediamine, which is a liner 1D building block, *o*-phenylenediamin can be considered as a 2D building block, thus the geometry of the condensation product of compound **98** with *o*-phenylenediamine is hard to predicte. For *m*-phenylenediamine, the two amimo groups are relatively close, and it is too difficult for the second DHA compound **98** to attack the phenylenediamine after the first DHA compound **98** reacts with the phenylenediamine due to steric repulsion. This may explain why there were no precipitates observed, since the polymerization between **98** and *m*-phenylenediamine is too difficult to occur.

3.3 Preparation of Cross-Linked Polymers Based on Ph_4-AQ

3.3.1 Synthesis of Cross-linked Ph_4-AQ Polymers Using *p*-Phenylenediamine as a Building Block

The first attempt to make Ph_4-DHA based cross-linked polymers was made through the condensation reaction illustrated in Scheme 3.1. In the experiment, compound **98** and 2 equiv. of *p*-phenylenediamine were mixed in 1,4-dioxane in a Teflon-lined hydrothermal reactor in the presence of 3 M HOAc (aq). After all the reagents were added, the reaction mixture was bubbled with N_2 flow for 10 min to remove oxygen. Then the reactor was sealed and heated in an oven, with the temperature slowly increased from rt to 105 °C and then kept at that temperature for 3 days. Afterwards, the reactor was taken out of the oven and cooled down to rt. The precipitates formed

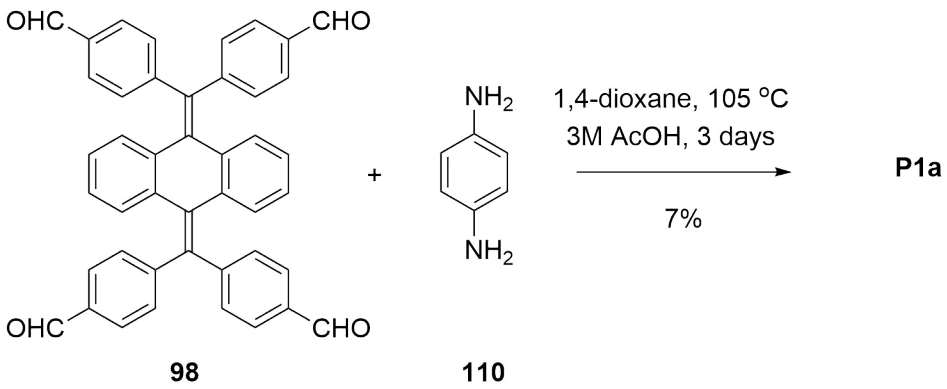

Scheme 3.1: Synthesis of cross-linked polymer **P1a** by Schiff base condensation reaction.

in the reaction mixture were collected by filtration, washed and dried under vacuum to afford a light brown solid product, **P1a**, with a yield of 7%. The product was found to be insoluble in common organic solvents, suggesting that it is a cross-linked polymer product. The outcome of this reaction was promising, although the yield was quite low. Modifications of reaction conditions were next carried out with the aim of improving the yield of the cross-linked condensation product.

The low yield of the above synthesis may be due to several reasons, such as the relatively short reaction time and low reaction temperature. Given this consideration, the second synthesis was performed with both the reaction time and temperature increased. Like the first synthesis, the required reactants and reagents were mixed and degassed before heating. This time the reaction was slowly heated to 115 °C and kept at this temperature for 7 days as shown in Table 3.1. After that, the reaction was slowly cooled down to rt during a period of 1 day. The resulting product, **P1b**, was a dark brown powder with a significantly increased yield of 68%. However, surface area analysis of this powder showed that the BET surface area of **P1b** was not as

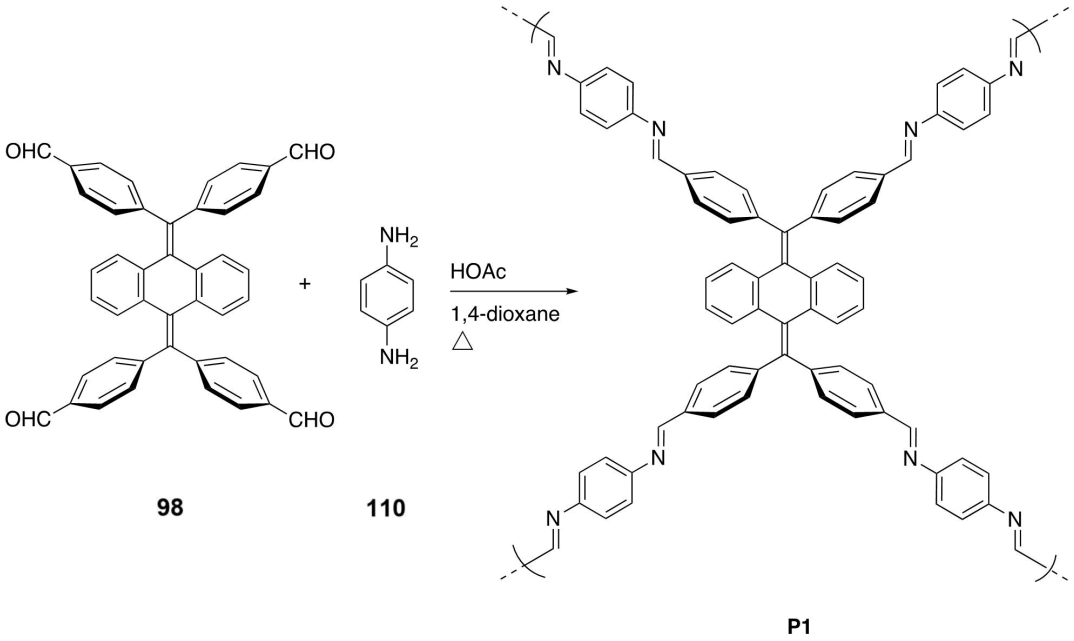

Scheme 3.2: Synthesis of cross-linked polymer networks **P1** under modified Schiff base condensation conditions.

high as expected, indicating limited porosity of the material.

The initiation of Schiff base condensation usually needs a relatively high temperature. On the other hand, in order to form highly ordered cross-linked microstructures, self-healing steps should be involved in the synthetic process and high temperature is not preferred. As such, an optimal reaction temperature is the key to the formation of an ordered cross-linked polymer. Subsequent modification was thus focused on tuning the reaction temperature. In the next experiment, the condensation reaction was slowly heated to 120 °C and kept at this temperature for 4 days, and then the temperature was cooled down to 110 °C and kept for another 3 days. Finally, the reaction was slowly cooled to rt, yielding product **P1c** as a yellow powder. The product was characterized by powder X-ray diffraction (PXRD) analysis, which showed that **P1c** is partially crystalline. Also **P1c** was shown to have

Temperature	Time	Product Color	Yield	Product
105 °C	3 days	Pale brown	7%	**P1a**
115 °C	7 days	Dark brown	68%	**P1b**
120-110 °C	7 days	Yellow	45%	**P1c**
120 °C	9 days	Dark brown	78%	**P1d**
110 °C	7 days	Yellow	48%	**P1e**

Table 3.1: Summary of experimental conditions and outcomes for the preparation of Ph_4-AQ based cross-linked polymers under different solvothermal conditions. Note that cross-linked polymer **P1e** was prepared by heating the reaction mixture in an oil bath.

a relatively large BET surface area, ca. 400 $m^2\ g^{-1}$, which is very close to the reported surface areas of some 2D COFs.[92–95,97–101] This results showed that the crystallinity of cross-linked products can be improved by slowly cooling the reaction temperature after initiating the reaction at a relatively high temperature.

In the fourth experiment, the reaction mixture was slowly heated to 120 °C and kept at this temperature for 9 days. Then it was slowly cooled to rt. The resulting reaction product, **P1d**, was found to possess a surface area not as high as that of **P1c**. PXRD analysis showed that **P1d** has a poorer crystallinity than that of **P1c** (vide infra).

In addition to the oven heating method, preparation of Ph_4-AQ cross-linked polymers under heating with an oil bath was also investigated. The oil bath heating method has the advantage in terms of easy monitoring of the progress of the reaction,

since it allows the reaction be carried out in a transparent glass reactor rather than the Teflon-lined hydrothermal reactor allowing for visual checking of the reaction. Also, the oil bath allows the reaction temperature to be more accurately controlled without significant fluctuation. In the experiment, compound **98** and 2 equiv of *p*-phenylenediamine were dissolved in 1,4-dioxane in a glass tube. 3 M HOAc (aq) was then added and the reaction mixture was bubbled with N_2 flow for 10 min to remove oxygen. After this treatment, the reaction tube was sealed and heated with an oil bath. The temperature was slowly raised to 110 °C and kept at this temperature for 7 days. Then the reaction was slowly cooled down to rt and the resulting precipitate was collected, washed and dried under vacuum to give cross-linked polymer **P1e** as a yellow powder with a yield of 48%.

3.3.2 Synthesis of Cross-Linked Polymers Using Other Phenylenediamines as Building Blocks

In addition to linear-shaped *p*-phenylenediamine, *m*-phenylenediamine (**111**) *o*-phenylenediamine (**112**) were also investigated as building blocks to undergo Schiff base condensation with compound **98** (Scheme 3.3). In each of these two phenylenediamines, the two amino groups are oriented at an angle of 60° and 120°, respectively. As such, their condensation reactions with **98** were expected to yield different products than the reaction between **98** and *p*-phenylenediamine.

As shown in Scheme 3.3, compound **98** and 2 equiv of *m*-phenylenediamine were mixed in 1,4-dioxane in a glass tube. 3 M HOAc (aq) was then added and the reaction mixture was bubbled with N_2 for 10 min to remove oxygen. After this

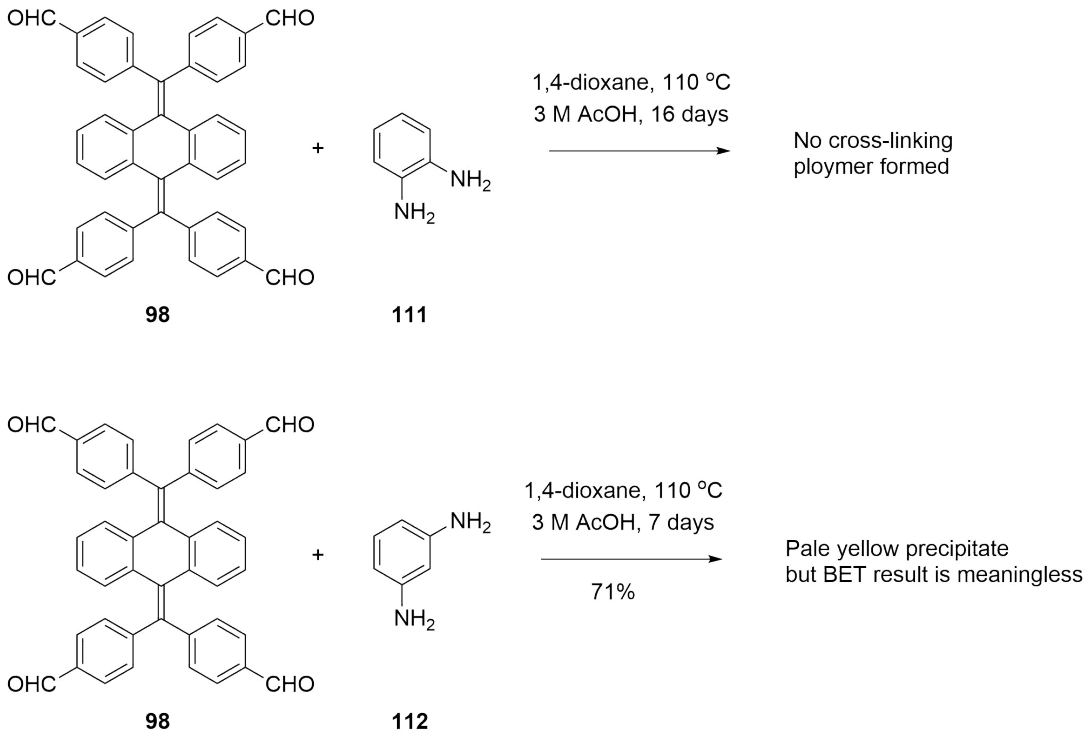

Scheme 3.3: Synthesis of cross-linked polymer networks **P1** under modified Schiff base condensation conditions.

treatment, the reaction tube was sealed and heated in an oil bath. The temperature was slowly raised to 110 °C and kept at this temperature for as long as 16 days. Unfortunately, no precipitates were observed during the course of this reaction, indicating that the condensation reaction between **98** and *m*-phenylenediamine, if it occurred, only yielded oligomeric products with good solubility. The reaction outcome hence indicates that the molecular shape of *m*-phenylenediamine, in particular the 120° angle between the two amino groups, is not suitable for cross-linking reactions.

The Schiff base condensation reactions between compound **98** and *o*-phenylenediamine was then tested. In the experiment, compound **98** and 2 equiv of *o*-phenylenediamine were mixed in 1,4-dioxane in a glass tube. 3 M HOAc (aq)

was then added and the reaction mixture was bubbled with N_2 for 10 min to remove oxygen. After this treatment, the reaction tube was sealed and heated with an oil bath. The temperature was slowly raised to 110 °C and kept at this temperature for 7 days. In contrast to the case of *m*-phenylenediamine, pale yellow precipitates were gradually formed during the course of reaction. The precipitates were collected by filteration, washed with solvents, and then dried under vacuum. Gas adsorption analysis showed that this cross-linked product does not possess a significant BET aurface area and is not porous in structure. The lack of porosity is likely due to the molecular shape of *o*-phenylenediamine which should lead to twisted and/or folded polymer structures rather than ordered and extended polymer networks with defined intrinsic porosity. Because of these results, further attempts to optimize the yields of cross-linked polymers using *o*-phenylenediamine as a building block were abandoned.

3.4 Characterizations of Ph_4-AQ Based Cross-linked Polymers

3.4.1 PXRD and SEM Analyses

The prepared cross-linked polymers **P1b**–**P1d** were subjected to PXRD analysis to characterize their crystalline properties in the solid state. For comparison purposes, the PXRD patterns of starting **98** and *p*-phenylenediamine were also measured. Figure 3.1 shows the detailed PXRD data. Cross-linked polymer **P1c** (black trace in the figure) exhibits distinctive diffraction peaks, suggesting relatively good crystallinity. Scanning electron microscopic (SEM) imaging of the product **P1c**

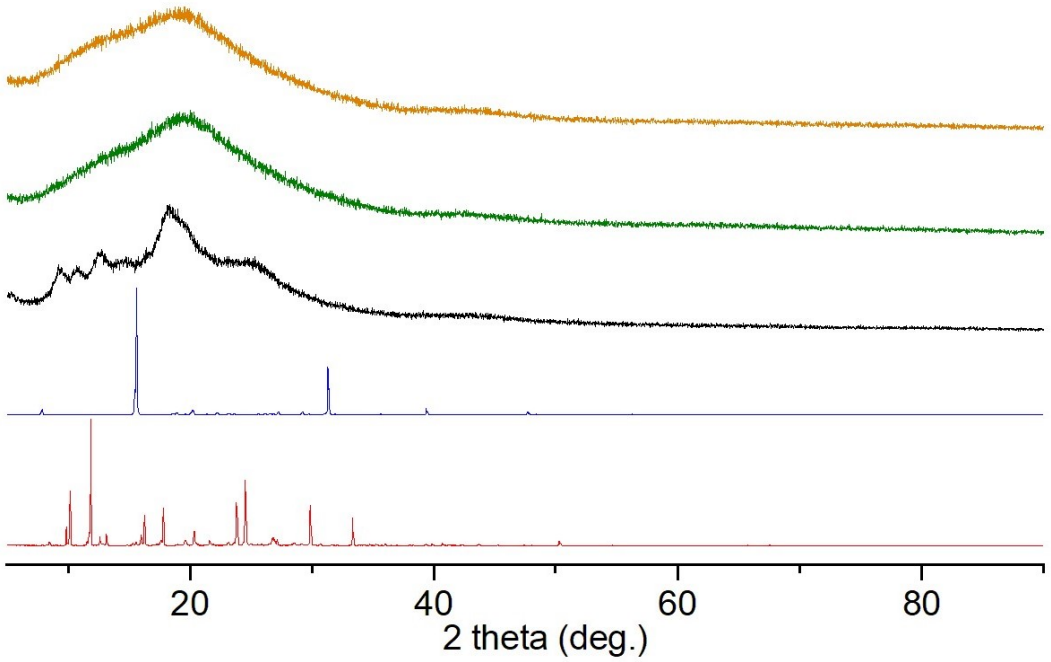

Figure 3.1: PXRD patterns of polymers **P1c** (black), **P1b** (green), **P1d** (orange), compound **98** (red), and *p*-phenylenediamine (blue).

also revealed the presence of microcrystals on the scale of hundreds of nanometers (Figure 3.2), which concurs with the PXRD results. Polymers **P1b** and **P1d** give similar PXRD patterns that are indicative of amorphous solids rather than crystalline materials. Clearly, the conditions applied for the preparation of **P1b** and **P1d** do not facilitate the formation of ordered cross-linked microstructures.

Figure 3.3 compares the PXRD patterns of polymers **P1c** and **P1e**, which were prepared in a hydrothermal reactor heated with an oven and a sealed glass tube heated with an oil bath, respectively. The PXRD results indicate that **P1e** has a certain degree of crystallinity, but compared with **P1c** the diffraction patterns are less distinctive. The results confirm that it is possible to generate relatively ordered

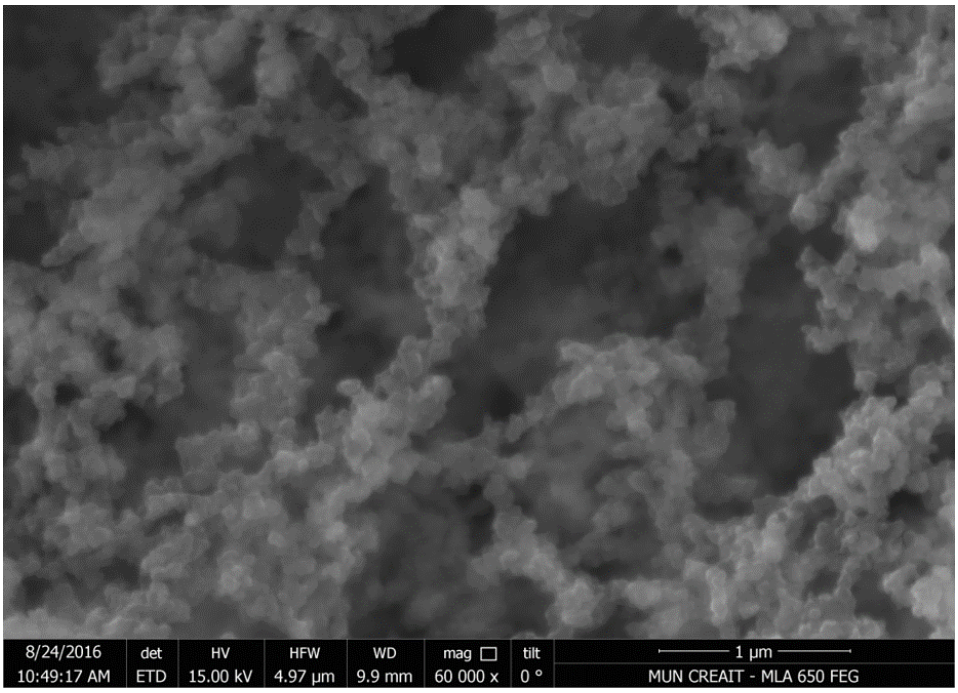

Figure 3.2: SEM image of polymer **P1c**.

cross-linked polymers by using oil bath heating in place of the solvothermal method.

3.4.2 IR Analysis

To investigate the covalent bonding properties of Ph_4-DHA cross-linked polymers, IR spectroscopic analysis was performed. Figure 3.4 shows the IR spectrum of polymer **P1c** in comparison with the IR spectra of starting materials **98** and *p*-phenylenediamine. As can be seen, the IR spectrum of **P1c** does not show the vibrational peaks due to the N–H (3400-3500 cm^{-1}) and C=O (1740 cm^{-1}) stretching modes, indicating the complete consumption of the aldehyde and amino groups during the Schiff base condensation reaction. In the meantime, a characteristic C=N stretching band at 1619 cm^{-1} is clearly observed in the spectrum of **P1c**, which provides evidence for the occurrence of Schiff base condensation.

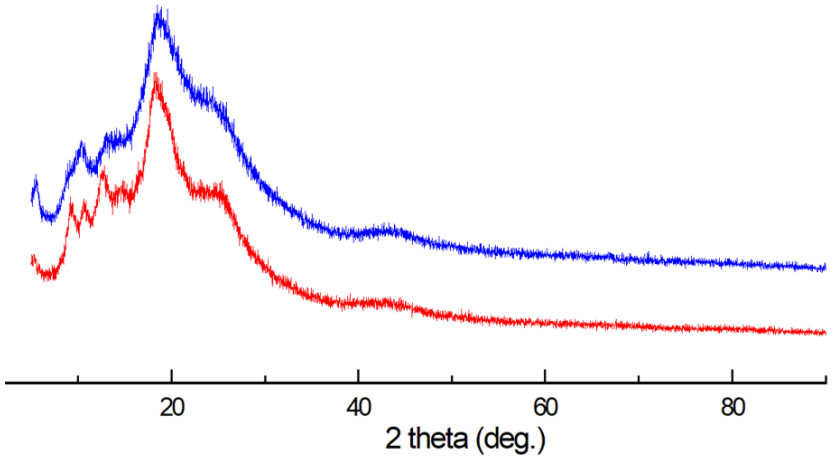

Figure 3.3: PXRD patterns of polymers **P1c** (red) and **P1e** (blue).

Figure 3.5 shows the IR spectra of polymers **P1a**–**P1d**. The IR data of **P1a** still show the presence of a weak C=O stretching band indicating that there are unreacted -CHO groups in the structure of **P1a**. After extending the reaction time, the C=O band disappears in the IR spectrum of polymers **P1b**–**P1d**. It is clear that the reaction time is an important factor for the preparation of cross-linking polymers. Indeed, the polymerization process is rather time consuming and prolonged reaction time is necessary. The IR spectra of **P1b**–**P1d** do not show much difference, suggesting that the chemical composition of these three polymers are quite similar to one another, even though PXRD results show that their crystalline properties are somewhat different.

3.4.3 Surface Area and Porosity Analysis

Given the twisted, butterfly-like molecular shape of compound **98**, it was expected that **P1** if formed with ordered (i.e., crystalline) microstructures would possess

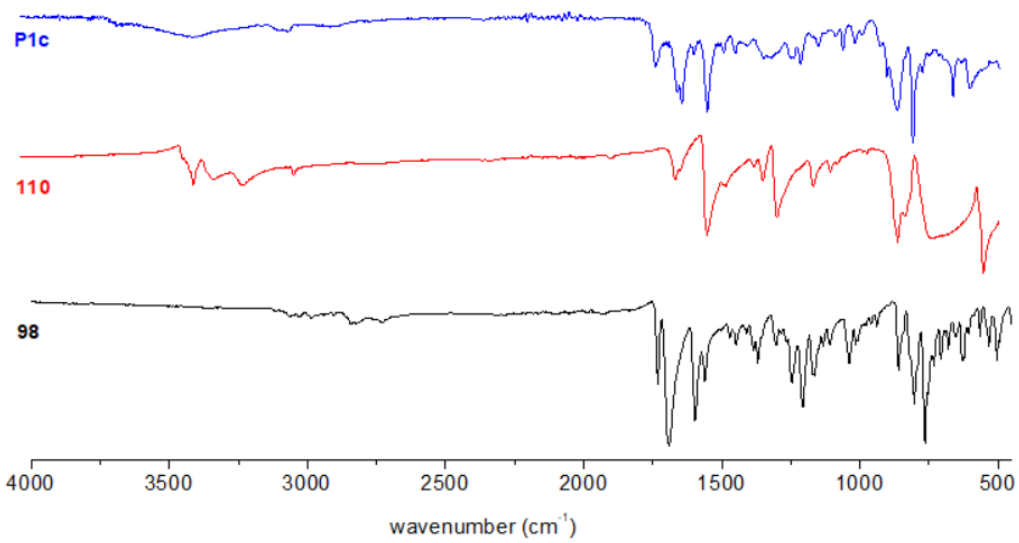

Figure 3.4: IR spectra of compound **98**, *p*-phenylenediamine, and cross-linked polymer **P1c**.

intrinsic microporosity. Indeed, the BET surface area of **P1** acquired under the hydrothermal conditions was determined to be 390.0 m^2 g^{-1}, and its BJH adsorption average pore width is 7.5 nm. As shown in Figure 3.6, the nitrogen gas adsorption of polymer **P1** gives a typical Type II isotherm. A Type II isotherm reflects the typical physical adsorption process on non-porous or macroporous adsorbents, which is the most common result in gas adsorption analysis. Due to the strong interactions of the adsorbate on the surface, the adsorption amount rises rapidly at low relative pressure, and the curve has a convex shape. The isotherm inflection point usually appears in the vicinity of single-layer adsorption. As the relative pressure continues to increase, multi-layer adsorption gradually takes place. When the saturated vapor pressure is reached, the adsorption layer is almost infinite, making it difficult to determine the accurate limit equilibrium adsorption value.

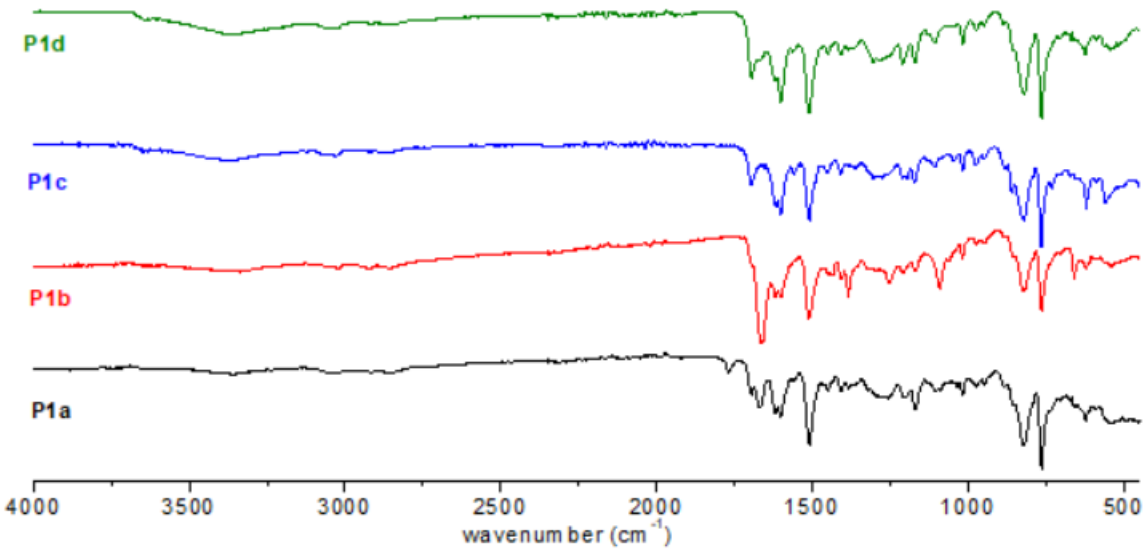

Figure 3.5: IR spectra of cross-linked polymers **P1a-P1d**.

3.4.4 Thermal Stability

The thermal stability of cross-linked polymer **P1** was examined by thermogravimetric analysis (TGA). Figure 3.8 shows the detailed TGA profile, from which it can be clearly seen that **P1** retains fairly good thermal stability up to 500 °C. The weight loss at 50 °C is about 16%, which can be ascribed to the loss of water or other low boiling-point solvents trapped in the polymer matrix. From 50 °C to 500 °C, the TGA trace shows a slightly decreasing trend, but the weight loss is relatively insignificant. Obviously, **P1** is thermally stable in this temperature range and the small degree of weight loss is likely due to the removal of some relatively high boiling point solvents trapped inside the polymer, such as DMF and 1,4-dioxane, since they were used in the preparation of the polymer as solvents. When the temperature is higher than 500 °C, the TGA curve shows a sharp decrease in weight, suggesting that chemical decomposition starts to occur significantly at high temperature. Overall, the TGA

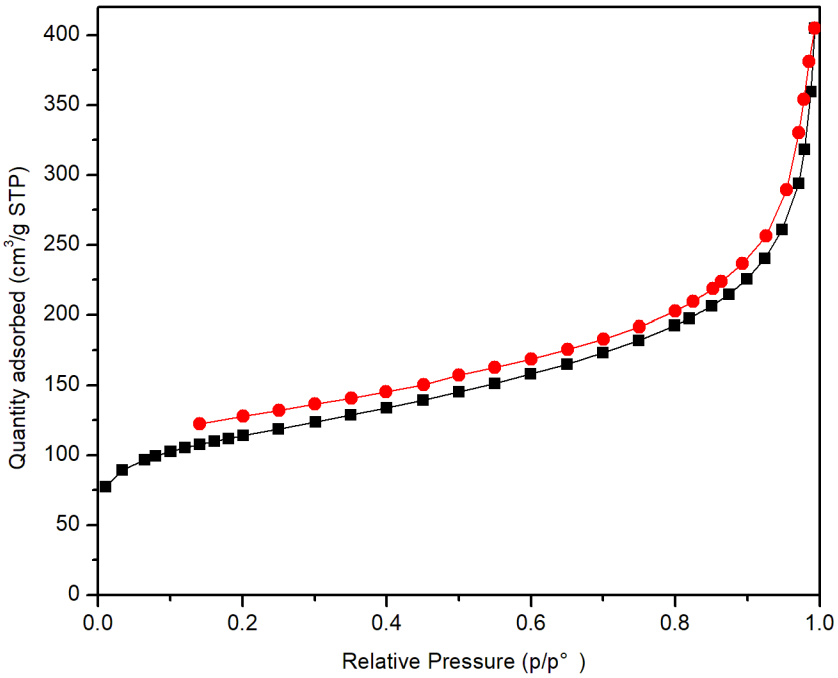

Figure 3.6: Nitrogen gas adsorption (black) and desorption (red) curve of cross-linked polymer **P1c**.

data indicate that the cross-linked polymer **P1** possesses good thermal stability which bodes well for its practical uses, such as functional adsorbents and/or catalysis.

3.5 Conclusions

A new class of cross-linked polymer networks using compound **98** and *p*-phenylenediamine as building blocks was investigated. Schiff base condensation served as an effective approach to form cross-linked polymers, while reaction conditions such as reaction temperature, heating method, and reaction time are important parameters for the quality of the resulting cross-linked polymers. Especially, if

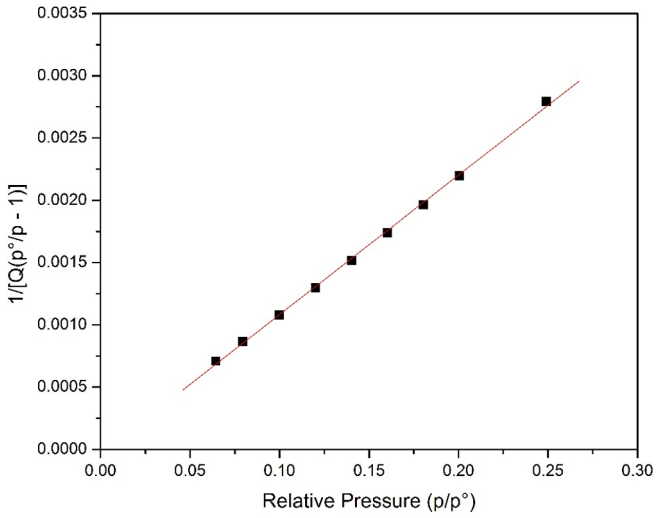

Figure 3.7: BET curve of cross-linked polymer **P1c**.

ordered crystalline microporous networks are desirable, the reaction conditions need to be carefully controlled. The polymerization reactions between compound **98** and *m*-phenylenediamine/*o*-phenylenediamine did not produce good quality cross-linked polymers. It has been confirmed that the molecular shape of the diamine building block is another key factor in the formation of microporous polymer networks.

3.6 Experimental Section

Chemicals were purchased from commercial suppliers and used directly without purification. Schiff based condensation reactions were performed in either a 15 mL Teflon-lined hydrothermal synthesis autoclave reactor or a 15 mL Pyrex glass tube reactor equipped with a Teflon screw cap. Infrared spectra (IR) were recorded on a Bruker Alfa spectrometer. Thermogravimetric analysis (TGA) was done on a

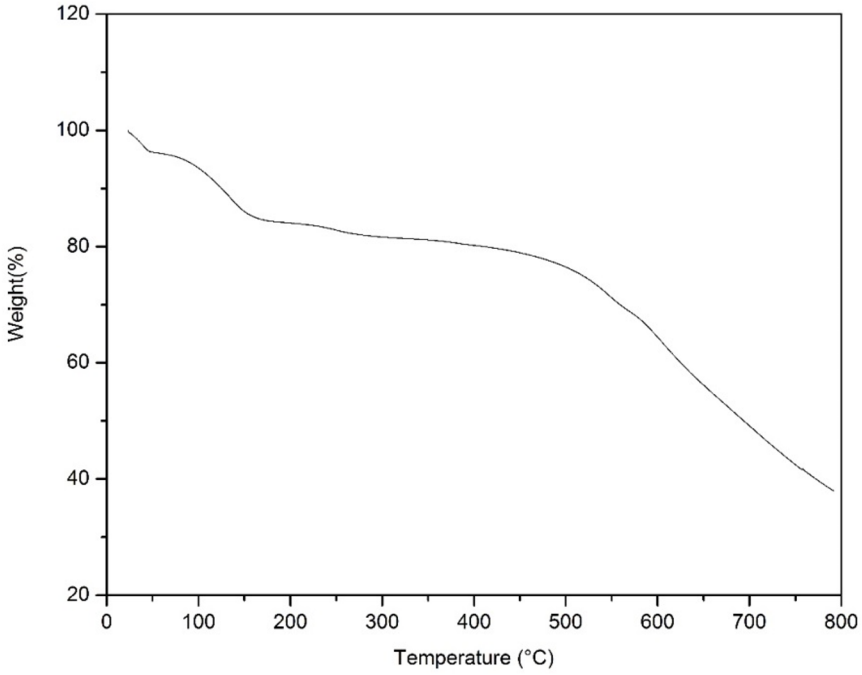

Figure 3.8: TGA profile of cross-linked polymer **P1c**.

TA Instruments TGA Q500 system. Scanning Electron Microscopes (SEM) were performed on a JEOL JSM-7100F instrument (Vacc = 30 kV, Imax = 400 nA). Powder X-ray diffraction (PXRD) analysis was carried out on the Rigaku Ultima IV x-ray diffractometer equipped with a copper x-ray source and a scintillation counter detector. Surface area and porosity analysis was performed on a Micrometrics Tristar II Plus instrument.

Synthesis of Polymer P1a

Compound **98** (60 mg, 0.096 mmol) and *p*-phenylenediamine (21 mg, 0.19 mmol) were dissolved in 1,4-dioxane (5 mL) in a 15 mL Teflon-lined hydrothermal synthesis autoclave reactor. The mixture was purged with N_2 flow for 10 min and then 3 M HOAc (aq) (0.26 mL) was added. The reactor was sealed and placed in an oven

to be slowly heated to 105 °C and the heating at this temperature was kept for 3 days. After cooling to rt, precipitates formed in the reaction mixture was collected by centrifugation followed by vacuum filtration. The solids were rinsed with DMF several times until the DMF filtrate became colorless. The rinsing was then repeated with copious THF. The resulting solids were air dried overnight and then placed under vacuum for 5 h to give **P1a** (5.1 mg, 7%) a pale brown solid. **P1a** obtained by this method shows reasonably good crystallinity as characterized by SEM imaging and PXRD analysis.

Synthesis of Polymer P1b

Compound **98** (60 mg, 0.096 mmol) and *p*-phenylenediamine (21 mg, 0.19 mmol) were dissolved in 1,4-dioxane (5 mL) in a 15 mL Teflon-lined hydrothermal synthesis autoclave reactor. The mixture was purged with N_2 flow for 10 min and then 3 M HOAc (aq) (0.26 mL) was added. The reactor was sealed and placed in an oven to be slowly heated to 115 °C and the heating at this temperature was kept for 7 days. After cooling to rt, precipitates formed in the reaction mixture was collected by centrifugation followed by vacuum filtration. The solids were rinsed with DMF several times until the DMF filtrate became colorless. The rinsing was then repeated with copious THF. The resulting solids were air dried overnight and then placed under vacuum for 5 h to give **P1b** (50 mg, 68%) a dark brown solid. **P1b** obtained by this method was characterized by SEM imaging and PXRD analysis.

Synthesis of Polymer P1c

Compound **98** (60 mg, 0.096 mmol) and *p*-phenylenediamine (21 mg, 0.19 mmol) were dissolved in 1,4-dioxane (5 mL) in a 15 mL Teflon-lined hydrothermal synthesis autoclave reactor. The mixture was purged with N_2 flow for 10 min and then 3 M

HOAc (aq) (0.26 mL) was added. The reactor was sealed and placed in an oven to be heated at 120 °C for 3 days. After that, the temperature was decreased to 110 °C and the heating at this temperature was kept for another 3 days. After cooling to rt, precipitate formed in the reaction mixture was collected by centrifugation and then vacuum filtration. The solids were rinsed with DMF several times until the DMF filtrate became colorless. The rinsing was then repeated with copious THF. The resulting solids were air dried overnight and then placed under vacuum for 5 h to give **P1c** (33 mg, 45%) a yellow solid. **P1c** obtained by this method shows reasonably good crystallinity as characterized by SEM imaging and PXRD analysis.

Synthesis of Polymer P1d

Compound **98** (60 mg, 0.096 mmol) and *p*-phenylenediamine (21 mg, 0.19 mmol) were dissolved in 1,4-dioxane (5 mL) in a 15 mL Teflon-lined hydrothermal synthesis autoclave reactor. The mixture was purged with N_2 flow for 10 min and then 3 M HOAc (aq) (0.26 mL) was added. The reactor was sealed and placed in an oven to be slowly heated to 120 °C and the heating at this temperature was kept for 7 days. After cooling to rt, precipitates formed in the reaction mixture was collected by centrifugation and then vacuum filtration. The solids were rinsed with DMF several times until the DMF filtrate became colorless. The rinsing was then repeated with copious THF. The resulting solids were air dried overnight and then placed under vacuum for 5 h to give **P1d** (57 mg, 78%) a dark brown solid. **P1d** obtained by this method was characterized by SEM imaging and PXRD analysis.

Synthesis of Polymer P1e

Compound **98** (60 mg, 0.096 mmol) and *p*-phenylenediamine (21 mg, 0.19 mmol) were dissolved in 1,4-dioxane (5 mL) in a Pyrex glass tube reactor. The mixture was

purged with N_2 flow for 10 min and then 3 M HOAc (aq) (0.26 mL) was added. The reactor was sealed with a Teflon screw cap and placed in an oil bath to be heated at 110 °C. After heating for 7 days, a yellow precipitate was formed. After cooling to rt, the precipitates were collected through vacuum filtration followed by sequential rinsing with copious amounts of DMF and THF. The resulting solids were air dried and then placed under vacuum for 5 h to give **P1e** (36 mg, 48%) as a yellow solid. **P1e** obtained by this method shows relatively poor crystallinity as evidenced by PXRD analysis.

Chapter 4

Acid-promoted Intramolecular Cyclization of *ortho*-Dithiafulvenyl-substituted Phenyacetylene Derivatives

The work reported in this chapter has been published as a full research article, see C. Wang, C. Flinn, Y. Zhao, Intramolecular Alkyne-Dithiolium Cycloaddition: a Joint Experimental and DFT Mechanistic Study *RSC Adv.*, **2017**, *7*, 36623–36631. Experimental work was solely carried out by C. Wang, while computational studies were conducted by Prof. C. Flinn and Prof. Y. Zhao. C. Wang also participated in data analysis and manuscript preparation.

4.1 Introduction

Organic π-conjugated materials have been widely applied in organic conductors semiconductors, chemo- and bio-sensors, light-emitting devices, organic photovoltaic devices, and many other fields. Among them, tetrathiafulvalene (TTF), which is the active component of the first organic conductor discovered, has played an indispensable and central role in the area of modern molecular electronics.[127,135,165–169] Over the past ten years, a class of π-extended TTF analogues, namely TTFVs, has been actively investigated as redox-active building blocks for various π-conjugated systems, many of which have demonstrated intriguing redox, optoelectronic, and supramolecular properties.[170–173] A particularly appealing aspect of TTFVs, especially the family of aryl-substituted TTFVs, lies in their redox controllable conformational switching behaviour. Built upon aryl-TTFVs, various functional molecular systems have been prepared and reported in the recent literature, including stimuli-responsive conjugated polymers, fluorescent molecular tweezers, redox-active ligands, shape-persistent macrocycles, molecular rotors.[82,141,174–176]

As mentioned in Chapter 1, dithiafulvenes (DTFs) can be readily converted into TTFVs through a straightforward oxidative dimerization reaction.[128,136–140] Scheme 4.1 describes the general mechanism for this type of dimerization reaction.[141–143] However, in a study by Yunfei Wang, a former member of the Zhao group, an unexpected reaction outcome was observed when a bis(DTF)-endcapped diphenylbutadiyne **117** was subjected to oxidative treatment with iodine (see Scheme 4.2).[144]

Quite surprisingly, the oxidation of **117** ended up with the formation of compound

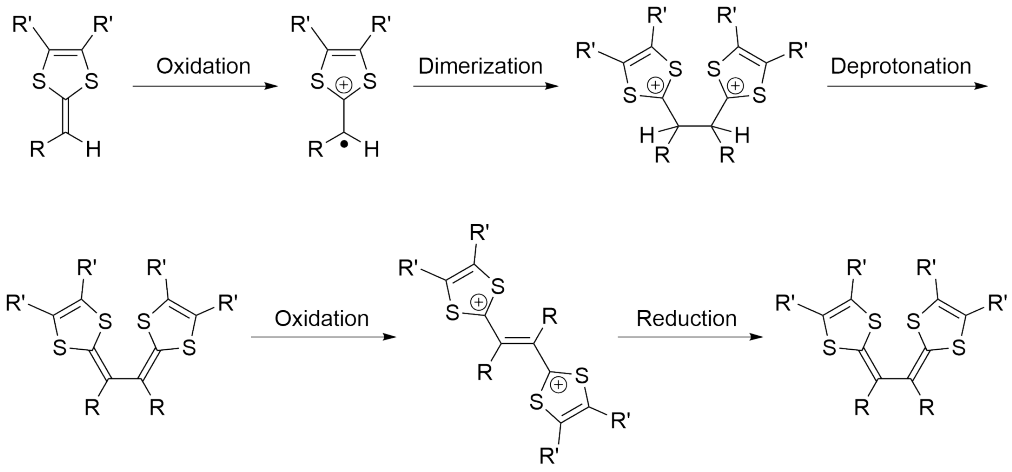

Scheme 4.1: Typical oxidative dimerization of DTF

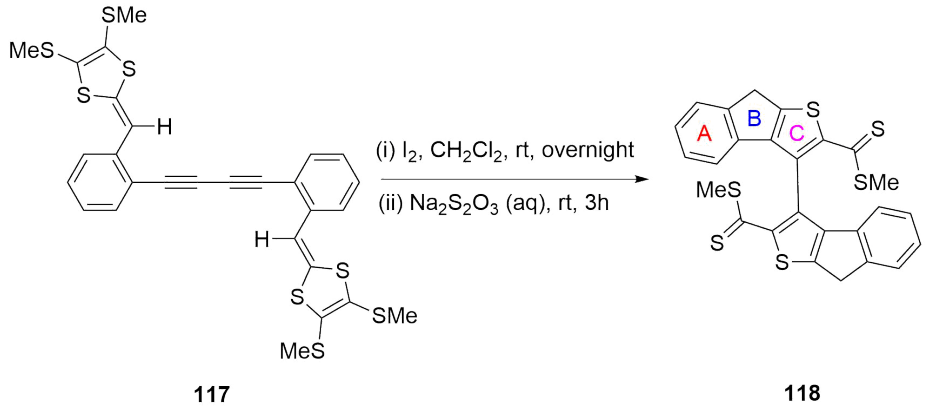

Scheme 4.2: An unusual iodine-promoted cycloaddition of bis-DTF compound **117**.

118 as the major product. In contrast to the generally expected dimerized product, the structure of **118** features a complex fused tricyclic indenothiophene motif. The newly formed rings in compound **118** are supposedly formed through an intramolecular cycloaddition process,[177,178] while the sp^3 benzylic carbon in the middle five-member ring B suggests that a protonation step takes place on the vinylic carbon adjacent to the dithiole group of compound **117** at the initial stage of the reaction.[179–181] Two plausible reaction pathways were thus proposed to account for the formation of product **118** as shown in Scheme 4.3.

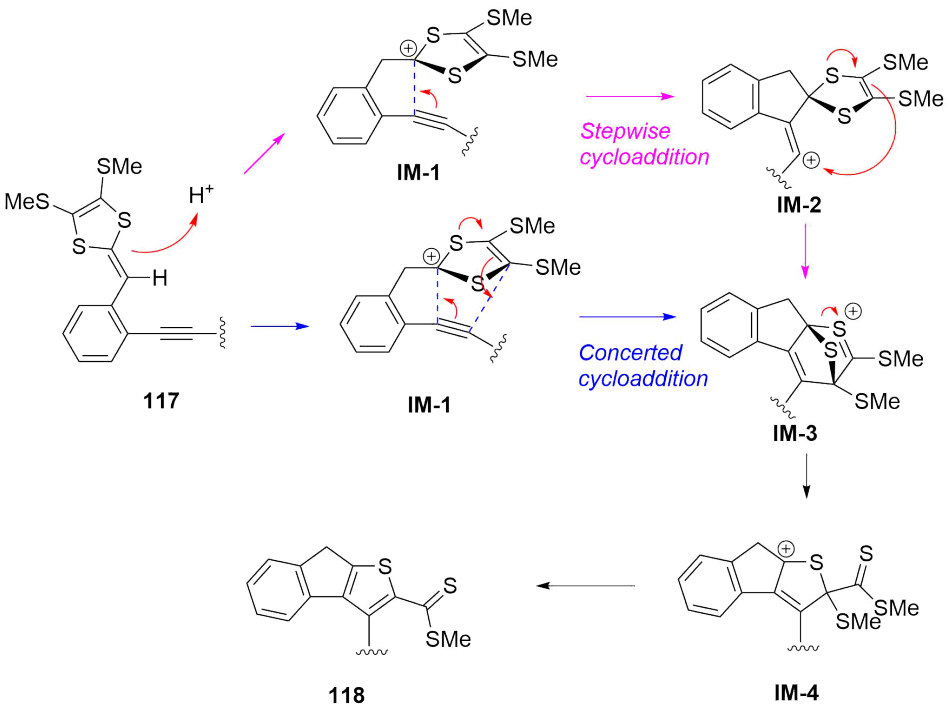

Scheme 4.3: Two plausible reaction pathways for the intramolecular alkyne-dithiolium cycloaddtion.

In the proposed mechanism, the reaction begins with the protonation of compound **117** to generate a dithiolium intermediate **IM-1**. The acid herein is believed to be HI, which comes from the redox reactions between compound **117** and iodine.[140] Once formed, the dithiolium moiety of **IM-1** can quickly react with the *ortho*-alkynyl group due to its close proximity. Following **IM-1**, two reaction pathways can be conceived based on commonly known organic reaction mechanisms. The first one is a concerted 1,3-dipolar cycloaddition that directly leads to **IM-3** with the backbones of B and C rings assembled at same time. The second one is a stepwise pathway, in which the alkynyl group attacks the dithiolium ring via an "alkyne Prins type cyclization" at first, forming the B ring only.[182–187] The resulting intermediate **IM-2** then undergoes another step of intramolecular nucleophilic addition to yield

intermediate **IM-3**, which then undergoes a ring-opening step to produce a cationic intermediate **IM-4**. At the final stage of the reaction, a desulfurization process occurs to give the neutral product compound **118**.

With the proposed reaction mechanisms, several important questions arise as follows. (i) The acid seems to be an essential reagent in the reaction, if the hypothesized mechanism holds true, will the introduction of a protic acid to the reaction make a improvement on the reaction rate and yield? (ii) Does the intramolecular alkyne-dithiolium cycloaddition prefer the concerted or stepwise pathway? (iii) How does the dethiomethylation occur in the final stage of the reaction? (iv) Is iodine a necessary agent to the reaction, or not?

To answer above questions, a series of experiments was designed and conducted. Computational density functional theory (DFT) calculations were also performed to investigate the detailed reaction mechanisms in combination with experimental evidence. The details of our mechanistic study on the intramolecular alkyne-dithiolium cycloaddition reaction are described in this chapter.

4.2 Results and Discussion

4.2.1 The Role of Protic Acids on Cyclization

Firstly, we investigated the role of protic acid in the intramolecular cyclization of compound **117**. A strong organic acid, trifluoroacetic acid (TFA), was chosen in our experiments based on its known ability to effectively protonate dithiole groups in nonpolar organic media.[188–190] Experimentally, TFA was slowly added into the

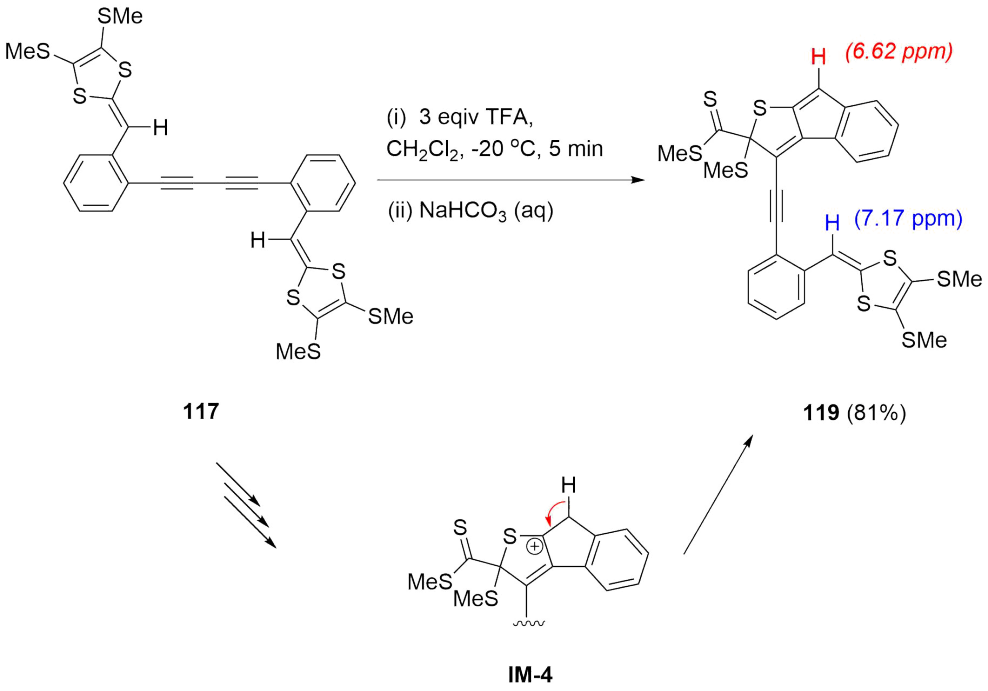

Figure 4.1: TFA-promoted intramolecular cyclization of compound **117**.

solution of compound **117** in CH_2Cl_2, which quickly led to a color change from yellowish to dark red. The reaction proceeded very fast. At -20 °C, compound **117** was completely consumed within 5 min as monitored by thin-layer chromatographic (TLC) analysis. Aqueous workup followed by quick silica column separation afforded a crude product as a red-color powder. Further purification of this product was unsuccessful due to its poor chemical stability and the presence of some inseparable byproducts. Nevertheless, the product **119** could still be reasonably deduced as the structure shown in 4.1, based on the two distinctive singlets at 6.12 ppm and 7.17 ppm in the ^{1}H NMR spectrum. The first peak is characteristic of the indenyl proton, while the second is the vinylic proton adjacent to the dithole group. The two proton signals show nearly equal integral values, indicating that only half of compound **117** has cyclized under the TFA treatment. The formation of an indenyl moiety in **119**

can be rationalized by a *beta*-hydrogen elimination on the reactive intermediate **IM-4** mentioned in 4.1. A strong protic acid can substantially accelerate the intramolecular alkyne-dithiolium cyclization, but it does not seem to be very effective at promoting the elimination of SMe. Without removal of the SMe group, the remaining alkynyl unit of compound **119** is prohibited from going through another step of intramolecular cyclization due to the pronounced steric hindrance surrounding it.

4.2.2 The Reactivity of Monoynes and Diynes towards Cyclization

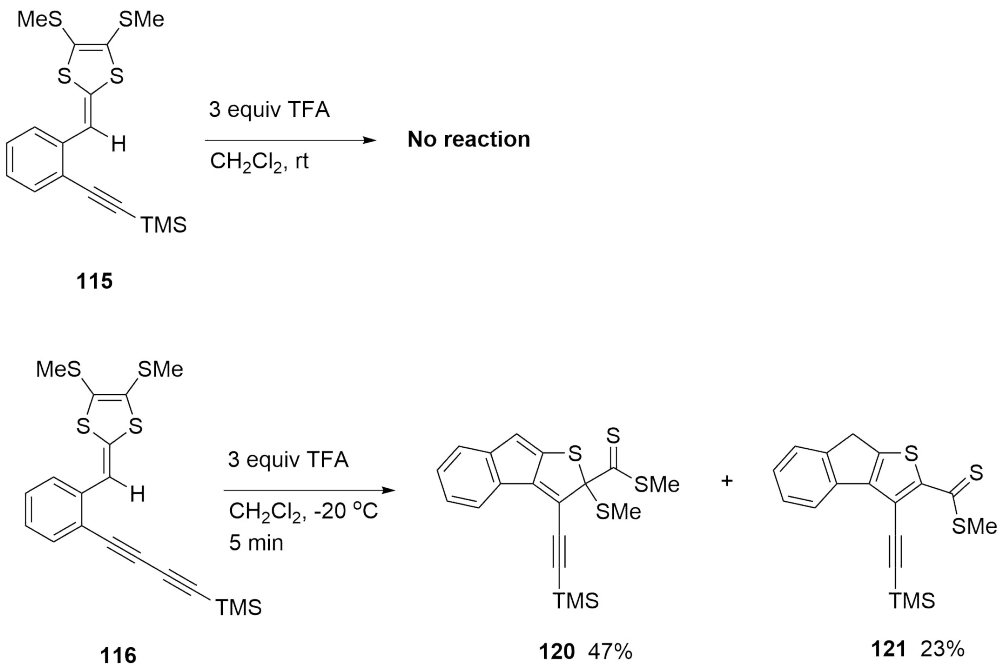

Scheme 4.4: TFA-promoted intramolecular cyclization of compound **115** and **116**.

To check whether this TFA-promoted intramolecular cyclization reaction would generally occur on *ortho* alkynyl substituted aryl-DTFs, two simple model compounds

115 and **116** were prepared and then subjected to TFA treatment in CH_2Cl_2 (see Scheme 4.4). Upon addition of an excess amount of TFA, the solution of compound **115** turned into a red color quickly at -20 °C. After 5 min, the mixture was worked up with aqueous $NaHCO_3$ and checked by TLC analysis. To our surprise, only the starting material **115** was observed and there was no indication of any other meaningful products. Increasing the reaction temperature to room temperature and prolonging the reaction time to 12 hours still led to the same result. Clearly, compound **115** lacks of the acid-promoted intramolecular cyclization reactivity.

Comparing the structures of compounds **115** and **117**, one can easily see that their alkynyl units are different in terms of π-conjugation degree. At this juncture, it was reasoned that the extended π-conjugation of the 1,3-butadiynylene segment of **117** exerted a key effect on the reactivity, most likely the key transition state(s) involved in the cyclization step would be stabilized by the extended π-conjugation at the alkynyl group resulting in lower activation energy barrier(s). This hypothesis is substantiated by the experimental observation that *ortho*-diyne substituted phenyl-DTF **116** was quickly consumed upon treatment with excess TFA in CH_2Cl_2 at -20 °C, yielding two compounds **120** and **121** as the major products at a molar ratio of ca. 2:1 as shown in Scheme 4.4. Both of the cyclized products were separated by silica column chromatography to yield samples pure enough for ^{1}H NMR analysis, based on which their molecular structures were determined. Mechanistically, compound **121** can be reasonably ascribed to the product of dethiomethylation of **120**, while this elimination step appears to more readily occur than in the case of compound **117**.

4.2.3 The Role of Iodine in Elimination of SMe

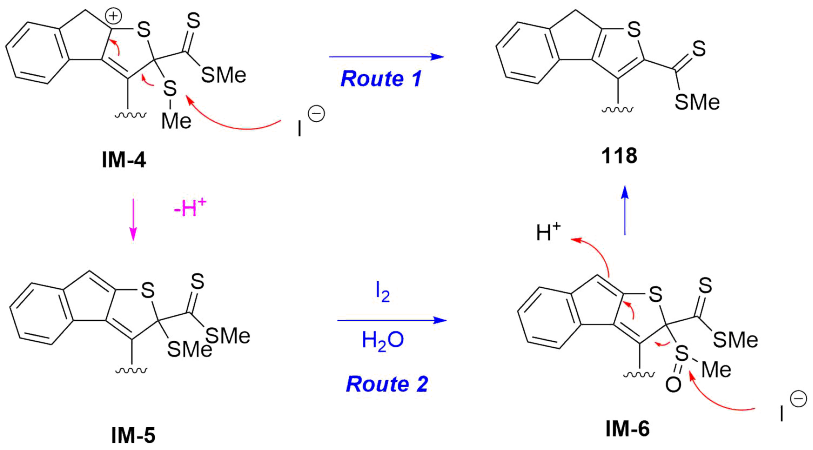

Scheme 4.5: Two plausible mechanisms proposed for the elimination of SMe group

In the reaction of compound **117** to form compound **118** shown in Scheme 4.2, iodine is believed to play a vital role in accelerating the dethiomethylation step as compared with the outcome of the TFA-promoted reaction in Scheme 4.1. The removal of the SMe group was proposed to occur through a simple elimination mechanism (shown as Route 1 in Scheme 4.5), in which iodide anion acts as a nucleophile to directly attack the SMe group. To validate whether this is a viable mechanism, a control reaction was conducted in which excess TFA and KI were co-added to the CH_2Cl_2 solution of **117**. The reaction was run at -20 °C for as long as 4 hours and monitored by TLC, but the TLC results showed no significant differences from the reaction with only TFA present. This observation suggested that Route 1 is not the actual dethiomethylation mechanism.

In an another control experiment, compound **117** was first treated with 6 equiv. of TFA in CH_2Cl_2 at -20 °C for 5 min. 1 equiv. of iodine was dissolved in CH_2Cl_2

and then added to the reaction mixture. The reaction was kept at -20 °C for another 10 min. After a reductive workup with aqueous $Na_2S_2O_3$, compound **118** was obtained with a 54% isolated yield. Compared with the reaction conducted in Yunfei Wang's work, the use of TFA in combination with iodine did make a remarkable improvement on both reaction rate and yield, hence offering a useful synthetic method for constructing complex indenothienyl motifs.[191–194]

The experimental results so far have confirmed that direct dethiomethylation cannot occur easily under non-oxidative conditions. The presence of an oxidant, such as iodine, plays an important role in this reaction.[195,196]Iodine has been known to induce the oxidation of thioether to form sulfoxide. Another elimination mechanism (shown as Route 2 in Scheme 4.5) is thus proposed. After the acid-promoted alkyne-dithiolium cyclization, oxidation of the -SMe group of **IM-5** ensues to afford compound **IM-6**. Conversion of the -SMe into sulfoxide leads to enhanced electrophilicity. Thus nucleophilic attack on it would readily produce the indenothiophene product compound **118**. The mechanism depicted in Route 2 agrees reasonably with the experimental observations and the known chemistry reported in the literature, but there is still lack of concrete evidence for this mechanism being the actual operative one. More systematic studies are warranted to gain deeper insight in this respect. Nevertheless, it is clear that oxidation of the cyclized intermediate(s) with iodine activates the dethiomethylation step. For the reaction of model compound **116** shown in Figure 4.4, the dethiomethylated product **121** was formed without the presence of any deliberately added oxidant. Since the reaction was run under open air, the elimination of -SMe in this case does not contradict the mechanism of Route 2. Oxygen diffused into the reaction solution is believed to act as an oxidant[197] to

facilitate the -SMe elimination in this case.

4.2.4 DFT Studies of the Intramolecular Alkyne-Dithiolium Cycloaddition

So far, the above investigations have disclosed several important aspects regarding the intramolecular alkyne-dithiolium cycloaddition. However, the experimental data cannot fully disclose the mechanistic details of the key cyclization process that transform the alkynyl-dithiolium intermediate into a fused tricyclic indenodihydrothiophene cation. As described in Scheme 4.3, the reaction from **IM-3** to **IM-4** can possibly follow two different cycloaddition mechanisms, stepwise and concerted cycloaddition. To find out which mechanism is more favored, density functional theory (DFT) calculations have been carried out in order to map out the detailed reaction pathways. Two model compounds **122** and **123** were utilized in the computational study to simulate the actual compounds **115** and **116** tested in our experimental work. Our computational study was only focused on the intermediates and transition states involved in the processes from the protonated phenyl-DTFs **122** and **123** to their corresponding indenodihydrothiophene cation intermediates.

Figure 4.2 shows the DFT calculated reaction pathways and energy profiles for the intramolecular cycloaddition of the monoyne-substituted dithiolium **122**. The reaction first overcomes a transition state **122-TS1** with an activation energy barrier of 28.1 kcal/mol, leading to a cage-like cationic intermediate **122-IM1**. The structure of **122-TS1** indicates a concerted asynchronous bond forming feature, wherein the distance between C1–C2 is significantly shorter than those of C3–C4 and C3—C5 (for

	122-TS1	**122-IM1**	**122-TS2**	**122-TS4**
C1-C2	1.83	1.51	1.54	1.37
C2-C3	1.26	1.44	1.38	1.46
C3-C4	2.79	1.56	2.00	1.55
C3-C5	2.79	1.56	1.53	1.53
C4-C5	1.37	1.49	1.48	1.49
C4-C7	1.73	1.83	1.73	1.81
C5-C6	1.73	1.83	1.84	1.85
C1-S6	1.79	1.85	1.83	1.86
C1-S7	1.79	1.85	1.90	2.46

Table 4.1: Selected bond distances (Å) for the transition states and intermediate involved in the intramolecular cycloaddition of compound **122**.

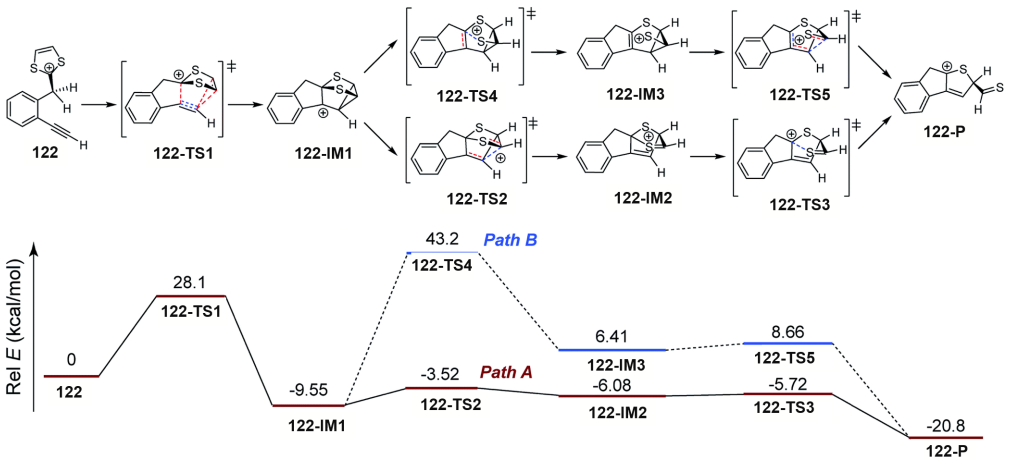

Figure 4.2: Calculated free energy profiles for steps involved in the intramolecular cycloaddition of compound **122**.

detailed bond distances, see Table 4.2.4). The C3–C4 and C3–C5 bond lengths are identical, rendering the transition state **122-TS1** planar symmetry. The development of the C1–C2 bond is associated with a notable distortion of the ditholium ring, allowing the π-bond of C4–C5 to have orbital interactions with the empty p-orbital of the C3 carbon. Natural bonding orbital (NBO) analysis[198,199]shows that the donor-acceptor orbital interactions between π(C4–C5) and p(C3) provide stabilization energy of 12.62 kcal/mol to the transition state. Transition state **122-TS1** is directly connected to a relatively stable intermediate **122-IM1** in which carbon atoms, C3, C4, and C5, are bonded to one another to form a three-membered ring.[200,201] Intermediate **122-IM1** is then subjected to sequential bond breaking at the C3–C4 and C1–S7 bonds to yield product **122-p**. Two reaction pathways (designated as paths A and B in Figure 4.2) were evaluated by the DFT calculations. In path A, the first step is C3–C4 bond cleavage going through transition state **122-TS2**, while path B begins with the breaking of C1–S7 bond first. Path A is the favoured one,

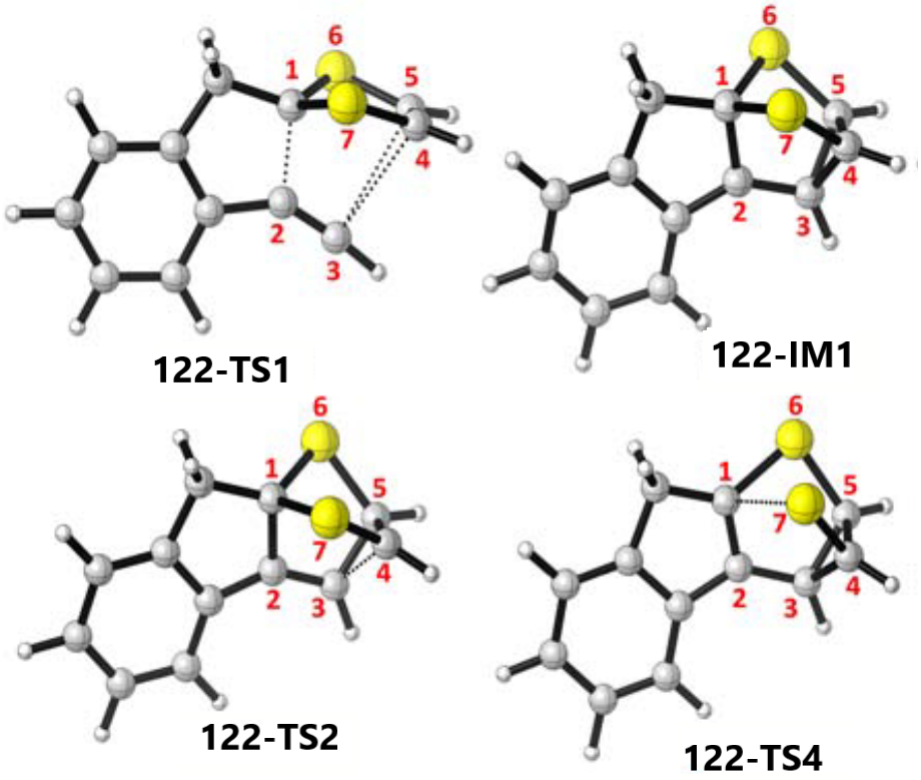

Figure 4.3: Structures of selected transition states and intermediate involved in the intramolecular cycloaddition of compound **122**.

since it has an energy barrier (6.03 kcal/mol) much lower than that of path B (52.75 kcal/mol).

The mechanistic details for the intramolecular cycloaddition of diyne-substituted dithiolium **123** are depicted in Figure 4.4. In contrast to the reaction mechanism of monoyne **122**, compound **123** undergoes the cycloaddition in a sequential manner.

In the first step, the C2–C3 alkynyl group attacks the C1 carbocation of the dithiolium ring, leading to a cationic intermediate **123-IM1**. This is a mechanism typical of the Prins-type cyclization reactions.[182–187] The transition state of this process **123-TS** clearly reveals a σ bond developing between C1–C2 , but the

	123-TS1	**123-IM1**	**123-TS2**	**123-TS4**
C1-C2	1.84	1.63	1.58	1.51
C2-C3	1.27	1.30	1.32	1.45
C3-C4	3.60	3.01	2.48	1.58
C3-C5	3.65	3.01	2.48	1.58
C4-C5	1.35	1.37	1.39	1.48
C4-C7	1.74	1.74	1.74	1.82
C5-C6	1.74	1.74	1.74	1.82
C1-S6	1.79	1.82	1.84	1.85
C1-S7	1.78	1.82	1.84	1.85
C3-C7	1.33	1.33	1.35	1.43
C7-C8	1.23	1.23	1.22	1.21

Table 4.2: Selected bond distances (Å) for the transition states and intermediate involved in the intramolecular cycloaddition of compound **123**

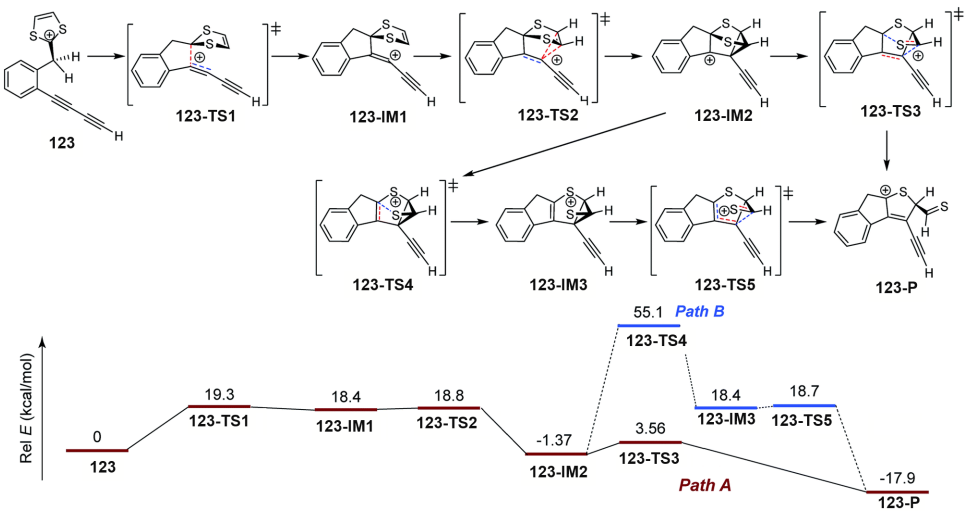

Figure 4.4: Calculated free energy profiles for steps involved in the intramolecular cycloaddition of compound **123**.

distances at C3–C4 and C3–C5 (3.60 Åand 3.65 Å) are, in contrast to the case of compound **122**, beyond the van der Waals contact distance and hence indicate little covalent interaction. NBO analysis shows that in transition state **123-TS1** there is an alkenyl carbocation character developing on C3, which is stabilized by the neighboring alkynyl group (C7–C8) through a π-conjugation effect. The donor-acceptor orbital interactions in **123-TS1** are calculated to deliver 55.50 kcal/mol of stabilization energy. The presence of such a resonance effect allows the transition state to avert further bending of the dithiolium ring to achieve π(C4–C5)–p(C3) interactions as occurring in the case of monoyne **122-TS**. Indeed, the stabilizing effect by the extra alkynyl group significantly lowers the energy barrier for the cyclization of diyne **123** by 8.8 kcal/mol in comparison with that of monoyne **122**.

After transition state **123-TS1**, the reaction then moves to a cationic intermediate **123-IM1**, the structure of which possesses a mirror symmetry plane bisecting the dithiolium ring. The C3–C4 and C3–C5 distances become identical at this stage

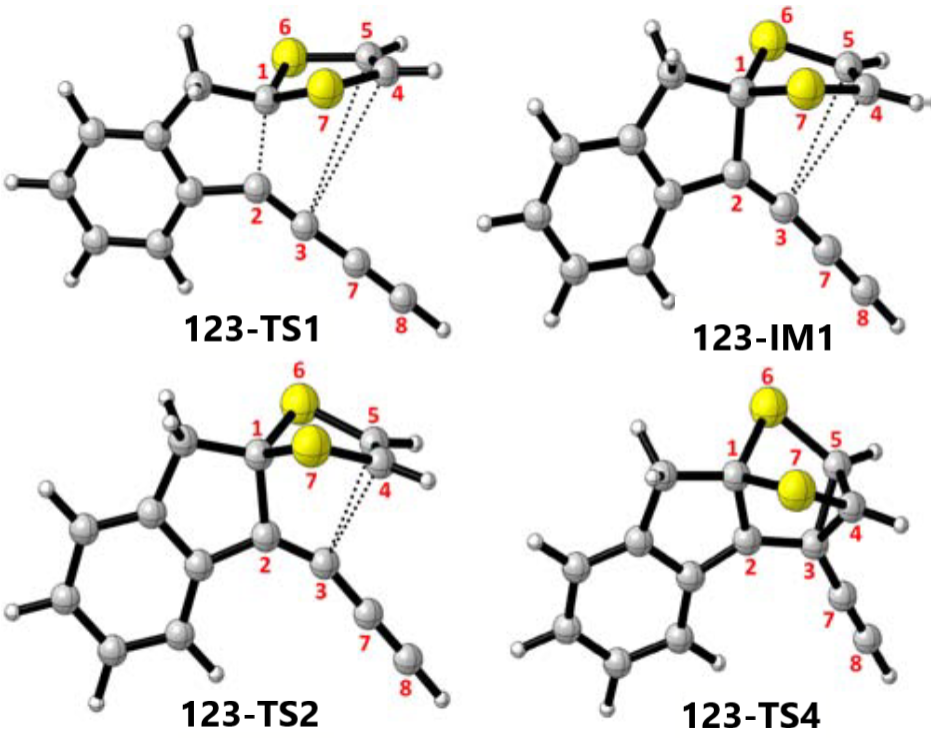

Figure 4.5: Structures of selected transition states and intermediate involved in the intramolecular cycloaddition of compound **123**.

(3.01 Å) and they are within the van der Waals contact distance. Intermediate **123-IM1** undergoes another transition state **123-TS2** in which the dithiolium ring is bent towards the C3 carbon to allow orbital interactions between π(C4–C5) and p(C3). Essentially, the second transition state **123-TS2** leads to a relatively stable intermediate **123-IM2**. It is worth noting that the potential energy surface connecting the three stationary points (**123-TS1**, **123-IM1**, and **123-TS2**) is very shallow, with their Gibbs free energies differing by less than 1.0 kcal/mol. This energetics feature suggests that intermediate **123-IM1** would be formed at a very fast rate once the first transition state **123-TS1** decomposes. Although it is theoretically predicted to be a stepwise cycloaddition mechanism, experimental exploration of this

mechanism would be very challenging. The second intermediate **123-IM2** possesses a cage-like structure similar to that of **123-IM1**, and from this point the reaction path is bifurcated. In the first approach (Path A, Figure 4.4, bond breaking at C3–C4 takes place to generate a transition state **123-TS3** ($\Delta G^{\ddagger}$ =5.93 kcal/mol), through which the product **123-P** is directly formed. The second pathway begins with bond breaking at C1–S7 first, which is energetically more demanding ($\Delta G^{\ddagger}$ = 56.47 kcal/mol) and therefore not likely to happen in the actual reaction.

The DTF investigations on the two model compounds **122** and **123** have yielded two different mechanisms for the intramolecular alkyne-dithiolium cycloaddition, concerted and stepwise. In the case of monoyne **122**, a concerted cycloaddition transition state is necessary to gain stabilization from the orbital interactions between the C=C π bond (donor) of the dithiolium and the empty p orbital (acceptor) on its alkyne counterpart. To arrive at the concerted transition state, the dithiolium ring is distorted which hence raises the strain energy within the molecule. The energy cost here makes the energy barrier relatively high and not so easy to overcome. It also accounts for the asynchronicity in the bond forming process. For diyne **123** the energetically demanding concerted transition state is averted owing to the contribution of the additional C–C triple bond. Through a resonance effect, the alkynyl p orbital offers stabilization to a Prins-type cyclization transition state that does not suffer from much strain energy as well. The theoretical results concur with the experimental observation that the diyne was much easier to cyclize than monoyne. With the theoretical models, it is also reasonable to assume that alkynyl groups directly connected to other pi-units (alkenes, arenes, etc.) should also have enhanced reactivity due to similar resonance effects. Further investigations on the

intramolecular cycloaddition between dithiolium and other 1,3-dipolarophiles are current underway.

4.3 Experimental Procedures

Chemicals were purchased from commercial suppliers and used directly without purification. All reactions were conducted in standard, dry glassware and under air. Evaporation and concentration were carried out with a rotary evaporator. Flash column chromatography was performed with 240-400 mesh silica gel, and thin-layer chromatography (TLC) was carried out with silica gel F254 covered on plastic sheets and visualized by UV light. ^{1}H and ^{13}C NMR spectra were measured on a Bruker Avance III 300 MHz multinuclear spectrometer. Chemical shifts (δ) are reported in ppm downfield relative to the signals of the internal reference $SiMe_4$ or residual solvents ($CHCl_3$: H = 7.24 ppm, C =77.2 ppm; CH_2Cl_2: H = 5.32 ppm, C = 54.0 ppm). Coupling constants (J) are given in Hz. Infrared spectra (IR) were recorded on a Bruker Alfa spectrometer. High resolution APCI-TOF MS analysis was done on a GCT premier Micromass Technologies instrument. Compounds **115** and **117**were prepared by the methods we reported previously.

Synthesis of 118

Compound **117** (0.22 g, 0.36 mmol) was dissolved in CH_2Cl_2 (25 mL) and the solution cooled down to -20 °C. To this solution was added TFA (0.25 g, 1.4 mmol, 0.17 mL) dropwise. The solution was observed to quickly change its color from yellow to dark red. The mixture was stirred at -20 °C for 5 min, then a solution of iodine (0.091 g, 0.36 mmol) dissolved in CH_2Cl_2 (10 mL) was slowly added into

the reaction vessel through an addition funnel. After the addition of TFA was complete, the reaction was stirred at -20 °C for another 10 min. The reaction mixture was then quenched by a saturated aqueous $NaHCO_3$ solution and a saturated aqueous $Na_2S_2O_3$ solution. The organic layer was separated, dried over anhydrous $MgSO_4$, and evaporated under vacuum. The residue was subjected to silica column chromatography (CH_2Cl_2/hexanes, 2:3) to afford compound **118** (0.12 g, 0.19 mmol, 54%) as a red solid. The ^{1}H and ^{13}C NMR data were consistent with those reported previously.

Synthesis of 119

Compound **117** (21 mg, 0.034 mmol) was dissolved in CH_2Cl_2 (5 mL) and the solution was cooled down to -20 °C. To this solution was added TFA (12 mg, 0.10 mmol, 0.0081 mL) dropwise via a microsyringe. The solution was observed to quickly change its color from yellow to dark red. The mixture was stirred at -20 °C for another 5 min and then quenched by a saturated aqueous $NaHCO_3$ solution (30 mL). The organic layer was separated, dried over anhydrous $MgSO_4$, and evaporated under vacuum. The residue was subjected to silica column chromatography (CH_2Cl_2/hexanes, 2:3) to afford compound **119** (17 mg, 0.028 mmol, 81%) as a red solid. ^{1}H NMR (300 MHz, $CDCl_3$) d 7.96 (d, J = 6.7 Hz, 1H), 7.59 (d, J = 7.0 Hz, 1H), 7.42 (d, J = 1.1 Hz, 1H), 7.39 (d, J = 1.6 Hz, 1H), 7.22–7.09 (m, 4H), 6.26 (s, 1H), 2.67 (s, 3H), 2.48 (s, 3H), 2.42 (s, 3H), 2.15 (s, 3H) ppm; ^{13}C NMR (75 MHz, $CDCl_3$) 214.8, 157.1, 154.6, 149.0, 147.2, 138.2, 128.6, 127.2, 125.4, 125.0, 120.3, 120.1, 112.9, 111.5, 108.2, 100.5, 47.6, 35.5, 34.2, 30.2, 23.5, 21.1, 17.8, 16.0, 14.6, 10.9, 0.5 ppm; FTIR (neat) 3052, 2986, 2915, 2184, 1561, 1396, 1263 cm^{-1}; HRMS (APPI-TOF, positive mode) m/z calcd for $C_{28}H_{22}S_8$ 613.9487, found 614.9501

$[M + H]^+$.

Synthesis of 116

Compound **116** was prepared from compound **115** reacted with excess amount of TMEDA. Compound **116** (0.18 g, 0.53 mmol) and K_2CO_3 (0.22 g, 1.6 mmol) were mixed in THF/methanol (15 mL /15 mL) and stirred at room temperature for 30 min. After the reaction, the solvent was removed by the rotary evaporator to obtain a yellow powder. The residual was dissolved in CH_2Cl_2 (40 mL), washed with H_2O and dried with anhydrous $MgSO_4$ for 20 min. The $MgSO_4$ was then removed by filtration. CuI (0.30 g, 1.6 mmol) and TMEDA (0.25 g, 2.1 mmol, 0.32 mL) were dissolved in CH_2Cl2 (10 mL). After all CuI was dissolved, the mixed solution was slowly added into the previous solution from the hydrolysis. The TMSA (0.73 g, 7.4 mmol, 1.056 mL) was added dropwise into the solution. The mixture was stirred under air at room temperature overnight. The solution was washed with H_2O and dried with anhydrous $MgSO_4$. The $MgSO_4$ was removed by filtration and the solvent was removed by rotary evaporator. The crude product was purified by silica column chromatography (ethyl acetate/hexane, 1:49) to obtain yellow oil-like compound **116** (0.066 g, 0.18 mmol , 34%). ^{1}H NMR (300 MHz, $CDCl_3$) δ 7.49 (dd, J = 7.7, 1.9 Hz, 1H), 7.41–7.30 (m, 2H), 7.10 (dd, J = 14.3, 2.0 Hz, 1H), 6.92 (s, 1H), 2.44 (d, J = 16.1 Hz, 6H), 2.44 (d, J = 16.1 Hz, 6H), 0.25 (s, 9H) ppm; ^{13}C NMR (75 MHz, $CDCl_3$) δ 139.6, 136.0, 134.5, 129.7, 128.5, 125.9, 125.5, 119.6,112.6, 92.4, 88.2, 19.5, 19.3 ppm; FTIR (neat) 3054, 2955, 2971, 2198, 2096, 1943, 1697, 1560, 1550, 1489, 1417, 1246 cm^{-1}; HRMS (APPI-TOF, positive) m/z calculated for $C_{19}H_{20}S_4Si$ 404.0217, found 405.0290 $[M + H]^+$.

Synthesis of 120 and 121

Compound **116** (0.029 g, 0.078 mmol) was dissolved in CH_2Cl_2 (5 mL) to form a dark brown solution. The mixture was cool down to -20 °C. Then TFA (0.027 g, 0.23 mmol, 0.018 mL) was added dropwise into the solution, the solution turns into red immediately once the TFA was added. The reaction was followed by TLC. All the starting material was reacted after 5 mins. The excess amount of TFA was removed by saturated $NaHCO_3$ solution (30 mL), and the product was dried with anhydrous $MgSO_4$ for 20 min. The $MgSO_4$ was removed by filtration and solvent removed using a rotars evaporator. The crude product was adark red powder and was further purified by the silica column chromatography (CH_2Cl_2/hexane, 1:2) to give two major product compound **120** (0.014 g, 47%) ^{1}H NMR (300 MHz, $CDCl_3$) δ 7.96 (d, J = 8.0 Hz, 1H), 7.60 (d, J = 8.1 Hz, 1H), 7.34 (d, J = 33.6 Hz, 2H), 4.83 (s, 1H), 2.80 (s, 3H), 1.61 (s, 3H), 0.37 (s, 9H) ppm; ^{13}C NMR (75 MHz, $CDCl_3$) δ 214.7, 177.1, 154.6, 147. 2, 138.2, 128.5, 127.2, 125.4, 120.1, 108.2, 106.1, 100.5, 47.6, 30.2, 21.1, 10.9, 0.5 ppm; FTIR (neat) 2954, 2918, 2851, 2147, 1390, 1259, 1180 cm^{-1}; HRMS (APPI-TOF, positive) *m/z* calculated for $C_{19}H_{20}S_4Si$ 404.0217, found 405.0282 $[M + H]^+$; and compound **121** (0.0058 g, 23%) ^{1}H NMR (300 MHz, $CDCl_3$) δ 8.04 (d, J = 7.5 Hz, 1H), 7.48 (d, J = 7.4 Hz, 1H), 7.37 (t, J = 7.0 Hz, 1H), 7.29 (d, J = 1.2 Hz, 1H), 7.24 (d, J = 1.2 Hz, 1H), 3.83 (s, 2H), 2.80 (s, 3H), 0.37 (s, 9H); ^{13}C NMR (75 MHz, $CDCl_3$) δ 214.8, 152.3, 145.9, 138.8, 127.4, 126.3, 125.1, 120.20, 113.1, 108.1, 100.8, 100.4, 35.6, 30.1, 21.0, 0.4 ppm; FTIR (neat) 3047, 2955, 2852, 2144, 1465, 1384, 1310, 1261, 1180, 1161cm^{-1}; HRMS (APPI-TOF, positive) *m/z* calculated for $C_{18}H_{18}S_3Si$ 358.0340, found 359.0382 $[M + H]^+$.

4.4 Computational Details

The molecular structures of the reactants, transitions states, and intermediates were optimized by the DFT calculations at the B3LYP level of theory.[202,203] The 6-31+G(d) basis set[204] was used for all atoms. Frequency calculations were performed at the same level of theory to identify all the stationary points as energy minima (zero imaginary frequencies) or transition states (one imaginary frequencies). An IRC analysis was performed to confirm that all the stationary points were smoothly connected to one another. All the DFT calculations were performed using the Gaussian 09 D.01 package, and Natural Bond Orbital (NBO) analysis was done using the NBO6 module included in the Gaussian 09 D.01 package.[205] The optimized molecular structures were plotted using CYLview[206] and the natural bond orbitals were visualized by GaussView 5.

Chapter 5

Conclusions

Overall, this thesis work mainly addresses the synthesis and properties of a certain class of polyarene-based π-conjugated systems, which show interesting photochemical and redox properties. Detailed conclusions are summarized as follows:

In Chapter 2, a series of Ar_4-AQs was synthesized and characterized. Their detailed photocyclization reactivity and mechanisms were investigated by NMR analysis. DDQ was proven to be an efficient promoter for the photocyclodehydrogenation of most Ar_4-AQs. However, for electron-donor substituted Ar_4-AQs, intramolecular charge transfer reactions could occur between electron-donor substituted Ar_4-AQs and DDQ, which hinder the photocyclization pathway. For the tetrachloro-substituted Ar_4-AQ, PCDHC was observed to occur much faster than photocyclodehydrogenation when there was no base to participate in the reaction. When there was a base present, only PCDHC was observed. Also, this part of my investigation for the first time demonstrates that photocyclodehydrogenation of Ar_4-AQ units embedded in solid-state polymer

networks is possible. The finding offers opportunities for the design and development of photo-responsive solid state materials in our future work.

In Chapter 3, a new class of cross-linked polymer networks using Ph_4–AQ **98** and *p*-phenylenediamine as building blocks was designed and investigated. The new class of cross-linked polymer networks was synthesized through Schiff base condensation. Experimental results showed that the quality of the resulting cross-linked polymers was greatly affected by reaction conditions, such as reaction temperature, heating method, and reaction time. The reaction conditions need to be carefully controlled to obtain ordered crystalline microporous networks. Moreover, The polymerization reactions between compound **98** and *m*-phenylenediamine/*o*-phenylenediamine did not produce good-quality cross-linked polymers. It has been confirmed that the molecular shape of the diamine building block is another key factor to the formation of microporous polymer networks.

In Chapter 4, the detailed mechanism of an intramolecular alkyne–dithiolium cycloaddition was investigated by a joint theoretical and experimental approach. Experimental results indicated that protonation on the vinyl group adjacent to the dithiole ring is an indispensable step to activate the dithiole group to form a reactive dithiolium ion. DFT calculations showed that two model compounds **122** and **123** undergo two different mechanisms for the intramolecular alkyne-dithiolium cycloaddition; that is, concerted and stepwise mechanisms. In the case of monoyne **122**, the reaction undergoes a concerted cycloaddition transition state to gain stabilization from the orbital interactions between the C=C π bond of the dithiolium and the empty p orbital on its alkyne counterpart. The dithiolium ring is bent to a certain extent in order to form the concerted transition state and hence

raises the strain energy within the molecule. Thus the energy barrier in this case is relatively high. For the case of diyne **123**, the energetically demanding concerted transition state is averted owing to the contribution of the additional C–C triple bond. Through the resonance effect, the alkynyl p orbital offers stabilization to a Prins-type cyclization transition state that does not suffer from significant strain energy as well. The theoretical results concur with the experimental observation that the diyne was much easier to cyclize than the monoyne. With the theoretical models, it is also reasonable to assume that alkynyl groups directly connected to other p-units (alkenes, arenes, etc.) should also have enhanced reactivity due to similar resonance effects.

Chapter 6

Perspectives

After the first discovery of TTF-based organic conductors by Fred Wudl and co-workers in 1970, TTF has attracted enormous attention in materials science and technology.[76] In the family of TTFs, a class of π-extended TTF analogues, namely TTFVs, are excellent organic electron donors and widely used as redox-active building blocks in various π-conjugated systems in the past ten years.[113–120,127,135,165–173] There has been lots of TTFV-based π-conjugated molecular and macromolecular materials reported over the past few years, such as stimuli-responsive conjugated polymers, fluorescent molecular tweezers, redox-active ligands, shape-persistent macrocycles, molecular rotors.[82,141,174–176]. Most of these TTFV polymers were prepared through Sonogashira cross-coupling or other coupling reactions. As mentioned in Chapters 1 and 4, TTFVs can be obtained from dithiafulvenes through a straightforward oxidative dimerization reaction.[128,136–140] However, TTFV polymers prepared from the oxidative dimerization reaction are rare. This may because that as the size of the polymer grows, the radical cation intermediates become stabilized by the resonance.

Thus preparation of large TTFV polymers by oxidative dimerization reaction is rather difficult.

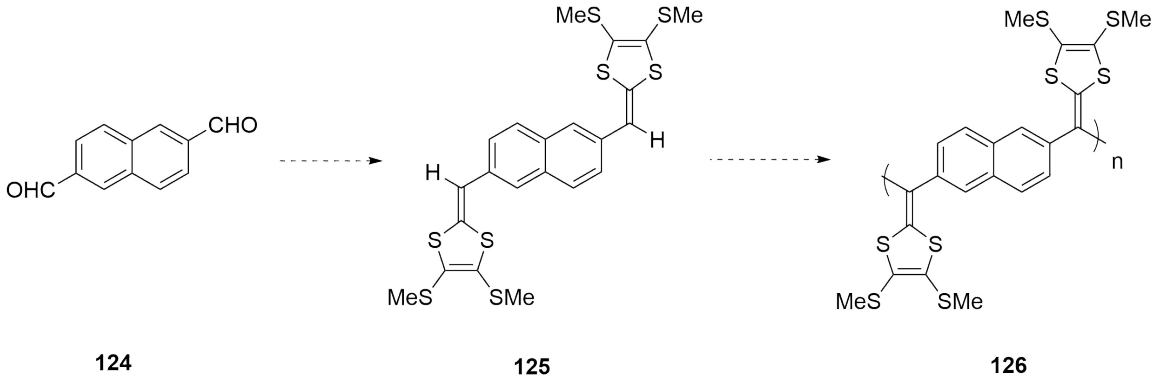

124 **125** **126**

Scheme 6.1: TTFVs polymers prepared from the oxidative dimerization reaction.

As shown in Scheme 6.1, a TTFV-naphthalene co-polymer **126** is expected to be produced from oxidative polymerization of precursor **125**. In the literature, a synthetic method for the dialdehyde compound **124** has been reported. With **124**, an olefination reaction with thione can possibly yield compound **125**. Preliminary efforts toward this synthesis were made, in which compound **124** and 2.5 equiv of thione were dissolve in $P(OMe)_3$, stirred and heated at 110 °C. The reaction was monitored by TLC and MS analysis. TLC results showed that a very polar compound was formed during the reaction, and MS data confirmed that only 1 equiv of the thione was reacted with the dialdehyde to form the mono-olefinated product. Reaction of a second equiv of thione reacted was found to be very difficult. Modifications of reaction temperature, reaction time, and use of $P(OEt)_3$ instead of $P(OMe)_3$ have been tried, but the results showed only minor differences. Overcoming this problem is a worthy target for the future work.

As discussed in Chapter 4, monoyne compound **122** and diyne compound **123**

can undergo unusual intramolecular alkyne-dithiolium cycloaddition. Based on these results, an interesting research topic arises; that is, will longer polynes (e.g., triyne, tetrayne) undergo similar reaction?

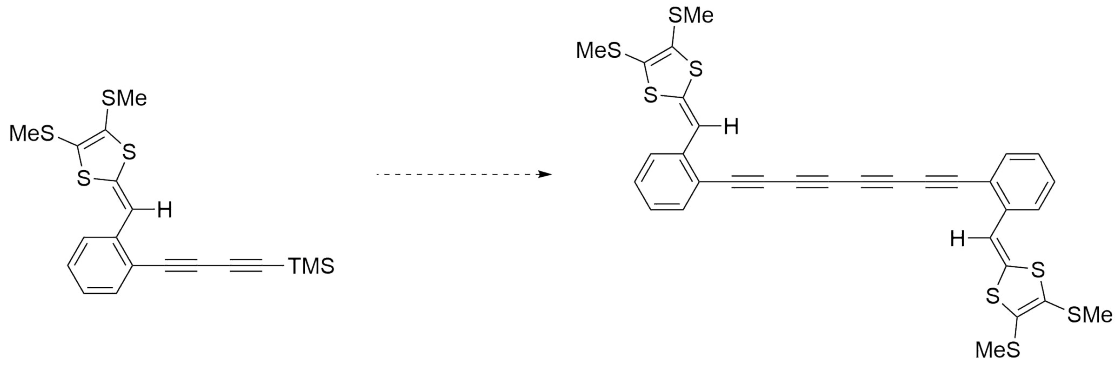

116 **127**

Scheme 6.2: Attempted synthesis of tetrayne compound **127** from diyne precursor **116**.

As shown in Scheme 6.2, preparation of tetrayne compound **127** was attempted starting with diyne compound **116** by Cu(I)-mediated homocoupling reaction. In the experiment, compound **116** and K_2CO_3 were dissolved in a mixed solvent of THF/MeOH and stirred at rt for 20 min. The reaction mixture was then concentrated under vacuum. The residue was dissolved in CH_2Cl_2, washed with H_2O, dried with anhydrous $MgSO_4$ and filtered to remove inorganic salts. CuI was dissolved in CH_2Cl_2, added to the organic layer and stirred for 5 h. Then the mixture was washed with H_2O, dried with anhydrous $MgSO_4$, and concentrated under vacuum. The crude product was purified by silica column chromatography to give homocoupled product **127** as a pale brown solid. However the product was found to be unstable. It decomposed quickly after purification, yielding a dark purple colored solid. The reason

for the instability is likely due to the facile solid-state topochemical polymerization of tetraynes. So, in future work, the issue of stability of **127** needs to be addressed. One possible solution to this problem is to keep the tetrayne product in the solution phase to prevent quick decomposition.

Finally, one of the objectives of this thesis work is to explore the possibility of synthesizing TBC derivatives by photocyclization of the corresponding Ar_4-AQs. TBC-based molecules are very interesting π-conjugated materials and have intriguing application in advanced electronic devices such as organic semiconductors. So far, all the Ar_4-AQ compounds examined in this thesis work underwent photocyclization to give only half-cyclized products. How to further promote the photocyclization to yield TBC products is still a challenging task and need more investigations. It is believed that better understanding of the detailed photochemical mechanisms of the photocyclization of Ar_4-AQs will of great benefit to the future work in this direction.

Bibliography

[1] Wu, J.; Pisula, W.; Müllen, K. Graphenes as potential material for electronics. *Chem. Rev.*, **2007**, *107*, 718–747.

[2] Goh, S. H.; Harvey, R. G. K-region arene oxides of carcinogenic aromatic hydrocarbons. *J. Am. Chem. Soc.*, **1973**, *95*, 242–243.

[3] Harvey, R. G.; Zhang, J.-T.; Luna, E.; Pataki, J. Synthesis of benzo[s]picene and its putative carcinogenic trans-3,4-dihydrodiol and fjord region anti-diol epoxide metabolites. *J. Org. Chem.*, **1998**, *63*, 6405–6408.

[4] Scholl, R.; Seer, C.; Weitzenböck, R. Perylen, ein hoch kondensierter aromatischer kohlenwasserstoff $C_{20}H_{12}$. *Chem. Ber.*, **1910**, *43*, 2202–2209.

[5] Scholl, R.; Seer, C. Liebigs ann. 394, 111 (1912). *Mh. Chem.*, **1912**, *33*, 1.

[6] Scholl, R. Annalen 1912, 394, 111.(c) scholl, r.; seer, c. *Chem. Ber.*, **1912**, *55*, 330–341.

[7] Clar, E.; Stewart, D. G. Aromatic hydrocarbons. lxv. triangulene derivatives1. *J. Am. Chem. Soc.*, **1953**, *75*, 2667–2672.

[8] Clar, E.; others. Localised vs delocalised molecular orbitals in aromatic hydrocarbons. *Tetrahedron*, **1979**, *35*, 2673–2680.

[9] Lawal, T. Polycyclic aromatic hydrocarbons. a review. *Cogent Environ. Sci.*, **2017**, *3*, 1339841.

[10] Miquel Solà. Forty years of clar's aromatic π-sextet rule. *Frontiers in chemistry*, **2013**, *1*, 22.

[11] Novoselov, K. S.; Geim, A. K.; Morozov, S. V.; Jiang, D.; Zhang, Y.; Dubonos, S. V.; Grigorieva, I. V.; Firsov, A. A. Electric field effect in atomically thin carbon films. *Science*, **2004**, *206*, 666–669.

[12] Zhong, M.; Xu, D.; Yu, X.; Huang, K.; Liu, X.; Qu, Y.; Xu, Y.; Yang, Deren. Interface coupling in graphene/fluorographene heterostructure for high-performance graphene/silicon solar cells. *Nano Energy*, **2016**, *28*, 12–18.

[13] Sundar, V. C.; Zaumseil, J.; Podzorov, V.; Menard, E.; Willett, R. L.; Someya, T.; Gershenson, M. E.; Rogers, J. A. Elastomeric transistor stamps: reversible probing of charge transport in organic crystals. *Science*, **2004**, *303*, 1644–1646.

[14] O'Neill, M.; Kelly, S. M. Liquid crystals for charge transport, luminescence, and photonics. *Adv. Mater.*, **2003**, *15*, 1135–1146.

[15] Sirringhaus, H. Device physics of solution-processed organic field-effect transistors. *Adv. Mater.*, **2005**, *17*, 2411–2425.

[16] Martin, R. E.; Diederich, F. Linear monodisperse π-conjugated oligomers:

Model compounds for polymers and more. *Angew. Chem., Int. Ed.*, **1999**, *38*, 1350–1377.

[17] Pisula, W.; Tomović, Ž.; Simpson, C.; Kastler, M.l; Pakula, T.; Müllen, K. Relationship between core size, side chain length, and the supramolecular organization of polycyclic aromatic hydrocarbons. *Chem. Mater.*, **2005**, *17*, 4296–4303.

[18] Beeson, J. C.; Fitzgerald, L. J.; Gallucci, J. C.; Gerkin, R. E.; Rademacher, J. T.; Czarnik, A. W. π-complexation in the solid state induced by intermolecular hydrogen bonding. *J. Am. Chem. Soc.*, **1994**, *116*, 4621–4622.

[19] Gearba, R. I.; Lehmann, M.; Levin, J.; Ivanov, D. A.; Koch, M. H. J.; barbera, j.; debije, mg; piris, j.; geerts, yh. *Adv. Mater*, **2003**, *15*, 1614–1618.

[20] Liu, C.; Bard, A. J. Pressure-induced insulator–conductor transition in a photoconducting organic liquid-crystal film. *Nature*, **2002**, *418*, 162.

[21] Warman, J. M.; Piris, J.; Pisula, W.; Kastler, M.; Wasserfallen, D.; Müllen, K. Charge recombination via intercolumnar electron tunneling through the lipid-like mantle of discotic hexa-alkyl-hexa-p eri-hexabenzocoronenes. *J. Am. Chem. Soc.*, **2005**, *127*, 14257–14262.

[22] Wu, J.; Baumgarten, M.; Debije, M. G.; Warman, J. M.; Müllen, K. Arylamine-substituted hexa-peri-hexabenzocoronenes: Facile synthesis and their potential applications as "coaxial" hole-transport materials. *Angew. Chem., Int. Ed.*, **2004**, *43*, 5331–5335.

[23] Alibert F. S.; Seguy, I.; Bobo, J.and Destruel, P.; Bock, H. Liquid-crystalline and electron-deficient coronene oligocarboxylic esters and imides by twofold benzogenic diels–alder reactions on perylenes. *Chem.: Eur. J.*, **2007**, *13*, 1746–1753.

[24] Shen, H., Tang J.; Chang, H.; Yang, C.; Liu, R. Short and efficient synthesis of coronene derivatives via ruthenium-catalyzed benzannulation protocol. *J. Org. Chem*, **2005**, *70*, 10113–10116.

[25] Rieger, R.and Kastler, M.and Enkelmann, V.; Müllen, K. Entry to coronene chemistry—making large electron donors and acceptors. *Chem.: Eur. J.*, **2008**, *14*, 6322–6325.

[26] C. T. Clar, E.; Ironside. *Proc. Chem. Soc.*, **1958**, 150.

[27] C. T.; Zander M. Clar, E.; Ironside. *J. Chem. Soc.*, **1959**, 142.

[28] R. H.; King GSD. Halleux, A.; Martin. Synthèses dans la série des dérivés polycycliques aromatiques hautement condensés. l'hexabenzo-1, 12; 2, 3; 4, 5; 6, 7; 8, 9; 10, 11-coronène, le tétrabenzo-4, 5; 6, 7; 11, 12; 13, 14-péropyrène et le tétrabenzo-1, 2; 3, 4; 8, 9; 10, 11-bisanthène. *Helv. Chim. Acta*, **1958**, *41*, 1177–1183.

[29] Hendel, W.; Khan, Z. H.; Schmidt, W. Hexa-peri-benzocoronene, a candidate for the origin of the diffuse interstellar visible absorption bands. *Tetrahedron*, **1986**, *42*, 1127–1134.

[30] Iyer, V. S.; Yoshimura, K.; Enkelmann, V.; Epsch, R.; Rabe, J. P.; Müllen, K. Ein löslicher C_{60}-graphitausschnitt. *Angew. Chem.*, **1998**, *110*, 2843–2846.

[31] Simpson, C. D.; Wu, J.and Watson, M. D.; Müllen, K. From graphite molecules to columnar superstructures–an exercise in nanoscience. *J. Mater. Chem.*, **2004**, *14*, 494–504.

[32] Watson, M. D.; Fechtenkötter, A.; Müllen, K. Big is beautiful-"aromaticity" revisited from the viewpoint of macromolecular and supramolecular benzene chemistry. *Chem. Rev.*, **2001**, *101*, 1267–1300.

[33] Wu, J.; Watson, M. D.; Tchebotareva, N.; Wang, Z.; Müllen, K. Oligomers of hexa-peri-hexabenzocoronenes as "super-oligophenylenes": Synthesis, electronic properties, and self-assembly. *J. Org. Chem.*, **2004**, *69*, 8194–8204.

[34] Megahed, S.and Scrosati, B. Lithium-ion rechargeable batteries. *J. Power Sources*, **1994**, *51*, 79–104.

[35] Müller, M.; Iyer, V. S.; Kübel, C.; Enkelmann, V.; Müllen, K. Polycyclische aromatische kohlenwasserstoffe durch cyclodehydrierung und gerüstumlagerung von oligophenylenen. *Angew. Chem.*, **1997**, *109*, 1679–1682.

[36] Wasserfallen, D.; Kastler, M.; Pisula, W.; Hofer, W. A.; Fogel, Y.; Wang, Z.; Müllen, K. Suppressing aggregation in a large polycyclic aromatic hydrocarbon. *J. Am. Chem. Soc.*, **2006**, *128*, 1334–1339.

[37] Fleming, A. J.; Coleman, J. N.; Dalton, A. B.; Fechtenkötter, A.; Watson, M. D.; Müllen, K.; Byrne, H. J.; Blau, W. J. Optical spectroscopy of isolated and

aggregate hexabenzocoronene derivatives: A study of self-assembling molecular nanowires. *J. Phys. Chem. B*, **2003**, *107*, 37–43.

[38] Bayer, A.; Hübner, J.; Kopitzke, J.; Oestreich, M.; Rühle, W.; Wendorff, J. H. Time-resolved fluorescence in 3-dimensional ordered columnar discotic materials. *J. Phys. Chem. B*, **2001**, *105*, 4596–4602.

[39] Marguet, S.; Markovitsi, D.; Millie, P.; Sigal, H.; Kumar, S. Influence of disorder on electronic excited states: an experimental and numerical study of alkylthiotriphenylene columnar phases. *J. Phys. Chem. B*, **1998**, *102*, 4697–4710.

[40] Wu, J.and Fechtenkötter, A.; Gauss, J.; Watson, M. D.; Kastler, M.; Fechtenkötter, C.; Wagner, M.; Müllen, K. Controlled self-assembly of hexa-peri-hexabenzocoronenes in solution. *J. Am. Chem. Soc.*, **2004**, *126*, 11311–11321.

[41] Ball, M.; Zhong, Y.; Wu, Y.; Schenck, C.; Ng, F.; Steigerwald, M.; Xiao, S.; Nuckolls, C. Contorted polycyclic aromatics. *Acc. Chem. Res.*, **2014**, *48*, 267–276.

[42] Xiao, S.nd Myers, M.; Miao, Q.; Sanaur, S.; Pang, K.; S., Michael L.; Nuckolls, C. Molecular wires from contorted aromatic compounds. *Angew. Chem., Int. Ed.*, **2005**, *44*, 7390–7394.

[43] Guo, X.; Myers, M.; Xiao, S.; Lefenfeld, M.; Steiner, R.; T.i, George S.; Tang, J.; Baumert, J.and Leibfarth, F.; Yardley, J. T.; others. Chemoresponsive monolayer transistors. *PNAS*, **2006**, *103*, 11452–11456.

[44] Luo, J.; Xu, X.; Mao, R.; Miao, Q. Curved polycyclic aromatic molecules that are π-isoelectronic to hexabenzocoronene. *J. Am. Chem. Soc.*, **2012**, *134*, 13796–13803.

[45] Xiao, S.; Tang, J.; Beetz, T.; Guo, X.; Tremblay, N.; Siegrist, T.; Zhu, Y.and Steigerwald, M.; Nuckolls, C. Transferring self-assembled, nanoscale cables into electrical devices. *J. Am. Chem. Soc.*, **2006**, *128*, 10700–10701.

[46] Guo, X.; Xiao, S.; Myers, M.; Miao, Q.and Steigerwald, M. L.; Nuckolls, Co. Photoresponsive nanoscale columnar transistors. *PNAS*, **2009**, *106*, 691–696.

[47] Schiros, T.; Mannsfeld, S.; Chiu, C.; Yager, K. G.; Ciston, J.; Gorodetsky, A. A.; Palma, M.; Bullard, Z.; Kramer, T.; Delongchamp, D.; others. Reticulated organic photovoltaics. *Adv. Funct. Mater.*, **2012**, *22*, 1167–1173.

[48] Kang, S. J.; Kim, J. B.; Chiu, C.; Ahn, S.; Schiros, T.; Lee, S. S.; Yager, K. G.; Toney, M. F.; Loo, Y.; Nuckolls, C. A supramolecular complex in small-molecule solar cells based on contorted aromatic molecules. *Angew. Chem., Int. Ed.*, **2012**, *51*, 8594–8597.

[49] Tremblay, N. J.; Gorodetsky, A. A.; Cox, M. P.; Schiros, T.; Kim, B.; Steiner, R.; Bullard, Z.; Sattler, A.; So, W.; Itoh, Y.; others. Photovoltaic universal joints: Ball-and-socket interfaces in molecular photovoltaic cells. *ChemPhysChem*, **2010**, *11*, 799–803.

[50] Gorodetsky, A. A.; Chiu, C.; Schiros, T.; Palma, M.; Cox, M.; Jia, Z.; Sattler, W.; Kymissis, I.; Steigerwald, M.; Nuckolls, C. Reticulated heterojunctions for photovoltaic devices. *Angew. Chem., Int. Ed.*, **2010**, *49*, 7909–7912.

[51] Cohen, Y. S.; Xiao, S.; Steigerwald, M. L.; Nuckolls, C.; Kagan, C. R. Enforced one-dimensional photoconductivity in core-cladding hexabenzocoronenes. *Nano Lett.*, **2006**, *6*, 2838–2841.

[52] Scholl, R.; Mansfeld, J. meso-benzdianthron (helianthron), meso-naphthodianthron, und ein neuer weg zum flavanthren. *Ber. Dtsch. Chem. Ges.*, **1910**, *43*, 1734–1746.

[53] Scholl, R.; Neumann, H. Abspaltung aromatisch gebundenen wasserstoffes unter verknüpfung aromatischer kerne durch aluminiumchlorid. 4. mitteilung: Über den ringschluß bei zweifach benzoylierten naphthalinen. *Ber. Dtsch. Chem. Ges.*, **1922**, *55*, 118–126.

[54] Scholl, R.; Seer, Ch. Abspaltung aromatisch gebundenen wasserstoffs und verknüpfung aromatischer kerne durch aluminiumchlorid. *J. Lieb. Ann. Chem.*, **1912**, *394*, 111–177.

[55] Kovacic, P.; Kyriakis, A. Polymerization of benzene to p-polyphenyl by aluminum chloride-cupric chloride. *J. Am. Chem. Soc.*, **1963**, *85*, 454–458.

[56] Müller, M.; Mauermann-Düll, H.; Wagner, M.; Enkelmann, V.; Müllen, K. Eine cycloadditions-cyclodehydrierungs-route von stilbenoiden zu ausgedehnten aromatischen kohlenwasserstoffen. *Angew. Chem.*, **1995**, *107*, 1751–1754.

[57] Simpson, C. D.; Brand, J. D.; Berresheim, A. J and Przybilla, L.; Räder, H. J.; Müllen, K. Synthesis of a giant 222 carbon graphite sheet. *Chem. Eur. J.*, **2002**, *8*, 1424–1429.

[58] Baddeley, G. 205. hydrogen chloride–aluminium chloride as an agent of isomerisation. *J. Chem. Soc.*, **1950**, 994–997.

[59] Boden, N.; Bushby, R.J.; Headdock, G.; Lozman, O. R.; Wood, A. Syntheses of new'large core'discogens based on the triphenylene, azatriphenylene and hexabenztrinaphthylene nuclei. *Liq. Cryst.*, **2001**, *28*, 139–144.

[60] Kübel, C.; Eckhardt, K.; Enkelmann, V.; Wegner, G.; Müllen, K. Synthesis and crystal packing of large polycyclic aromatic hydrocarbons: hexabenzo [bc, ef, hi, kl, no, qr] coronene and dibenzo [fg, ij] phenanthro [9, 10, 1, 2, 3-pqrst] pentaphene. *J. Mater. Chem.*, **2000**, *10*, 879–886.

[61] Simpson, C. D.; Mattersteig, G.; Martin, K.; Gherghel, L.; Bauer, R. E.; Räder, H. J.; Müllen, K. Nanosized molecular propellers by cyclodehydrogenation of polyphenylene dendrimers. *J. Am. Chem. Soc.*, **2004**, *126*, 3139–3147.

[62] Kramer, B.; Fröhlich, R.; Waldvogel, S. R. Oxidative coupling reactions mediated by $MoCl_5$ leading to 2, 2-cyclolignans: The specific role of hcl. *Eur. J. Org. Chem.*, **2003**, *2003*, 3549–3554.

[63] Waldvogel, S. R.; Aits, E.; Holst, C.; Fröhlich, R. Dehydrodimerization of iodobenzenes to iodinated biaryls. *Chem. Comm.*, **2002**, 1278–1279.

[64] Kovacic, P.; Jones, M. B. Dehydro coupling of aromatic nuclei by catalyst-oxidant systems: poly (p-phenylene). *Chem. Rev.*, **1987**, *87*, 357–379.

[65] Takada, T.; Arisawa, M.; Gyoten, M.; Hamada, R.; Tohma, H.; Kita,

Y. Oxidative biaryl coupling reaction of phenol ether derivatives using a hypervalent iodine (iii) reagent. *J. Org. Chem*, **1998**, *63*, 7698–7706.

[66] Churruca, F.; SanMartin, R.; Carril, M.; Urtiaga, M. K.; Solans, X.; Tellitu, I.; Domínguez, E. Direct, two-step synthetic pathway to novel dibenzo [a, c] phenanthridines. *J. Org. Chem*, **2005**, *70*, 3178–3187.

[67] Aylward, J. B. Boron trifluoride–lead tetra-acetate: the oxidation of some benzenoid compounds. *J, Chem. Soc. B: Phys. Org.*, **1967**, 1268–1270.

[68] McKillop, A.; Turrell, A. G.; Young, D. W.; Taylor, E. C. Thallium in organic synthesis. 58. regiospecific intermolecular oxidative dehydrodimerization of aromatic compounds to biaryls using thallium (iii) trifluoroacetate. *J. Am. Chem. Soc.*, **1980**, *102*, 6504–6512.

[69] Holl, R.; Meyer, K.; Donat, J. Vom pyren in das gebiet höher anellierter ringsysteme. *Ber. Dtsch. Chem. Ges.*, **1937**, *70*, 2180–2189.

[70] Scholl, R.; Meyer, K. Die aromatischen grundkohlenwasserstoffe des anth-anthrons, anth-dianthrons (2.3, 4.5-dibenz-coronenchinons-(1.6)), pyranthrons bzw. amphi-isopyranthrons, violanthrons, iso-violanthrons, 1.2. 3, 7.8. 9-dinaphthocoronenchinons-(4.10) und das dibenz-rubicen. *Ber. Dtsch. Chem. Ges.*, **1934**, *67*, 1229–1235.

[71] Avlasevich, Y.; Kohl, C.; Müllen, K. Facile synthesis of terrylene and its isomer benzoindenoperylene. *J. Mater. Chem.*, **2006**, *16*, 1053–1057.

[72] Vingiello, F. A.; Ojakaar, L. New polycyclic aromatic hydrocarbons with seven fused rings. *Tetrahedron*, **1966**, *22*, 847–860.

[73] Marchetti, F.; Pampaloni, G.; Zacchini, S. The reactivity of molybdenum pentachloride with ethers: routes to the synthesis of Mo(IV) Cl_4 adducts, Mo (V) chlorido-alkoxides and mo (v) oxydo-chlorides. *Dalton Trans.*, **2013**, *42*, 15226–15234.

[74] Rempala, P.; Kroulík, J.; King, B. T. A slippery slope: mechanistic analysis of the intramolecular scholl reaction of hexaphenylbenzene. *J. Am. Chem. Soc.*, **2004**, *126*, 15002–15003.

[75] Rempala, P.; Kroulík, J.; King, B. T. Investigation of the mechanism of the intramolecular scholl reaction of contiguous phenylbenzenes. *J. Org. Chem.*, **2006**, *71*, 5067–5081.

[76] Wudl, F.; Smith, G. M.; Hufnagel, E. J. Bis-1, 3-dithiolium chloride: an unusually stable organic radical cation. *J. Chem. Soc. D: Chem. Commun.*, **1970**, 1453–1454.

[77] Amsharov, K. Y.; Kabdulov, M. A.; Jansen, M. Facile bucky-bowl synthesis by regiospecific cove-region closure by hf elimination. *Angew. Chem. Int. Ed.*, **2012**, *51*, 4594–4597.

[78] Amsharov, K. Y.; Merz, .P. Intramolecular aryl–aryl coupling of fluoroarenes through al2o3-mediated hf elimination. *J. Org. Chem*, **2012**, *77*, 5445–5448.

[79] Rüdiger, E. C.; Porz, M.; Schaffroth, M.; Rominger, F.; Bunz, U. H. Synthesis

of soluble, alkyne-substituted trideca-and hexadeca-starphenes. *Chem. Eur. J.*, **2014**, *20*, 12725–12728.

[80] Schuler, B.; Collazos, S.; Gross, L.; Meyer, G.; Pérez, D.; Guitián, E.; Peña, D. From perylene to a 22-ring aromatic hydrocarbon in one-pot. *Angew. Chem. Int. Ed.*, **2014**, *53*, 9004–9006.

[81] Li, C.; Wang, C.; Liao, H.; Chaudhuri, R.; Liu, R. Synthesis of dibenzo [g, p] chrysenes from bis (biaryl) acetylenes via sequential icl-induced cyclization and mizoroki- heck coupling. *J. Org. Chem.*, **2007**, *72*, 9203–9207.

[82] Chen, T.; Liu, R. Synthesis of large polycyclic aromatic hydrocarbons from bis (biaryl) acetylenes: large planar pahs with low π-sextets. *Org. Lett.*, **2011**, *13*, 4644–4647.

[83] Sato, T.; Shimada, S.; Hata, K. A new route to polycondensed aromatics: photolytic formation of dibenzo [fg, op] naphthacene. *J. Chem. Soc. D: Chem. Commun.*, **1970**, 766–767.

[84] Mei, X.; Wen, G.; Wang, J.; Yao, H.; Zhao, Y.; Lin, Z.; Ling, Q. A λ-shaped donor–π–acceptor–π–donor molecule with aiee and ciee activity and sequential logic gate behaviour. *J. Mater. Chem. C*, **2015**, *3*, 7267–7271.

[85] He, J.; Mathew, S.; Kinney, Z. J.; Warrell, R. M.; Molina, J. S.; Hartley, C. S. Tetrabenzanthanthrenes by mitigation of rearrangements in the planarization of ortho-phenylene hexamers. *Chem. Comm.*, **2015**, *51*, 7245–7248.

[86] Ke, Z.; Hao, L.; Gao, X.; Zhang, H.; Zhao, Y.; Yu, B.; Yang, Zh.; Chen,

Y.; Liu, Z. Reductive coupling of co2, primary amine, and aldehyde at room temperature: A versatile approach to unsymmetrically n, n-disubstituted formamides. *Chem. Eur. J.*, **2017**, *23*, 9721–9725.

[87] Daigle, M.; Picard L., A.; Soligo, E.; Morin, J. F. Regioselective synthesis of nanographenes by photochemical cyclodehydrochlorination. *Angew. Chem. Int. Ed.*, **2016**, *55*, 2042–2047.

[88] Rosi, N. L.; Eckert, J.; Eddaoudi, M.; Vodak, D. T.; Kim, J.; O'keeffe, M.; Yaghi, O. M. Hydrogen storage in microporous metal-organic frameworks. *Science*, **2003**, *300*, 1127–1129.

[89] Long, J. R.; Yaghi, O. M. The pervasive chemistry of metal–organic frameworks. *Chem. Soc. Rev.*, **2009**, *38*, 1213–1214.

[90] Tranchemontagne, D. J.; Mendoza-Cortés, J. L.; O'Keeffe, M.; Yaghi, O. M. Secondary building units, nets and bonding in the chemistry of metal–organic frameworks. *Chem. Soc. Rev.*, **2009**, *38*, 1257–1283.

[91] Perry IV, J. J.; Perman, J. A.; Zaworotko, M. J. Design and synthesis of metal–organic frameworks using metal–organic polyhedra as supermolecular building blocks. *Chem. Soc. Rev.*, **2009**, *38*, 1400–1417.

[92] Cote, A. P.; Benin, A. I and Ockwig, N. W.; O'keeffe, M.; Matzger, A. J.; Yaghi, O. M. Porous, crystalline, covalent organic frameworks. *Science*, **2005**, *310*, 1166–1170.

[93] Rowan, S. J.; Cantrill, S. J.; Cousins, G. R.; Sanders, J. K.; Stoddart, J. F. Dynamic covalent chemistry. *Angew. Chem. Int. Ed.*, **2002**, *41*, 898–952.

[94] Spitler, E. L.; Giovino, M. R.; White, S. L.; Dichtel, W. R. A mechanistic study of lewis acid-catalyzed covalent organic framework formation. *Chem. Sci.*, **2011**, *2*, 1588–1593.

[95] Hunt, J. R.; Doonan, C. J.; LeVangie, J. D.; Côté, A. P.; Yaghi, O. M. Reticular synthesis of covalent organic borosilicate frameworks. *J. Am. Chem. Soc.*, **2008**, *130*, 11872–11873.

[96] Lanni, L. M.; Tilford, R. W.; Bharathy, M.; Lavigne, J. J. Enhanced hydrolytic stability of self-assembling alkylated two-dimensional covalent organic frameworks. *J. Am. Chem. Soc.*, **2011**, *133*, 13975–13983.

[97] Uribe-Romo, F.J.; Doonan, C. J.; Furukawa, H.; Oisaki, K.and Yaghi, O. M. Crystalline covalent organic frameworks with hydrazone linkages. *J. Am. Chem. Soc.*, **2011**, *133*, 11478–11481.

[98] Uribe-Romo, F. J.; Hunt, J. R.; Furukawa, H.; Klock, C.; O'Keeffe, M.; Yaghi, O. M. A crystalline imine-linked 3-d porous covalent organic framework. *J. Am. Chem. Soc.*, **2009**, *131*, 4570–4571.

[99] Innocenzi, P.; Malfatti, L.; Soler-Illia, G. J. Hierarchical mesoporous films: from self-assembly to porosity with different length scales. *Chem. Mater.*, **2011**, *23*, 2501–2509.

[100] Kuhn, P.; Antonietti, M.; Thomas, A. Porous, covalent triazine-based

frameworks prepared by ionothermal synthesis. *Angew. Chem. Int. Ed.*, **2008**, *47*, 3450–3453.

[101] Bojdys, M. J.; Jeromenok, J.; Thomas, A.; Antonietti, M. Rational extension of the family of layered, covalent, triazine-based frameworks with regular porosity. *Adv. Mater.*, **2010**, *22*, 2202–2205.

[102] Ding, X.and Guo, J.and Feng, X.; Honsho, Y.; Guo, J.; Seki, S.; Maitarad, P.; Saeki, A.; Nagase, S.; Jiang, D. Synthesis of metallophthalocyanine covalent organic frameworks that exhibit high carrier mobility and photoconductivity. *Angew. Chem. Int. Ed.*, **2011**, *50*, 1289–1293.

[103] Tilford, R. W.; Gemmill, W. R.; Zur-Loye, H. C.; Lavigne, J. J. Facile synthesis of a highly crystalline, covalently linked porous boronate network. *Chem. Mater.*, **2006**, *18*, 5296–5301.

[104] Zwaneveld, N. A.; Pawlak, R.; Abel, M.; Catalin, D.; Gigmes, D.; Bertin, D.; Porte, L. Organized formation of 2d extended covalent organic frameworks at surfaces. *J. Am. Chem. Soc.*, **2008**, *130*, 6678–6679.

[105] Guan, C.; Wang, D.; Wan, L. Construction and repair of highly ordered 2d covalent networks by chemical equilibrium regulation. *Chem. Comm.*, **2012**, *48*, 2943–2945.

[106] Colson, J. W.; Woll, A. R.; Mukherjee, A.; Levendorf, M. P.; Spitler, E. L.; Shields, V. B.; Spencer, M. G.; Park, J.; Dichtel, W. R. Oriented 2d covalent organic framework thin films on single-layer graphene. *Science*, **2011**, *332*, 228–231.

[107] Spitler, E. L.; Colson, J. W.; Uribe-Romo, F. J.; Woll, A. R.; Giovino, M. R.; Saldivar, A.; Dichtel, W. R. Lattice expansion of highly oriented 2D phthalocyanine covalent organic framework films. *Angew. Chem. Int. Ed.*, **2012**, *51*, 2623–2627.

[108] Spitler, E. L.; Koo, B. T.; Novotney, J. L.; Colson, J. W.; Uribe-Romo, F. J.; Gutierrez, G. D.; Clancy, P.; Dichtel, W. R. A 2D covalent organic framework with 4.7 nm pores and insight into its interlayer stacking. *J. Am. Chem. Soc.*, **2011**, *133*, 19416–19421.

[109] Campbell, N. L.; Clowes, R.and Ritchie, L. K.; Cooper, A. I. Rapid microwave synthesis and purification of porous covalent organic frameworks. *Chem. Mater.*, **2009**, *21*, 204–206.

[110] Dogru, M.; Sonnauer, A.; Gavryushin, A.; Knochel, P.; Bein, T. A covalent organic framework with 4 nm open pores. *Chem. Comm.*, **2011**, *47*, 1707–1709.

[111] Hünig, S.; Kiesslich, G.; Sceutzow, D.; Zhrandik, R.; Carsky, P. *Int. J. Sulfur Chem., Part C*, **1971**, 109–122.

[112] Coffen, D. L.; Chambers, J. Q.; Williams, D. R.; Garrett, P. E.; Canfield, N. D. Tetrathioethylenes. *J. Am. Chem. Soc.*, **1971**, *93*, 2258–2268.

[113] C. Rovira. TTF Chemistry. Fundamentals and Applications of Tetrathiafulvalene. Edited by Jun-ichi Yamada and Toyonari Sugimoto. *Angew. Chem. Inter. Ed.*, **2006**, *45*, 3003-3003.

[114] Segura, J. L.; Martín, N. New concepts in tetrathiafulvalene chemistry. *Angew. Chem. Int. Ed.*, **2001**, *40*, 1372–1409.

[115] Simonsen, K. B.; Becher, J. Tetrathiafulvalene thiolates: Important synthetic building blocks for macrocyclic and supramolecular chemistry. *Synlett*, **1997**, 1211–1220.

[116] Nielsen, M. B.; Lomholt, C.; Becher, J. Tetrathiafulvalenes as building blocks in supramolecular chemistry ii. *Chem. Soc. Rev.*, **2000**, *29*, 153–164.

[117] Canevet, D.; Sallé, M.and Zhang, G.; Zhang, D.; Zhu, D. Tetrathiafulvalene (TTF) derivatives: key building-blocks for switchable processes. *Chem. Comm.*, **2009**, 2245–2269.

[118] VandeVondele, J.; Lynden-Bell, R.; Meijer, E. J.; Sprik, M. Density functional theory study of tetrathiafulvalene and thianthrene in acetonitrile: Structure, dynamics, and redox properties. *J. Phys. Chem. B*, **2006**, *110*, 3614–3623.

[119] Nielsen, M. B.; Sauer, S. P. On the aromaticity of tetrathiafulvalene cations. *Chem. Phys. Lett.*, **2008**, *453*, 136–139.

[120] Bendikov, M.; Wudl, F.; Perepichka, D. F. Tetrathiafulvalenes, oligoacenenes, and their buckminsterfullerene derivatives: the brick and mortar of organic electronics. *Chem. Rev.*, **2004**, *104*, 4891–4946.

[121] Wang, Y.; Urban, C.; Rodríguez-Fernández, J.; Gallego, J.; Otero, R.; Martín, N.; Miranda, R.; Alcamí, M.; Martín, F. Formation of self-assembled chains

of tetrathiafulvalene on a cu (100) surface. *J. Phys. Chem. A*, **2011**, *115*, 13080–13087.

[122] Cooper, W. F.; Kenny, N. C.; Edmonds, J. W.; Nagel, A.; Wudl, F.; Coppens, P. Crystal and molecular structure of the aromatic sulphur compound 2, 2-bi-1, 3-dithiole. evidence for d-orbital participation in bonding. *J. Chem. Soc. D*, (16):889–890, **1971**,889–890.

[123] Batsanov, A. S. Tetrathiafulvalene revisited. *Acta Cryst. C*, **2006**, *62*, o501–o504.

[124] Bozio, R.; Zanon, I.; Girlando, A.; Pecile, C. Vibrational spectroscopy of molecular constituents of one-dimensional organic conductors. Tetrathiofulvalene (TTF), TTF^+, and $(TTF^+)_2$ dimer. *J. Chem. Phys.*, **1979**, *71*, 2282–2293.

[125] Ellern, A.; Bernstein, J.; Becker, J. Y.; Zamir, S.; Shahal, L.; Cohen, S. A new polymorphic modification of tetrathiafulvalene. crystal structure, lattice energy and intermolecular interactions. *Chem. Mater.*, **1994**, *6*, 1378–1385.

[126] Frere, P.; Skabara, P. J. Salts of extended tetrathiafulvalene analogues: relationships between molecular structure, electrochemical properties and solid state organisation. *Chem. Soc. Rev.*, **2005**, *34*, 69–98.

[127] Zhao, Y.and Chen, G.; Mulla, K.; Mahmud, I.; Liang, S.; Dongare, P.; Thompson, D. W.; Dawe, L. N.; Bouzan, S. Tetrathiafulvalene vinylogues as versatile building blocks for new organic materials. *Pure Appl. Chem.*, **2012**, *84*, 1005–1025.

[128] Roncali, J. Linearly extended π-donors: when tetrathiafulvalene meets conjugated oligomers and polymers. *J. Mater. Chem.*, **1997**, *7*, 307–2321.

[129] Bryce, M. R.; Coffin, M. A.; Clegg, W. New vinylogous tetrathiafulvalene. π-electron donors with peripheral alkylseleno substitution. *J. Org. Chem.*, **1992**, *57*, 1696–1699.

[130] Carlier, R.; Hapiot, P.; Lorcy, D.; Robert, A.; Tallec, A. Electrosynthesis and redox behavior of vinylogous TTF displaying strong conformational changes associated with electron transfers. *Electrochim. Acta*, **2001**, *46*, 3269–3277.

[131] Schou, S. S.; Parker, C. R.; Lincke, K.; Jennum, K.; Vibenholt, J.; Kadziola, A.; Nielsen, M. B. On the phosphite-mediated synthesis of dithiafulvenes and π-extended tetrathiafulvalenes. *Synlett*, **2013**, *24*, 231–235.

[132] Christensen, C. A.; Batsanov, A. S.; Bryce, M. R. Thiolated π-extended tetrathiafulvalenes: Versatile multifunctional π-systems. *J. Org. Chem.*, **2007**, *72*, 1301–1308.

[133] Steimecke, G.; Sieler, H. J.; Kirmse, R.; Hoyer, E. 1.3-dithiol-2-thion-4.5-dithiolat aus schwefelkohlenstoff und alkalimetall. *Phosphorus Sulfur Silicon Relat. Elem.*, **1979**, *7*, 49–55.

[134] He, Z.; Zhang, L.; Mei, J.; Zhang, T.; Lam, J. W.; Shuai, Z.; Dong, Yong Q.; Tang, B. Z. Polymorphism-dependent and switchable emission of butterfly-like bis (diarylmethylene) dihydroanthracenes. *Chem. Mater.*, **2015**, *27*, 6601–6607.

[135] Khadem, M.; Zhao, Y. Multivalent dithiafulvenyl functionalization of dendritic

oligo (phenylene vinylene) s with an anthraquinodimethane core. *Chem. Commun.*, **2017**, *53*, 1821–1824.

[136] Inagi, S.and Naka, K.; Chujo, Y. Functional polymers based on electron-donating ttf and derivatives. *J. Mater. Chem.*, **2007**, *17*, 4122–4135.

[137] Fourmigue, M.; Johannsen, I.; Boubekeur, K.; Nelson, C.; Batail, P. Tetrathiafulvalene-and dithiafulvene-substituted mesitylenes, new. pi.-donor molecules with 3-fold symmetry and the formation of an unprecedented new class of electroactive polymers. *J. Am. Chem. Soc.*, **1993**, *115*, 3752–3759.

[138] Guerro, M.; Lorcy, D. A simple route to novel functionalized tetrathiafulvalene vinylogues. *Tetrahedron Lett.*, **2005**, *46*, 5499–5502.

[139] Yamashita, Y.; Tomura, M.; Zaman, M. B. Synthesis and properties of novel tetrathiafulvalene vinylogues. *Chem. Commun.*, **1998**, 1657–1658.

[140] Hapiot, P.; Lorcy, D.; Tallec, A.; Carlier, R.; Robert, A. Mechanism of dimerization of 1, 4-dithiafulvenes into TTF vinylogues. *J. Phys. Chem.*, **1996**, *100*, 14823–14827.

[141] Massue, J.; Ghilane, J.; Bellec, N.; Lorcy, D.; Hapiot, P. Facile electrochemical generation of polyoxyethyl-vinylogous tetrathiafulvalene films. *Electrochem. Commun.*, **2007**, *9*, 677–682.

[142] Woolridge, K.; Goncalves, L. C.; Bouzan, S.n and Chen, G.; Zhao, Y. Aryl-substituted dithiafulvenes: synthesis, electronic properties, and redox reactivity. *Tetrahedron Lett.*, **2014**, *55*, 6362–6366.

[143] Bouzan, S.; Dawe, L. N.; Zhao, Y. Bromophenyl substituted dithiafulvenes and tetrathiafulvalene vinylogues: synthesis, structure, and electronic properties. *Tetrahedron Lett.*, **2013**, *54*, 4666–4669.

[144] Wang, Y.; Zhao, Y. Dithiafulvenyl-substituted phenylacetylene derivatives: synthesis and structure–property–reactivity relationships. *Org. Biomol. Chem.*, **2015**, *13*, 9575–9579.

[145] Davy, N. C.; Man, G.; Kerner, R. A.; Fusella, M. A.; Purdum, G. E.; Sezen, M.; Rand, B. P.; Kahn, A.; Loo, Y. Contorted hexabenzocoronenes with extended heterocyclic moieties improve visible-light absorption and performance in organic solar cells. *Chem. Mater.*, **2016**, *28*, 673–681.

[146] He, Z.; Shan, L.; Mei, J.; Wang, H.; Lam, J. W.; Sung, H. H.; Williams, I. D.; Gu, X.; Miao, Q.; Tang, B. Z. Aggregation-induced emission and aggregation-promoted photochromism of bis (diphenylmethylene) dihydroacenes. *Chem. Sci.*, **2015**, *6*, 3538–3543.

[147] Rieger, R.; Müllen, K. Forever young: polycyclic aromatic hydrocarbons as model cases for structural and optical studies. *J. Phys. Org. Chem.*, **2010**, *23*, 315–325.

[148] Grzybowski, M.; Skonieczny, K.; Butenschoen, H.; Gryko, D. T. Comparison of oxidative aromatic coupling and the scholl reaction. *Angew. Chem. Int. Ed.*, **2013**, *52*, 9900–9930.

[149] Pola, S.; Kuo, C.; Peng, W.; Islam, M. M.; Chao, I.; Tao, Y. Contorted

tetrabenzocoronene derivatives for single crystal field effect transistors: correlation between packing and mobility. *Chem. Mater.*, **2012**, *24*, 2566–2571.

[150] Miyaura, N.; Yamada, K.; Suzuki, A. A new stereospecific cross-coupling by the palladium-catalyzed reaction of 1-alkenylboranes with 1-alkenyl or 1-alkynyl halides. *Tetrahedron Lett.*, **1979**, *20*, 3437–3440.

[151] Franzén, R.; Xu, Y. Review on green chemistry suzuki cross coupling in aqueous media. *Can. J. Chem.*, **2005**, *83*, 266–272.

[152] Bai, L.; Wang, J. Environmentally friendly suzuki aryl-aryl cross-coupling reaction. *Curr. Org. Chem.*, **2005**, *9*, 535–553.

[153] Sołoducho, J.; Olech, K.; Świst, A.; Zajac, D.; Cabaj, J. Recent advances of modern protocol for cc bonds–the suzuki cross-coupling. *Adv. Chem. Eng. Sci.*, **2013**, *3*, 19–32.

[154] Polshettiwar, V.; Decottignies, A.; Len, C.; Fihri, A. Suzuki–miyaura cross-coupling reactions in aqueous media: Green and sustainable syntheses of biaryls. *ChemSusChem*, **2010**, *3*, 502–522.

[155] Freundlich, J. S.; Landis, H. E. An expeditious aqueous suzuki–miyaura method for the arylation of bromophenols. *Tetrahedron Lett.*, **2006**, *47*, 4275–4279.

[156] Qiu, J.; Wang, L.; Liu, M.; Shen, Q.; Tang, J. An efficient and simple protocol for a $PdCl_2$-ligandless and additive-free suzuki coupling reaction of aryl bromides. *Tetrahedron. Lett.*, **2011**, *52*, 6489–6491.

[157] Lee, N. R.; Linstadt, R. T.; Gloisten, D. J.; Gallou, F.; L., B. H. B-alkyl sp^3–sp^2 suzuki–miyaura couplings under mild aqueous micellar conditions. *Org. Lett.*, **2018**, *20*, 2902–2905.

[158] Wilson, K. L.; Murray, J.; Jamieson, C.; Watson, A. J. Cyrene as a bio-based solvent for the suzuki–miyaura cross-coupling. *Synlett*, **2018**, *29*, 650–654.

[159] Kirchhoff, J. H.; Netherton, M. R.; Hills, I. D.; Fu, G. C. Boronic acids: new coupling partners in room-temperature suzuki reactions of alkyl bromides. crystallographic characterization of an oxidative-addition adduct generated under remarkably mild conditions. *J. Am. Chem. Soc.*, **2002**, *124*, 13662–13663.

[160] Kingston, J. V.; Verkade, J. G. Synthesis and characterization of $R_2PN\,P(iBuNCH_2CH_2)_3N$: A new bulky electron-rich phosphine for efficient Pd-assisted suzuki- miyaura cross-coupling reactions. *J. Org. Chem.*, **2007**, *72*, 2816–2822.

[161] Liu, W.; Xie, Y.; Liang, Y.; Li, J. Reusable and Efficient $Pd\,(OAc)\,2$/TBAB/PEG-400 System for Suzuki-Miyaura Cross-Coupling Reaction under Ligand-Free Conditions. *Synthesis*, **2006**, 860–864.

[162] Baxter, J. M.; Steinhuebel, D.; Palucki, M.; Davies, I. W. Stereoselective enol tosylation: Preparation of trisubstituted α, β-unsaturated esters. *Org. Lett.*, **2005**, *7*, 215–218.

[163] Saito, B.; Fu, G. C. Alkyl- alkyl suzuki cross-couplings of unactivated secondary alkyl halides at room temperature. *J. Am. Chem. Soc.*, **2007**, *129*, 9602–9603.

[164] Brunauer, S.; Emmett, P. H.; Teller, E. Adsorption of gases in multimolecular layers. *J. Am. Chem. Soc.*, **1938**, *60*, 309–319.

[165] Mulla, K.; Zhao, Y. TTFV molecular tweezers with phenylboronic acid and phenylboronate endgroups: modular synthesis and electrochemical responses to saccharides and fluoride ion. *Tetrahedron Lett.*, **2014**, *55*, 382–386.

[166] Mulla, K.; Shaik, H.; Thompson, D. W.; Zhao, Y. TTFV-based molecular tweezers and macrocycles as receptors for fullerenes. *Org. Lett.*, **2013**, *15*, 4532–4535.

[167] Mulla, K.; Dongare, P.; Thompson, D. W.; Zhao, Y. Click synthesized dianthryl–TTFV: an efficient fluorescent turn-on probe for transition metal ions. *Org. Biomol. Chem.*, **2012**, *10*, 2542–2544.

[168] Shao, M.; Dongare, P.; Dawe, L. N.; Thompson, D. W.; Zhao, Y. Biscrown-annulated TTFAQ- dianthracene hybrid: synthesis, structure, and metal ion sensing. *Org. Lett.*, **2010**, *12*, 3050–3053.

[169] Massue, J.; Bellec, N.; Guerro, M.; Bergamini, J.; Hapiot, P.; Lorcy, D. Crown ether vinylogous tetrathiafulvalene receptors: Complexation interference on the molecular movements triggered by electron transfer. *J. Org. Chem.*, **2007**, *72*, 4655–4662.

[170] Chen, G; Zhao, Y;. Redox-regulated rotary motion of a bis (9-triptycyl)-TTFV system. *Org. Lett.*, **2014**, *16*, 668–671.

[171] Lorcy, D.; Guerro, M.; Bergamini, J.s and Hapiot, P. Vinylogous

tetrathiafulvalene based podands: Complexation interferences on the molecular movements triggered by electron transfer. *J. Phys. Chem. B*, **2013**, *117*, 5188–5194.

[172] Chen, G.; Mahmud, I.; Dawe, L. N.; Zhao, Y. Acetylenic Phenyldithiafulvene: A Versatile Synthon for TTFV-Based Macromolecules. *Org. Lett.*, **2010**, *12*, 704–707.

[173] Åxman P. M.; Zhu, L.; Jensen, S. H.; Andersson, A. S.; Kadziola, A.; Kilså, K.; Brøndsted N. M. Photoswitches containing a dithiafulvene electron donor. *Adv. Funct. Mater.*, **2007**, *17*, 797–804.

[174] Khadem, M.; Zhao, Y. Tetrathiafulvalene vinylogue–fluorene co-oligomers: Synthesis, properties, and supramoleclar interactions with carbon nanotubes. *J. Org. Chem.*, **2015**, *80*, 7419–7429.

[175] Cocherel, N.; Leriche, P.; Ripaud, E.; Gallego-Planas, N.; Frère, P.; Roncali, J. Electropolymerization of triphenylamine–dithiafulvene hybrid extended π-conjugated systems. *New J. Chem.*, **2009**, *33*, 801–806.

[176] Ripaud, E.; Leriche, P.; Cocherel, N.; Cauchy, T.; Frère, P.; Roncali, J. Tristhienylphenylamine–extended dithiafulvene hybrids as bifunctional electroactive species. *Org. Biomol. Chem.*, **2011**, *9*, 1034–1040.

[177] Mancuso, R.; Gabriele, B. Recent advances in the synthesis of thiophene derivatives by cyclization of functionalized alkynes. *Molecules*, **2014**, *19*, 15687–15719.

[178] Meazza, G.; Zanardi, G.; Guglielmetti, G.; Piccardi, P. Synthesis of 2, 3, 5-triaryl-4-trifluoromethyl thiophenes. *J. Fluor. Chem.*, **1997**, *82*, 175–180.

[179] Adeel, S. M.; Li, Q.; Nafady, A.; Zhao, C.; Siriwardana, A. I.; Bond, A. M.; Martin, L. L. A csystemati study of the variation of tetrathiafulvalene (TTF), $TTF^{+\cdot}$ and TTF^{2+} reaction pathways with water in the presence and absence of light. *RSC Adv.*, **2014**, *4*, 49789–49795.

[180] Giffard, M.; Alonso, P.; Garín, J.; Gorgues, A.; Nguyen, T. P.; Richomme, P.; Robert, A.; Roncali, J.; Uriel, S. The first evidence for the generation of radicals and formation of electrically conducting molecular materials by protic doping of tetrathiafulvalenes. *Adv. Mater.*, **1994**, *6*, 298–300.

[181] Roncali, J.; Giffard, M.; Frère, P.; Jubault, M.; Gorgues, A. Extensively conjugated tetrathiafulvalene (TTF) π-electron donors with oligothiophenes spacer groups. *J. Chem. Soc., Chem. Commun.*, **1993**, 689–691.

[182] Han, X.; Peh, G.and Floreancig, P. E. Prins-type cyclization reactions in natural product synthesis. *Eur. J. Org. Chem.*, **2013**, 1193–1208.

[183] Miranda, P. O.; Ramírez, M. A.; Martín, V. S.; Padrón, J. I. Factors controlling the alkyne prins cyclization: the stability of dihydropyranyl cations. *Chem. Eur. J.*, **2008**, *14*, 6260–6268.

[184] Shin, C.; Chavre, S. N.; Pae, A. N.; Cha, J. H.; Koh, H. Y.; Chang, M. H.; Choi, J. H.; Cho, Y. S. Highly stereoselective synthesis of 2, 5-disubstituted 3-vinylidene tetetrahydrofurans via prins-type cyclization. *Org. Lett.*, **2005**, *7*, 3283–3285.

[185] Chavre, S. N.; Choo, H.; Lee, J. K.; Pae, A. N.; Kim, Y.; Cho, Y. S. 5-and 6-exocyclic products, cis-2, 3, 5-trisubstituted tetrahydrofurans, and cis-2, 3, 6-trisubstituted tetrahydropyrans via prins-type cyclization. *J. Org. Chem.*, **2008**, *73*, 7467–7471.

[186] Gilmore, K.; Alabugin, I. V. Cyclizations of alkynes: revisiting baldwin's rules for ring closure. *Chem. Rev.*, **2011**, *111*, 6513–6556.

[187] Chavre, S. N.; Choo, H.; Cha, J. H.; Pae, A. N.; Choi, K. I.; Cho, Y. S. 5-exocyclic products, 2, 3, 5-trisubstituted tetrahydrofurans via prins-type cyclization. *Org. Lett.*, **2006**, *8*, 3617–3619.

[188] Liang, S.; Zhao, Y.; Adronov, A. Selective and reversible noncovalent functionalization of single-walled carbon nanotubes by a ph-responsive vinylogous tetrathiafulvalene–fluorene copolymer. *J. Am. Chem. Soc.*, **2014**, *136*, 970–977.

[189] Liang, S.; Chen, G.; Zhao, Y. Conformationally switchable TTFV–phenylacetylene polymers: synthesis, properties, and supramolecular interactions with single-walled carbon nanotubes. *J. Mater. Chem. C*, **2013**, *1*, 5477–5490.

[190] Liang, S.; Chen, G.; Peddle, J.; Zhao, Y. Reversible dispersion and releasing of single-walled carbon nanotubes by a stimuli-responsive TTFV-phenylacetylene polymer. *Chem. Commun.*, **2012**, *48*, 3100–3102.

[191] Wang, M.; Cai, D.; Yin, Z.; Chen, S.; Du, C.; Zheng, Q. Asymmetric-

indenothiophene-based copolymers for bulk heterojunction solar cells with 9.14% efficiency. *Adv. Mater.*, **2016**, *28*, 3359–3365.

[192] Lee, J. K.; Kim, J.; Choi, H.; Lim, K.; Song, K.; Ko, J. Push–pull organic semiconductors with planar indenothiophene bridges for solution-processed small-molecule organic solar cells. *Tetrahedron*, **2014**, *70*, 6235–6240.

[193] Chao, T.; Wong, K.; Hung, W.i and Hou, T.; Chen, W. Structural effects on the hole mobilities of indenothiophene-embedded homologs. *Tetrahedron Lett.*, **2009**, *50*, 3422–3424.

[194] MacDowell, D.; Jeffries, A. T. Chemistry of indenothiophenes. III. Metalation of 3-benzylthiophene and an alternative synthesis of 4H-indeno [1, 2-b] thiophene-4-carboxylic acid. *J. Org. Chem.*, **1971**, *36*, 1053–1056.

[195] Gensch, K. H.; Pitman, I. H.; Higuchi, T. Oxidation of thioethers to sulfoxides by iodine. II. Catalytic role of some carboxylic acid anions. *J. Am. Chem. Soc.*, **1968**, *90*, 2096–2104.

[196] Higuchi, T.; Gensch, K. H. Oxidation of thioethers by iodine to sulfoxides. catalytic role of certain inorganic nucleophiles1. *J. Am. Chem. Soc.*, **1966**, *88*, 5486–5491.

[197] Correa, P. E.; Riley, D. P. Highly selective direct oxidation of thioethers to sulfoxides using molecular oxygen. *J. Org. Chem.*, **1985**, *50*, 1787–1788.

[198] Weinhold, F.; Landis, C. R. Natural bond orbitals and extensions of localized bonding concepts. *Chem. Educ. Res.*, **2001**, *2*, 91–104.

[199] Foster, J. P.; Weinhold, F. Natural hybrid orbitals. *J. Am. Chem. Soc.*, **1980**, 7211–7218.

[200] Fukui, K. Formulation of the reaction coordinate. *J. Phys. Chem.*, **1970**, *74*, 4161–4163.

[201] Fukui, K. The path of chemical reactions-the irc approach. *Acc. Chem. Res.*, **1981**, *14*, 363–368.

[202] Becke, A.D. Density-functional thermochemistry. III. The role of exact exchange. *J. Chem. Phys.*, **1993**, *98*, 5648-5652.

[203] Stephens, P. J.; Devlin, F. J.; Chabalowski, C.; Frisch, M. J. Ab initio calculation of vibrational absorption and circular dichroism spectra using density functional force fields. *J. Chem. Phys.*, **1994**, *98*, 11623–11627.

[204] Hariharan, P. C.; Pople, J. A. The influence of polarization functions on molecular orbital hydrogenation energies. *Theor. Chim. Acta*, **1973**, *28*, 213–222.

[205] M. J. Frisch, G. W. Trucks, H. B. Schlegel, G. E. Scuseria, M. A. Robb, J. R. Cheeseman, G. Scalmani, V. Barone, G. A. Petersson, H. Nakatsuji, X. Li, M. Caricato, A. V. Marenich, J. Bloino, B. G. Janesko, R. Gomperts, B. Mennucci, H. P. Hratchian, J. V. Ortiz, A. F. Izmaylov, J. L. Sonnenberg, D. Williams-Young, F. Ding, F. Lipparini, F. Egidi, J. Goings, B. Peng, A. Petrone, T. Henderson, D. Ranasinghe, V. G. Zakrzewski, J. Gao, N. Rega, G. Zheng, W. Liang, M. Hada, M. Ehara, K. Toyota, R. Fukuda, J. Hasegawa, M. Ishida, T. Nakajima, Y. Honda, O. Kitao, H. Nakai, T. Vreven, K. Throssell,

J. A.; J. E. Peralta Montgomery, Jr., F. Ogliaro, M. J. Bearpark, J. J. Heyd, E. N. Brothers, K. N. Kudin, V. N. Staroverov, T. A. Keith, R. Kobayashi, J. Normand, K. Raghavachari, A. P. Rendell, J. C. Burant, S. S. Iyengar, J. Tomasi, M. Cossi, J. M. Millam, M. Klene, C. Adamo, R. Cammi, J. W. Ochterski, R. L. Martin, K. Morokuma, O. Farkas, J. B. Foresman, and D. J. Fox. Gaussian˜16 Revision B.01, 2016. Gaussian Inc. Wallingford CT.

[206] C. Y. Legault. Cylview, 1.0b, 2009. Université de Sherbrooke (http://www.cylview.org).

Appendix: NMR Spectra of New Compounds

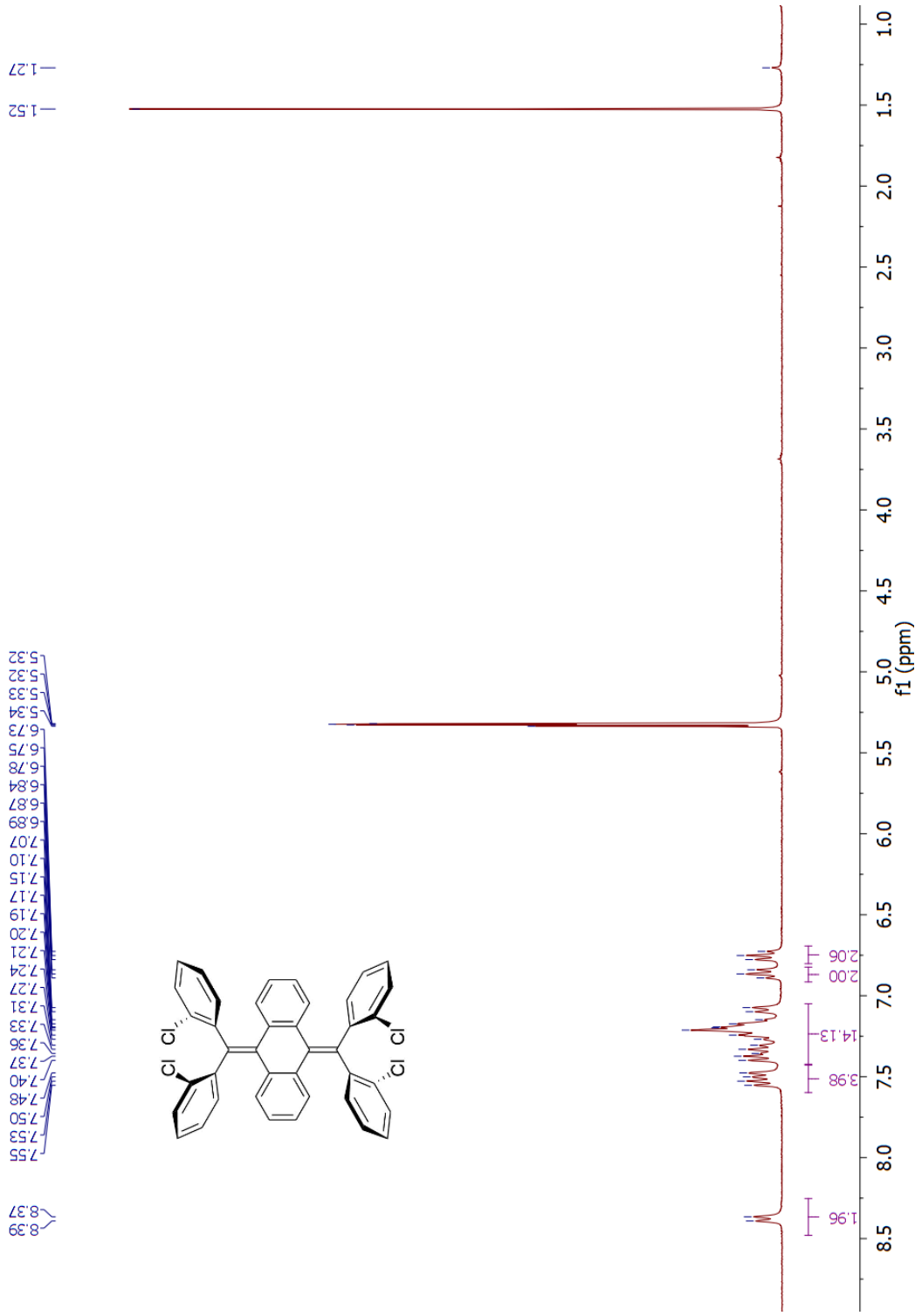

Figure 1: ^{1}H NMR (300 MHz, CD_2Cl_2) spectrum for compound **99**.

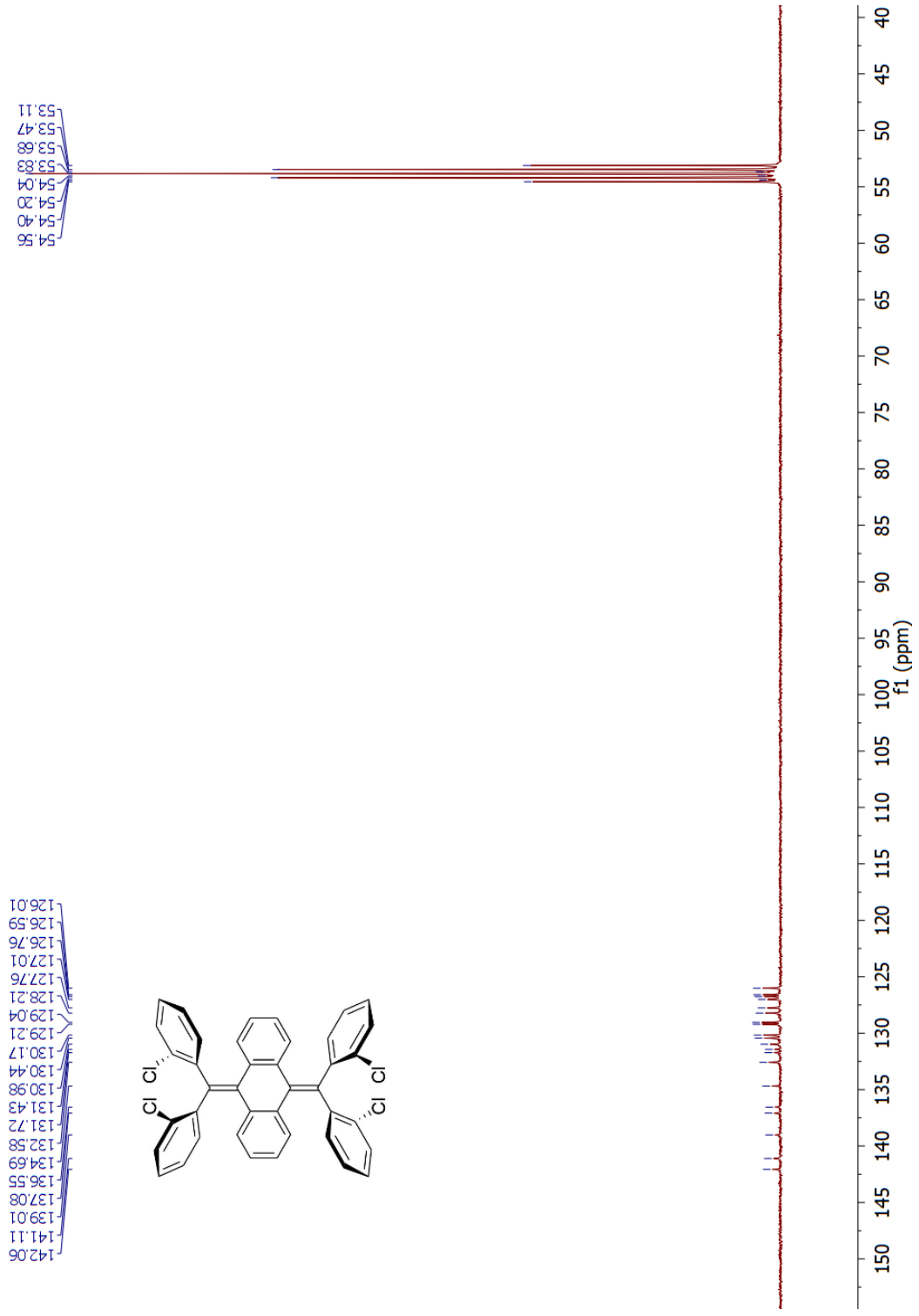

Figure 2: ^{13}H NMR (75 MHz, CD_2Cl_2) spectrum for compound **99**.

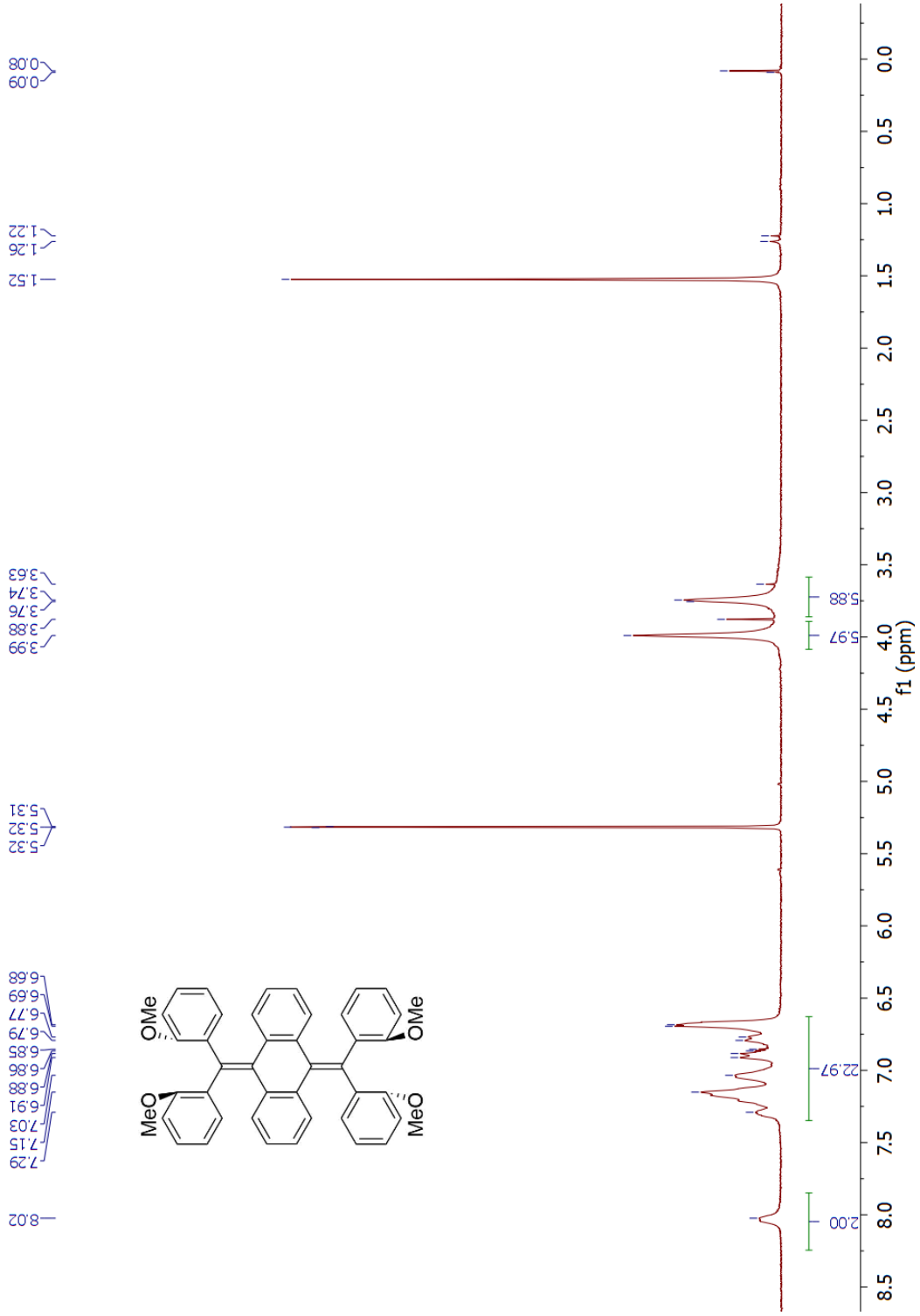

Figure 3: ^{1}H NMR (300 MHz, CD_2Cl_2) spectrum for compound **101**.

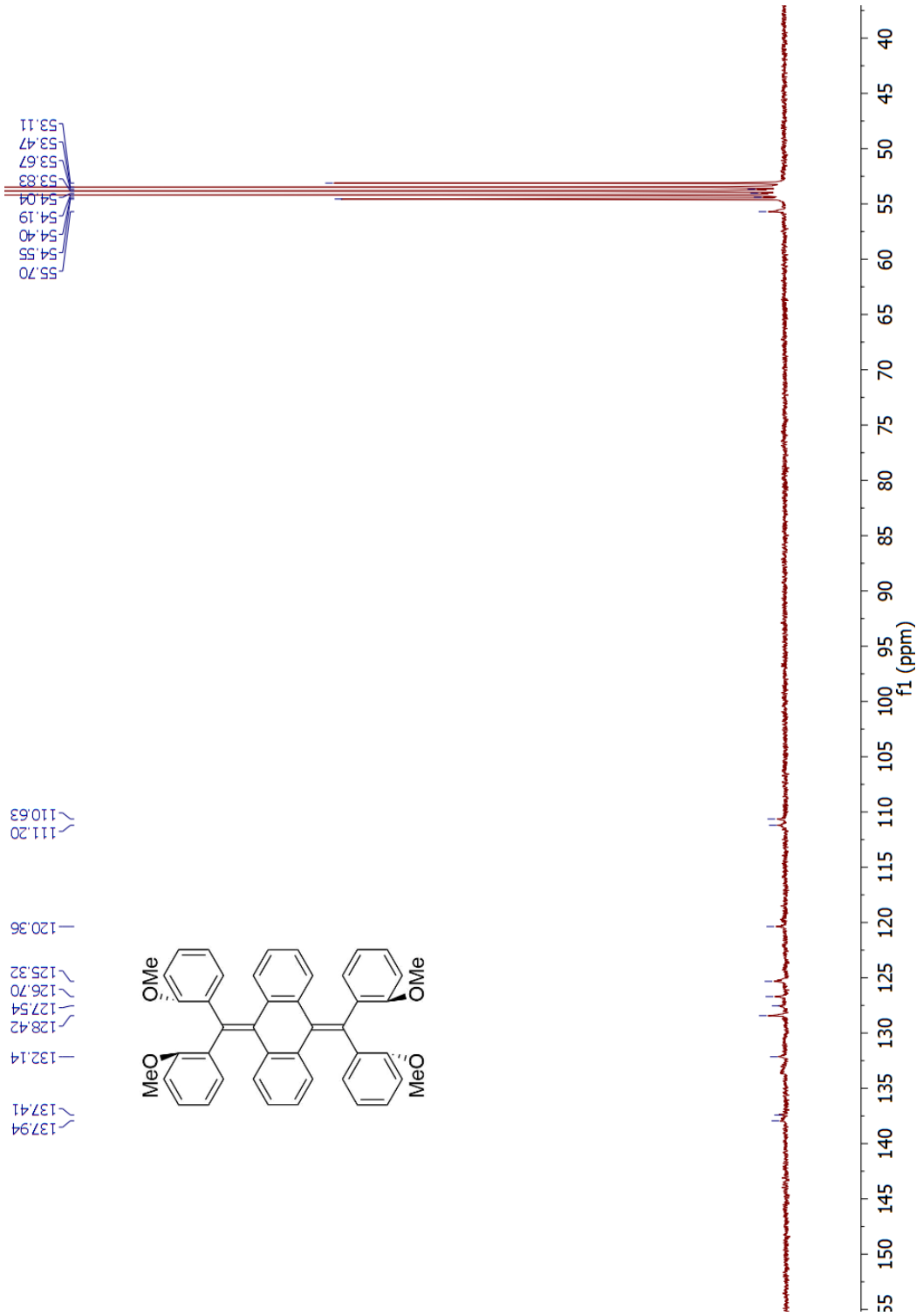

Figure 4: ^{13}H NMR (75 MHz, CD_2Cl_2) spectrum for compound **101**.

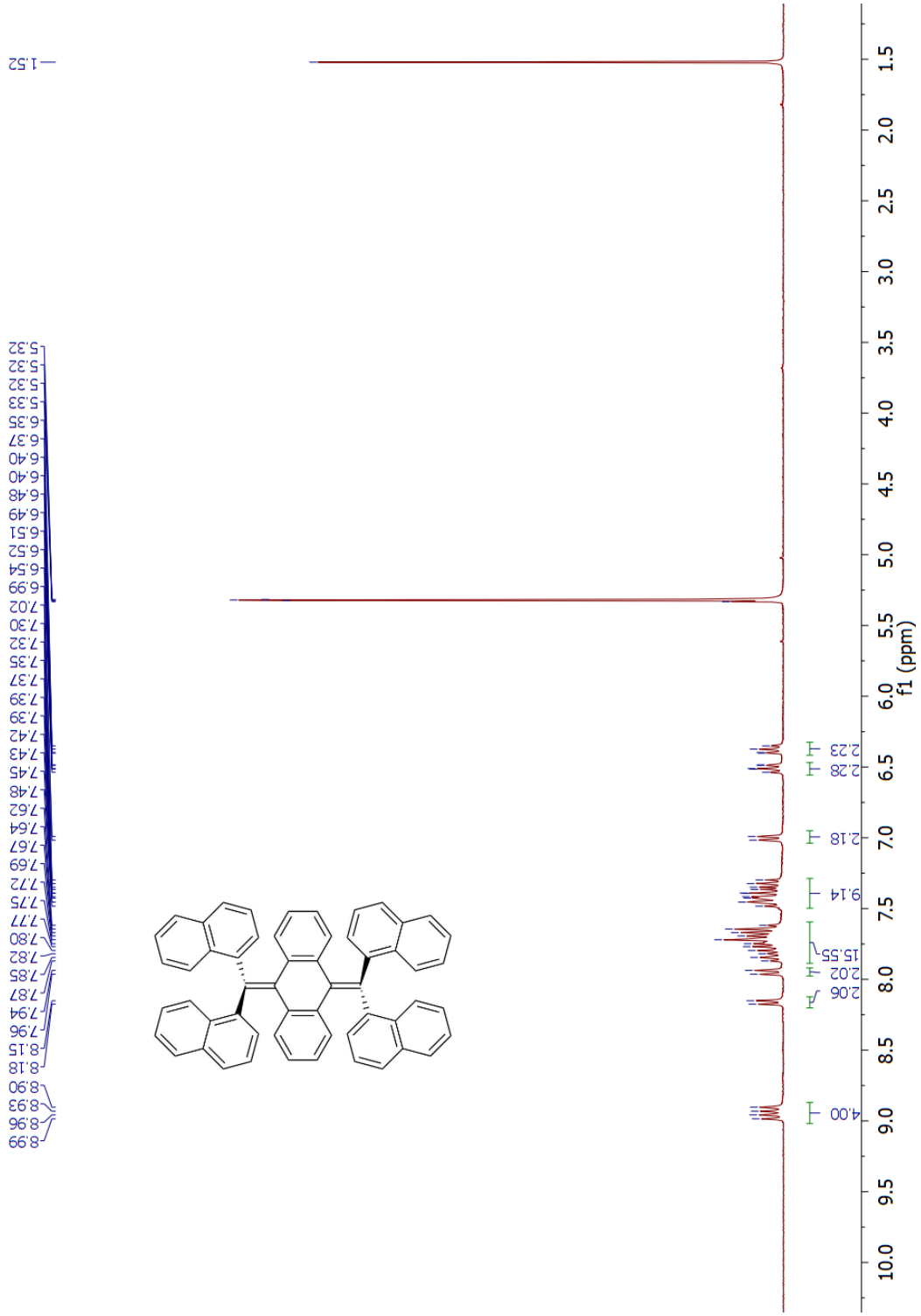

Figure 5: ^{1}H NMR (300 MHz, CD_2Cl_2) spectrum for compound **102**.

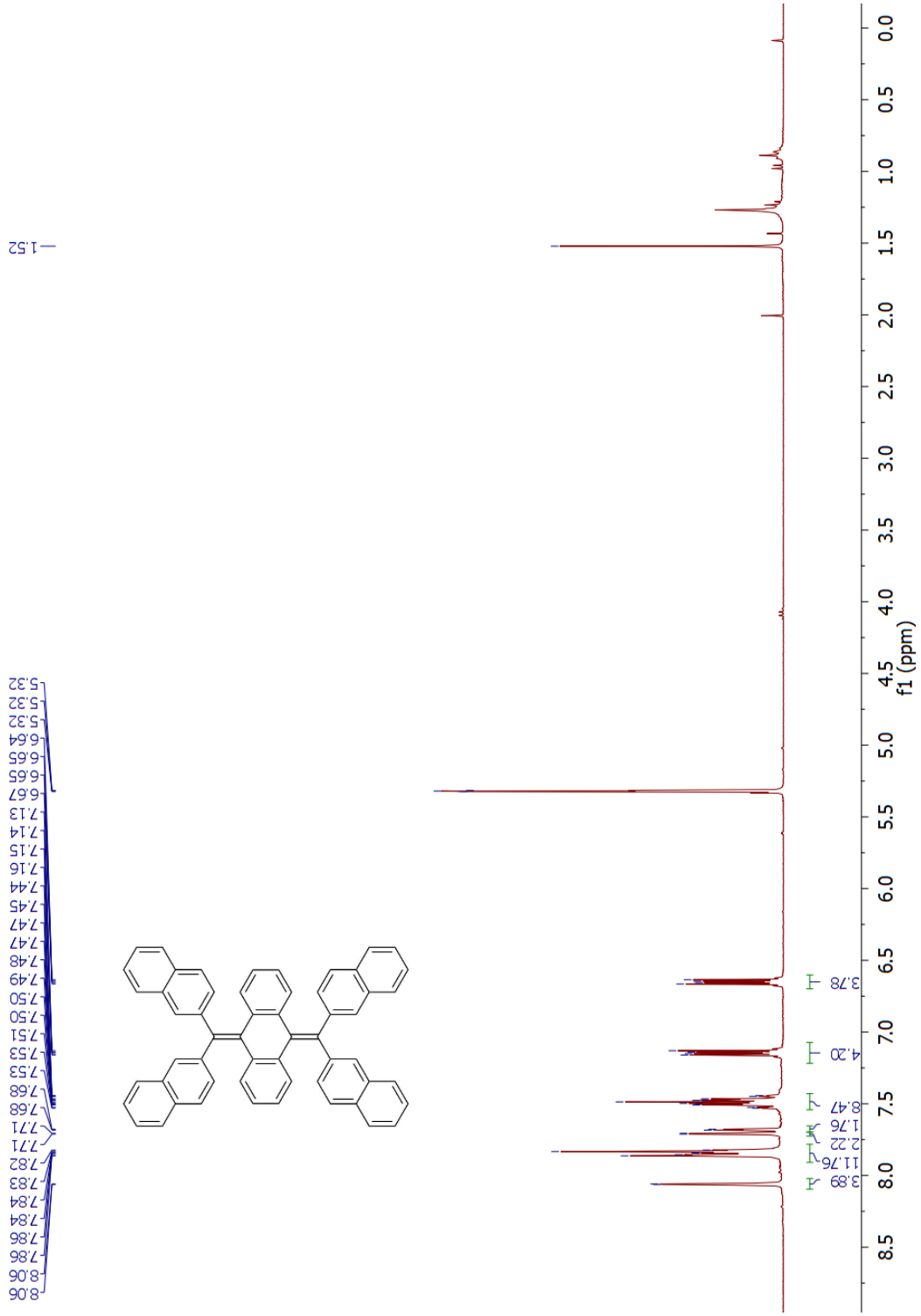

Figure 6: ^{1}H NMR (300 MHz, CD_2Cl_2) spectrum for compound **103**.

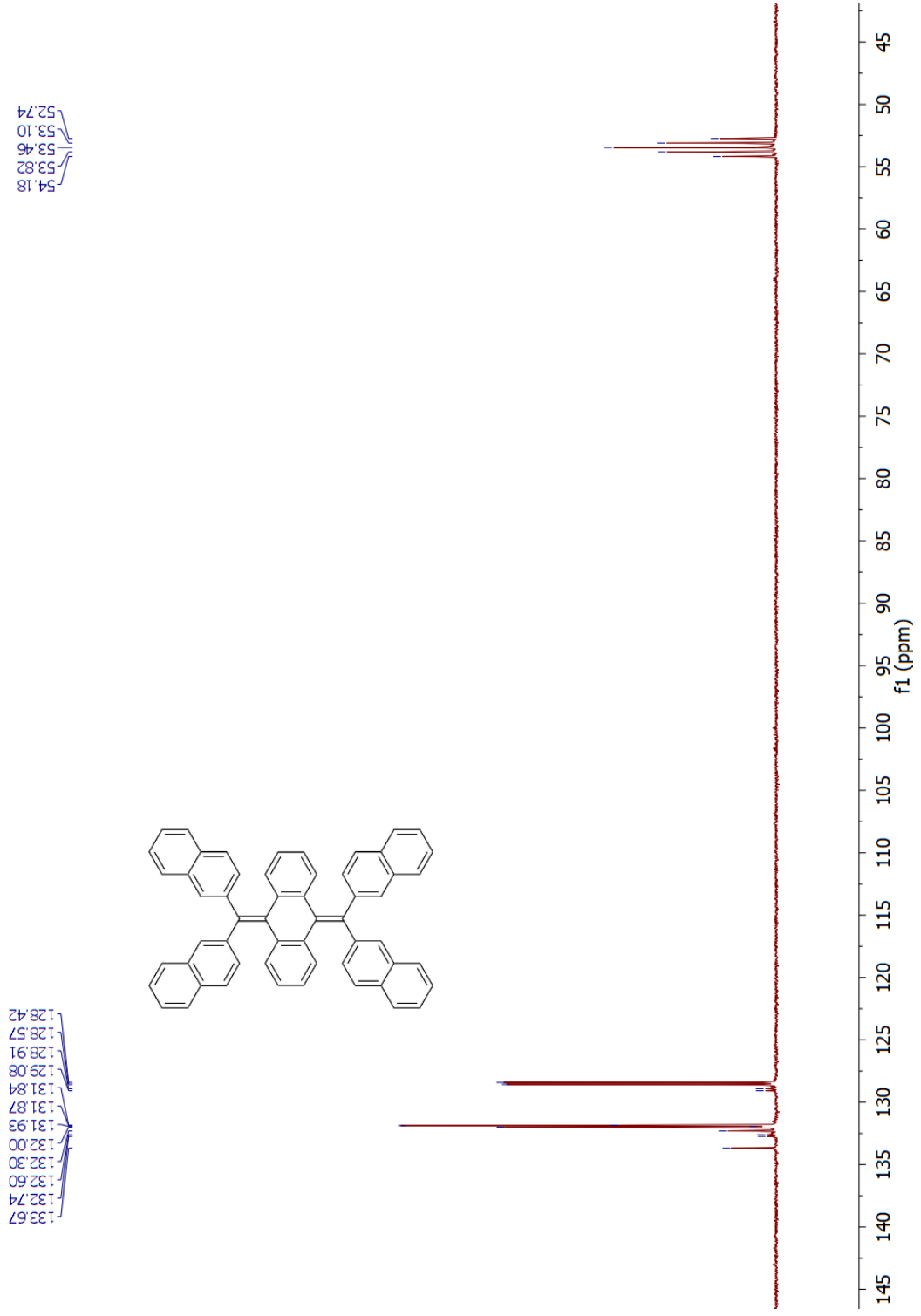

Figure 7: ^{13}H NMR (75 MHz, CD_2Cl_2) spectrum for compound **103**.

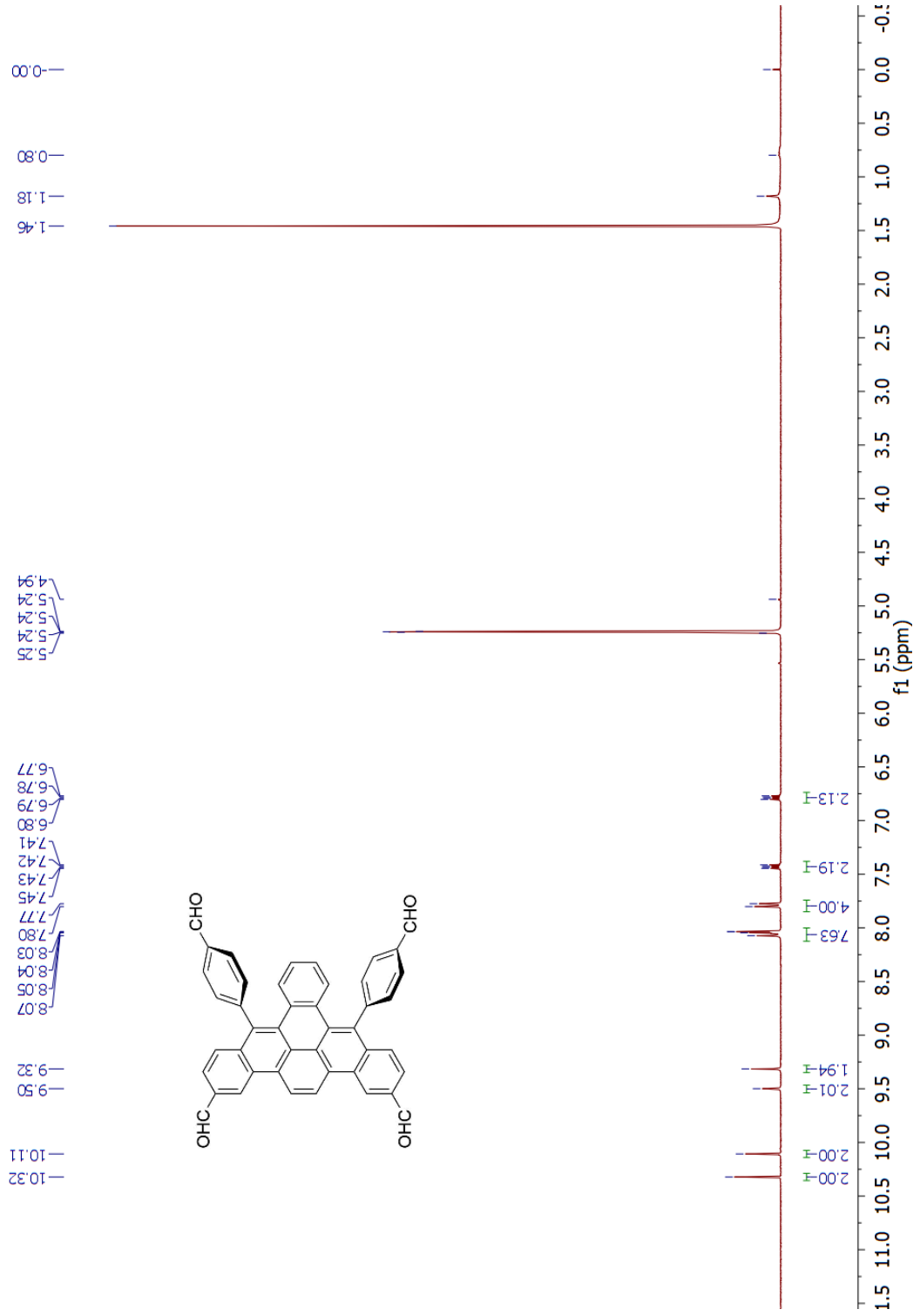

Figure 8: ^{1}H NMR (300 MHz, CD_2Cl_2) spectrum for compound **104**.

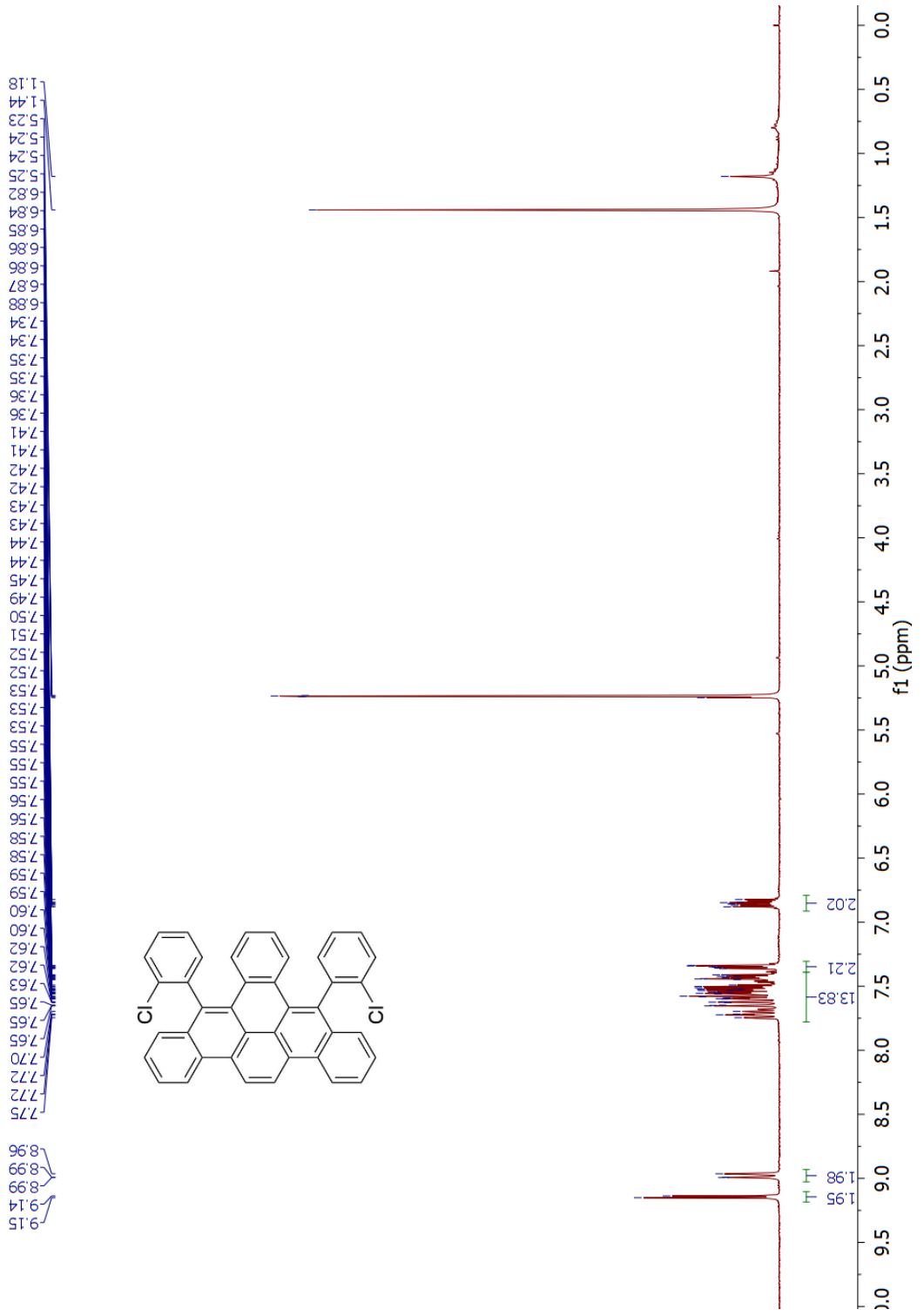

Figure 9: ^{1}H NMR (300 MHz, CD_2Cl_2) spectrum for compound **105**.

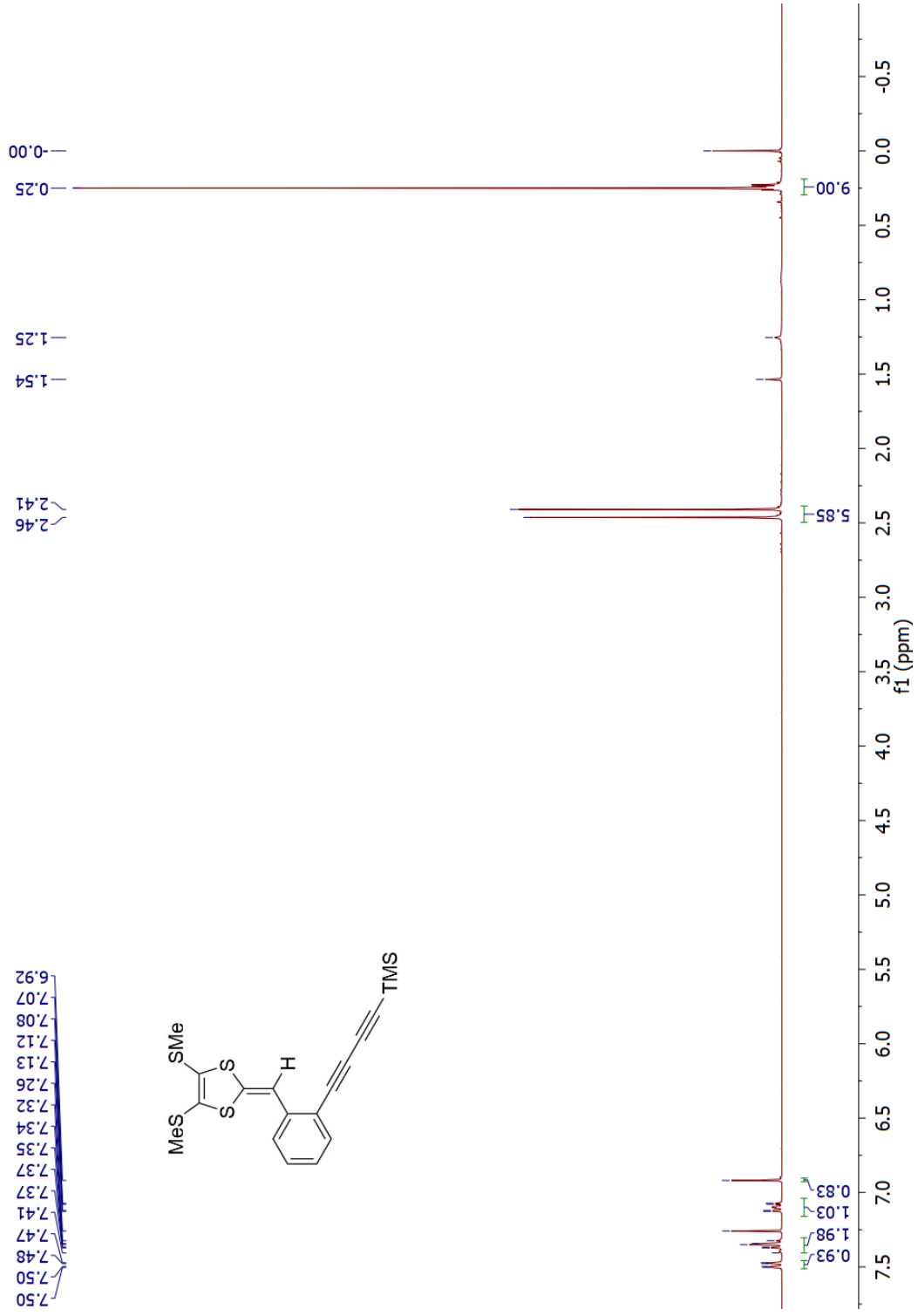

Figure 10: ^{1}H NMR (300 MHz, CD_2Cl_2) spectrum for compound **116**.

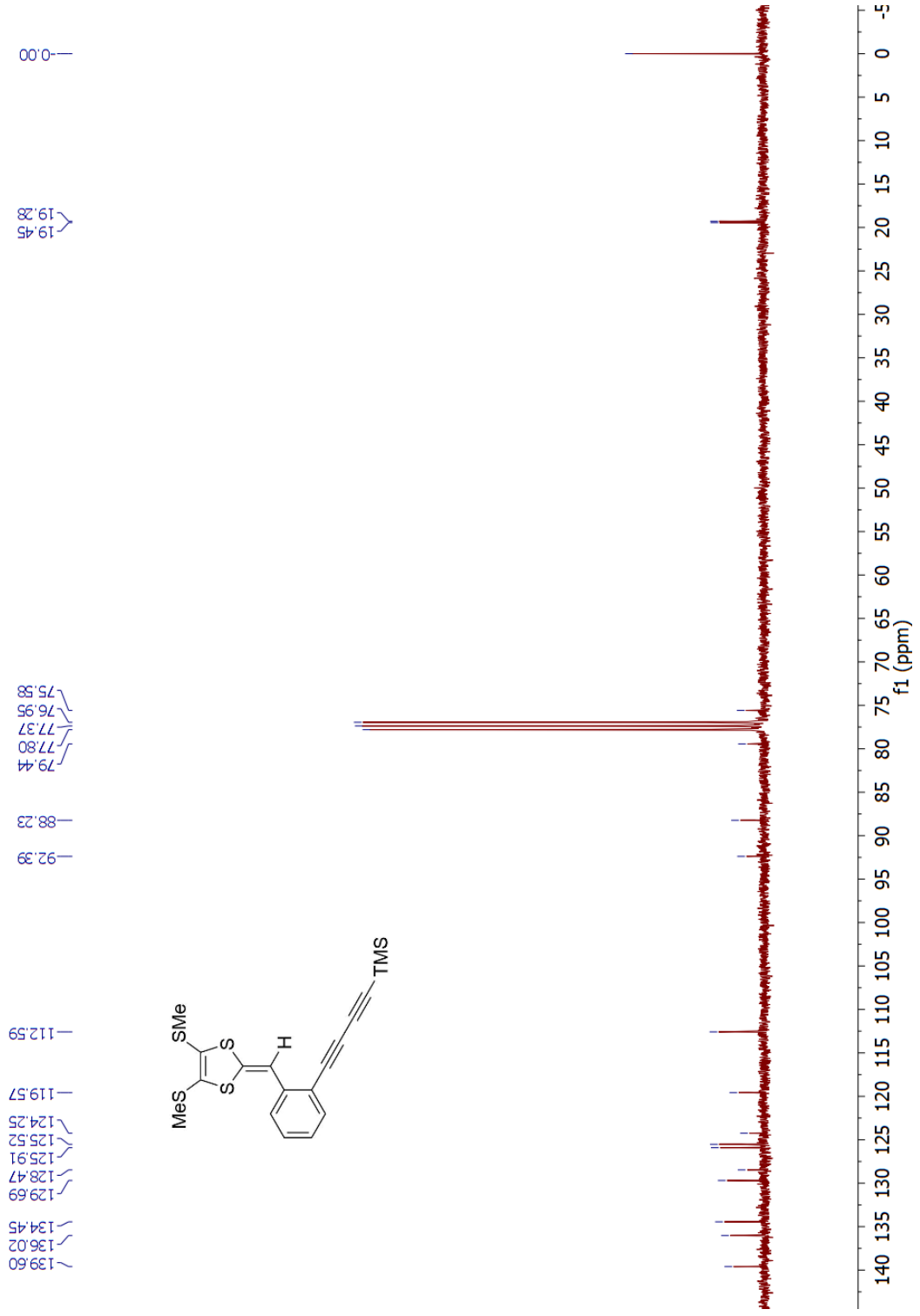

Figure 11: ^{13}H NMR (75 MHz, CD_2Cl_2) spectrum for compound **116**.

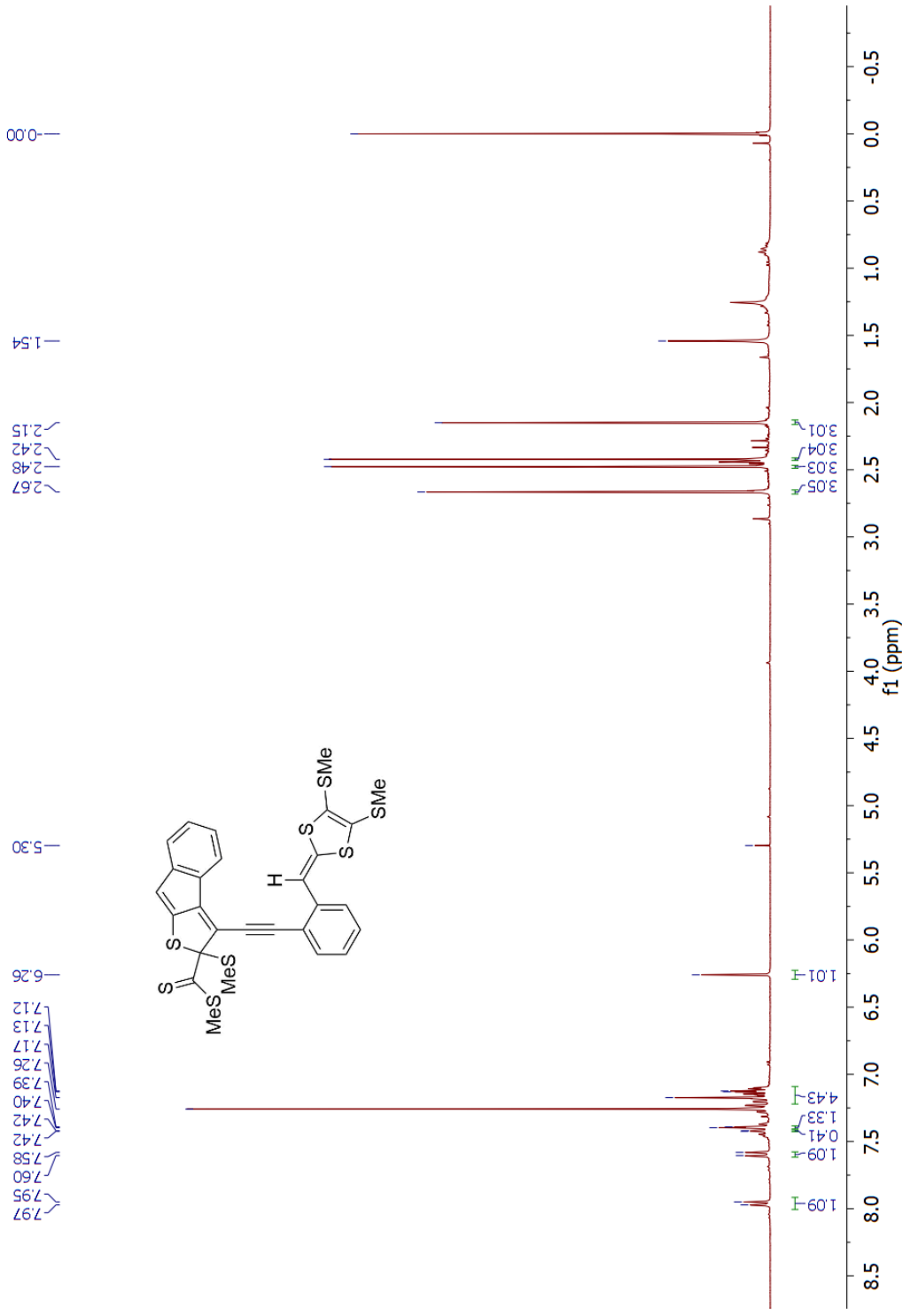

Figure 12: ^{1}H NMR (300 MHz, CD_2Cl_2) spectrum for compound **119**.

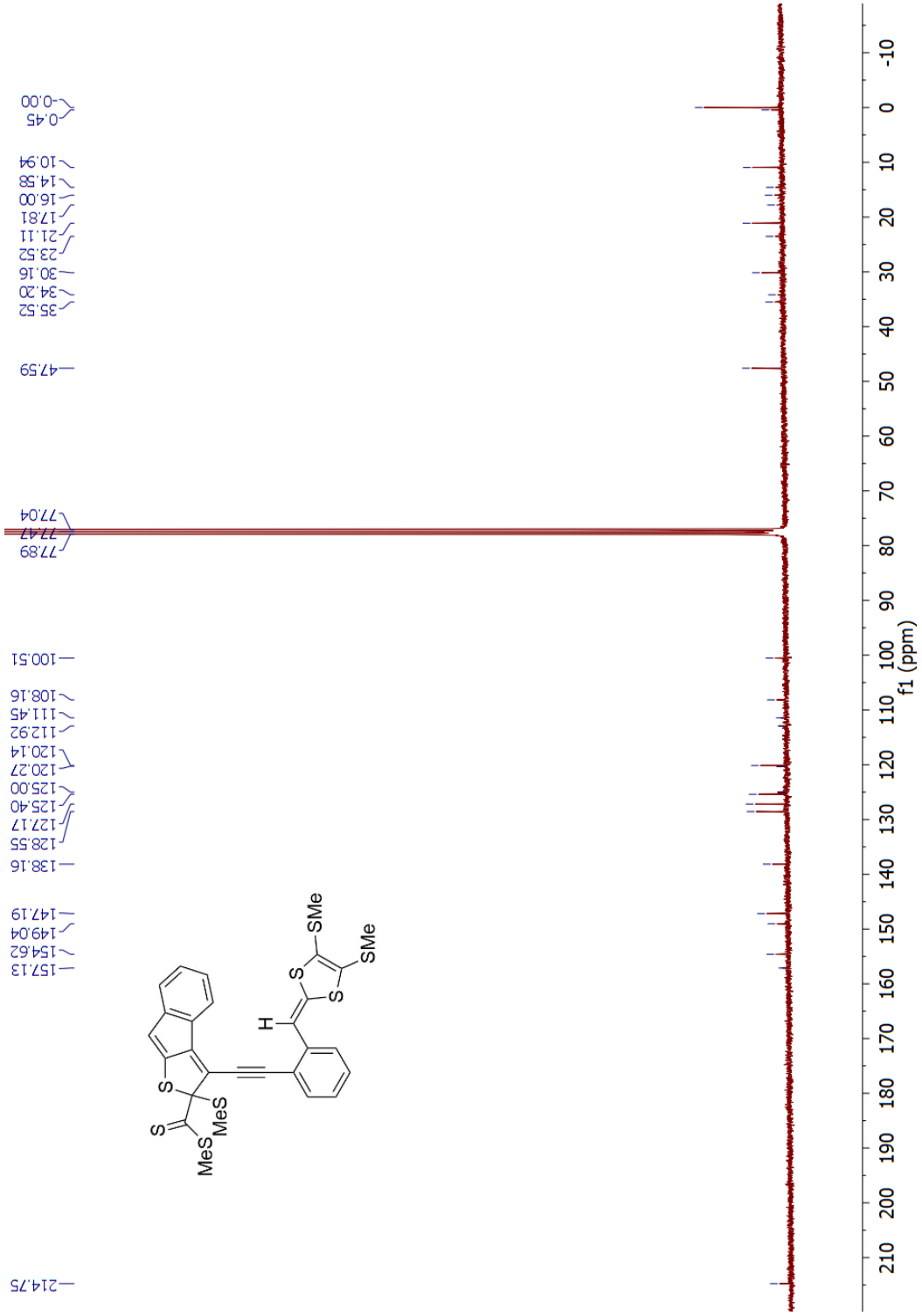

Figure 13: ^{13}H NMR (75 MHz, CD_2Cl_2) spectrum for compound **119**.

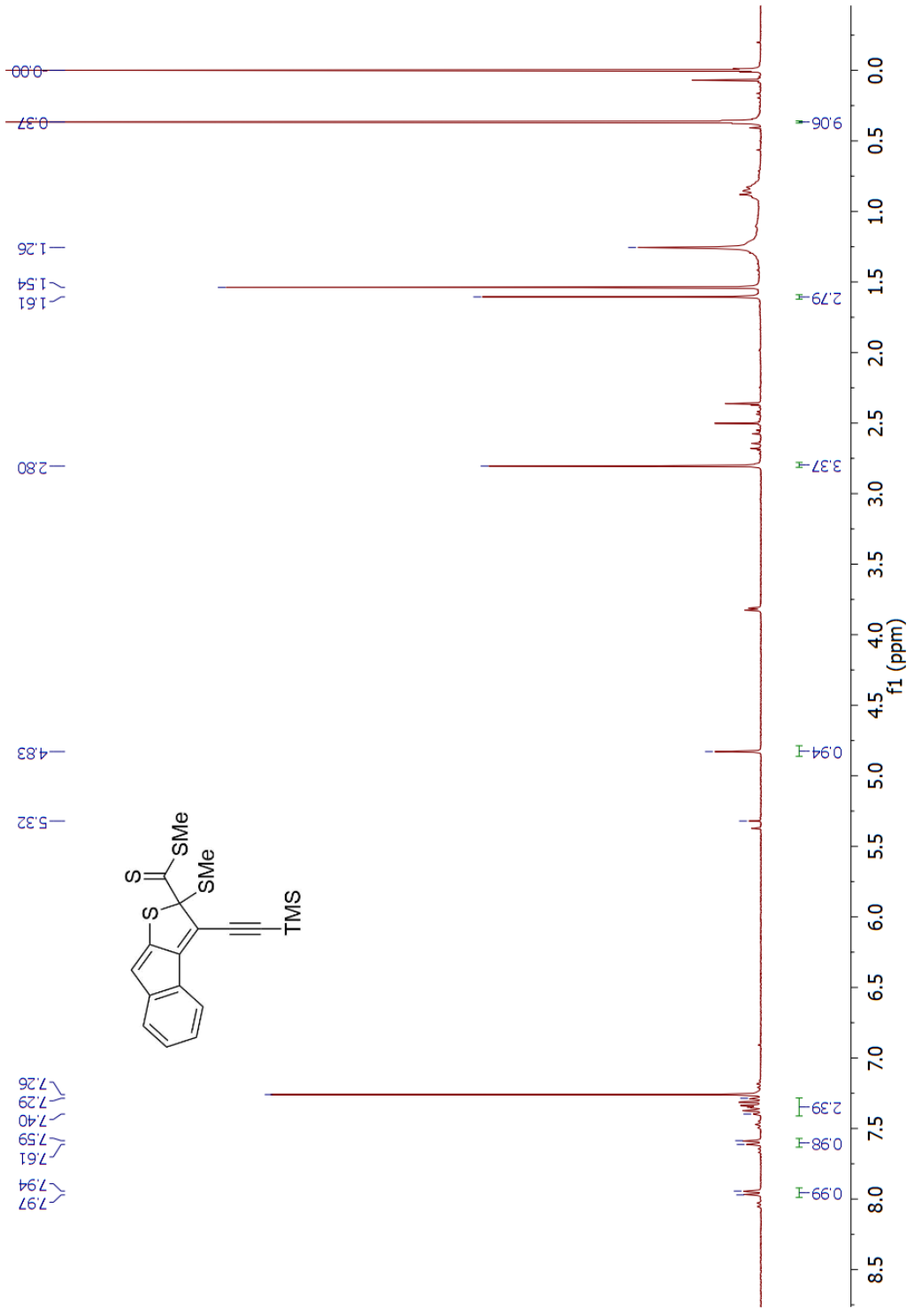

Figure 14: ^{1}H NMR (300 MHz, CD_2Cl_2) spectrum for compound **120**.

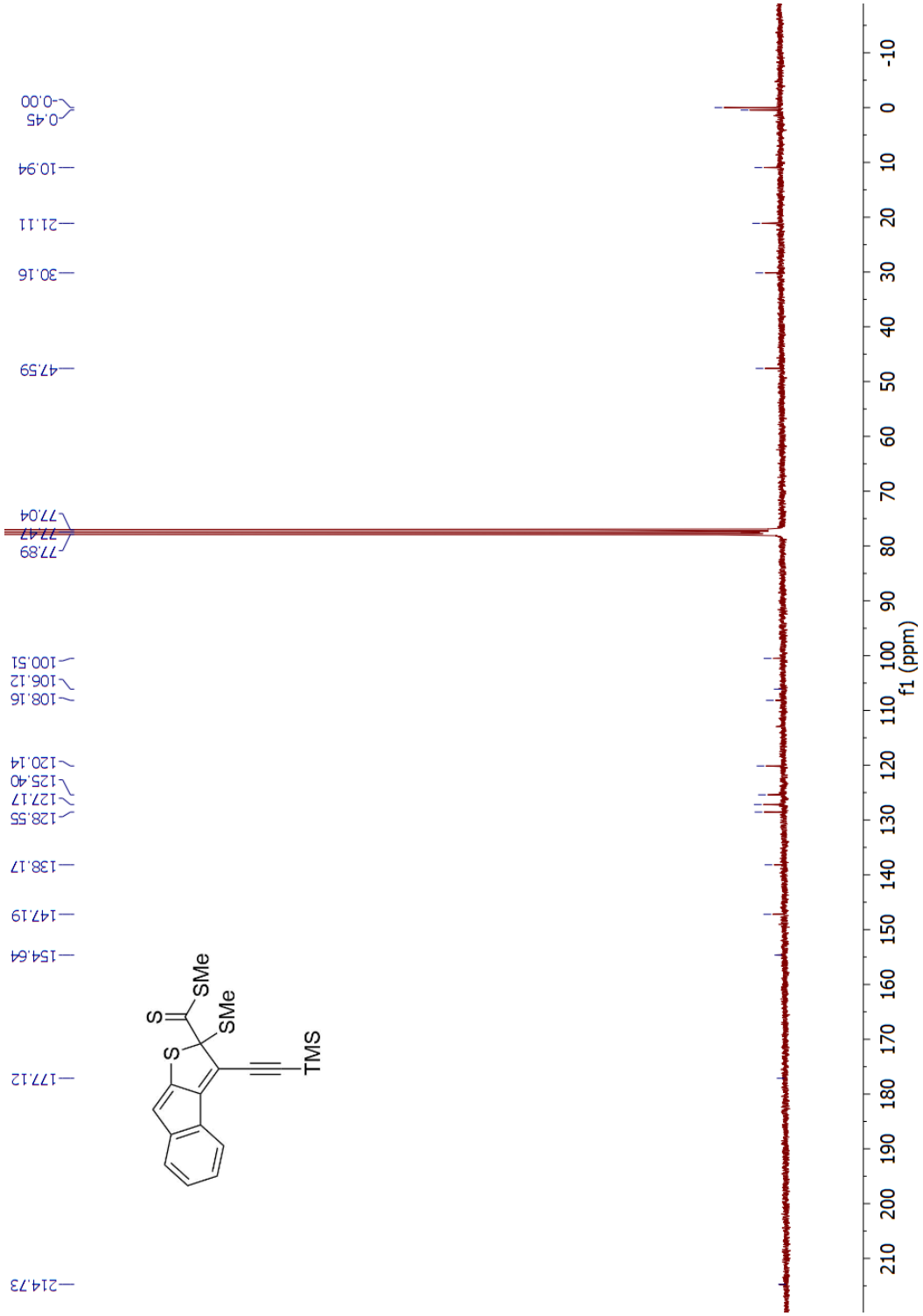

Figure 15: ^{13}H NMR (75 MHz, CD_2Cl_2) spectrum for compound **120**.

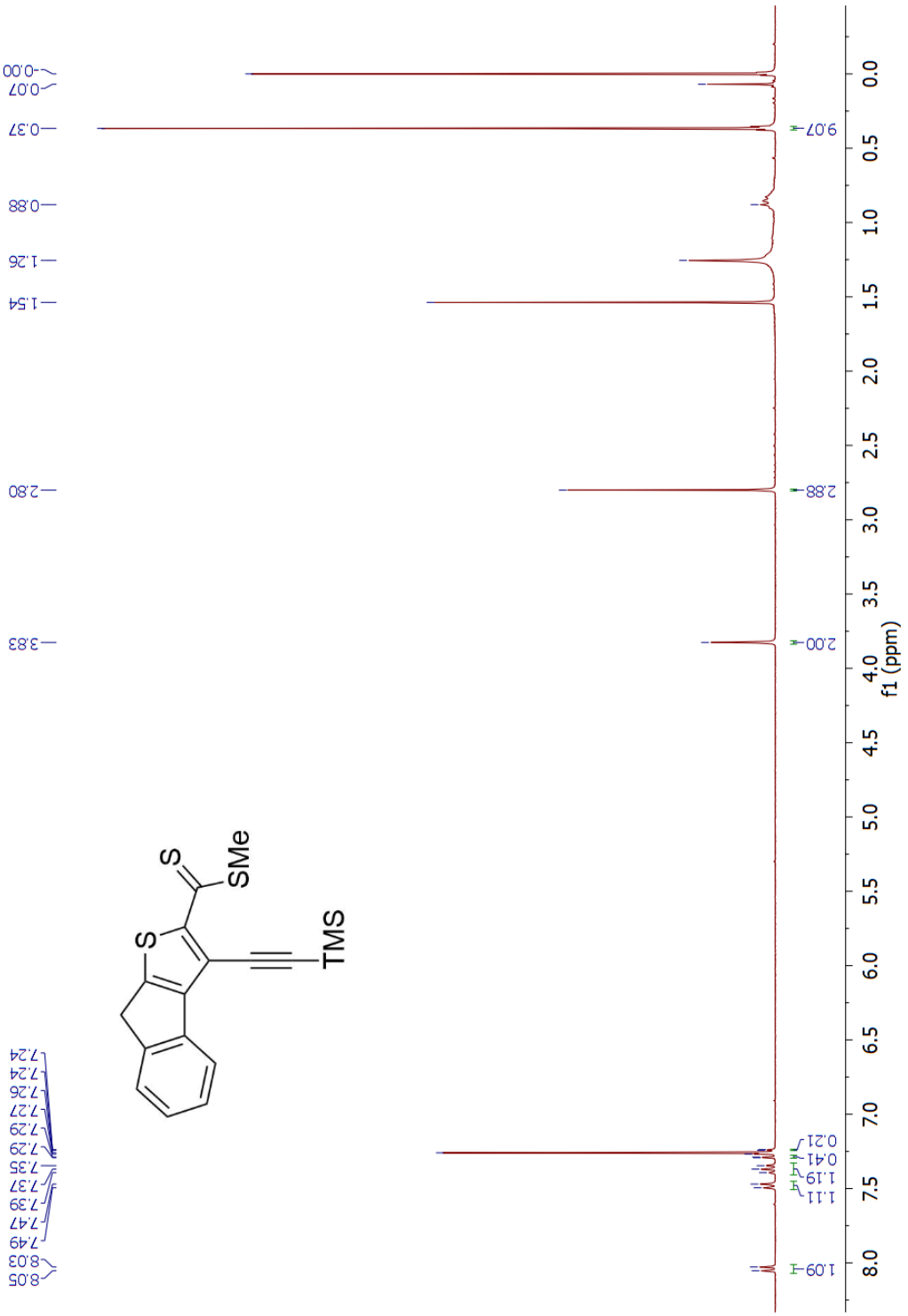

Figure 16: ^{1}H NMR (300 MHz, CD_2Cl_2) spectrum for compound **121**.

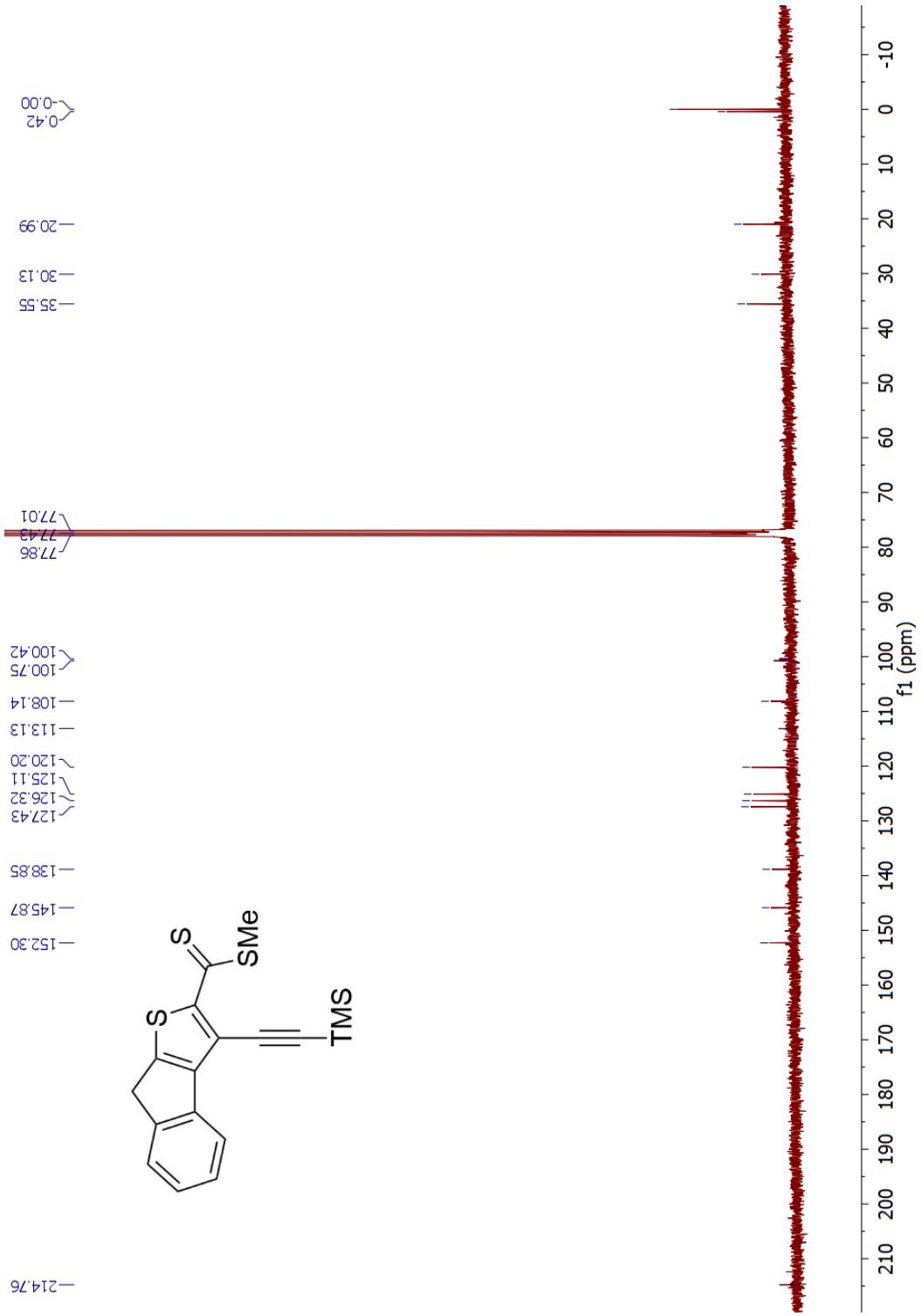

Figure 17: ^{13}H NMR (75 MHz, CD_2Cl_2) spectrum for compound **121**.

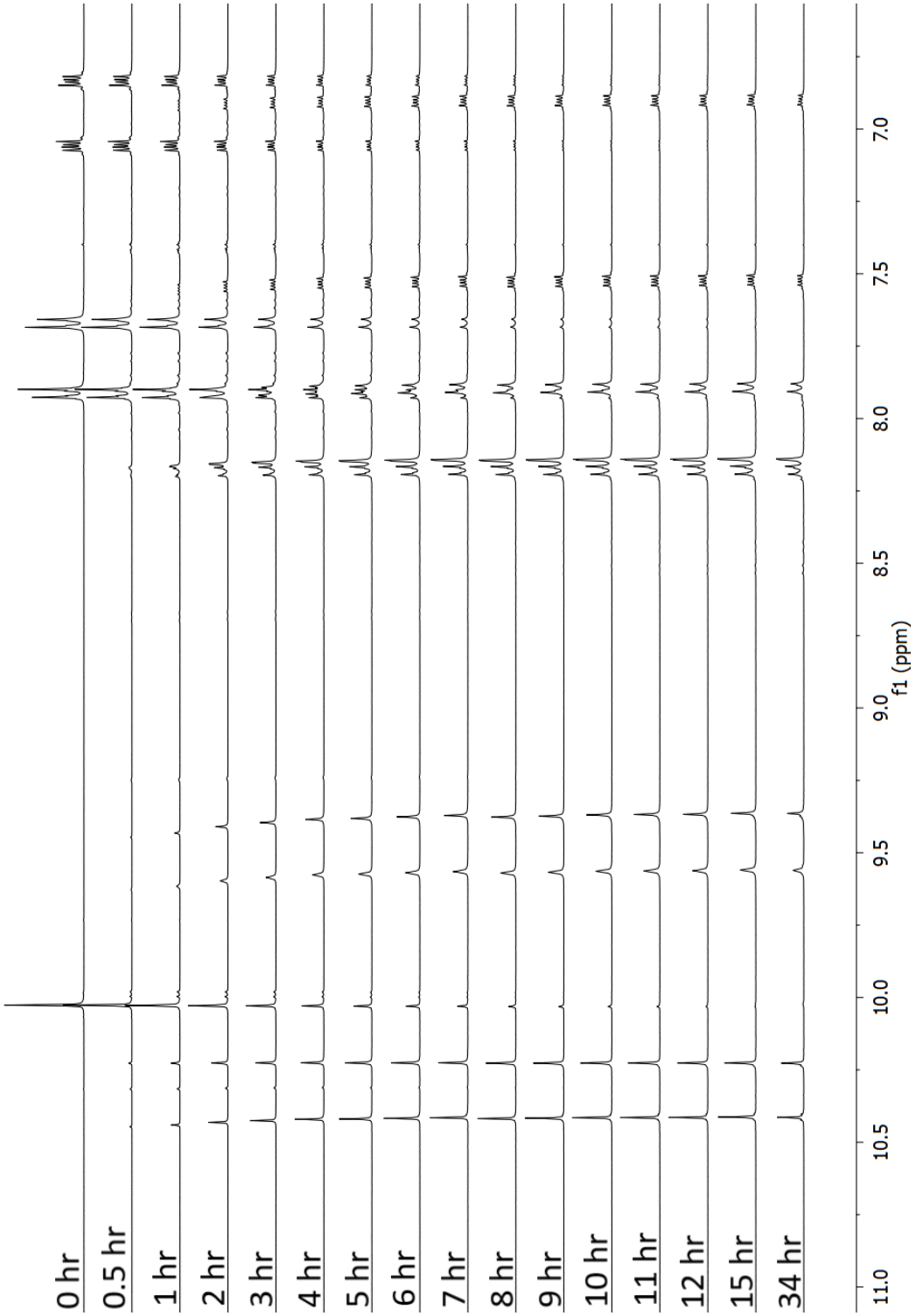

Figure 18: ^{1}H NMR (300 MHz, CD_2Cl_2) monitoring the photocyclodehydrogenation of compound **98** in the presence of DDQ at various reaction times.

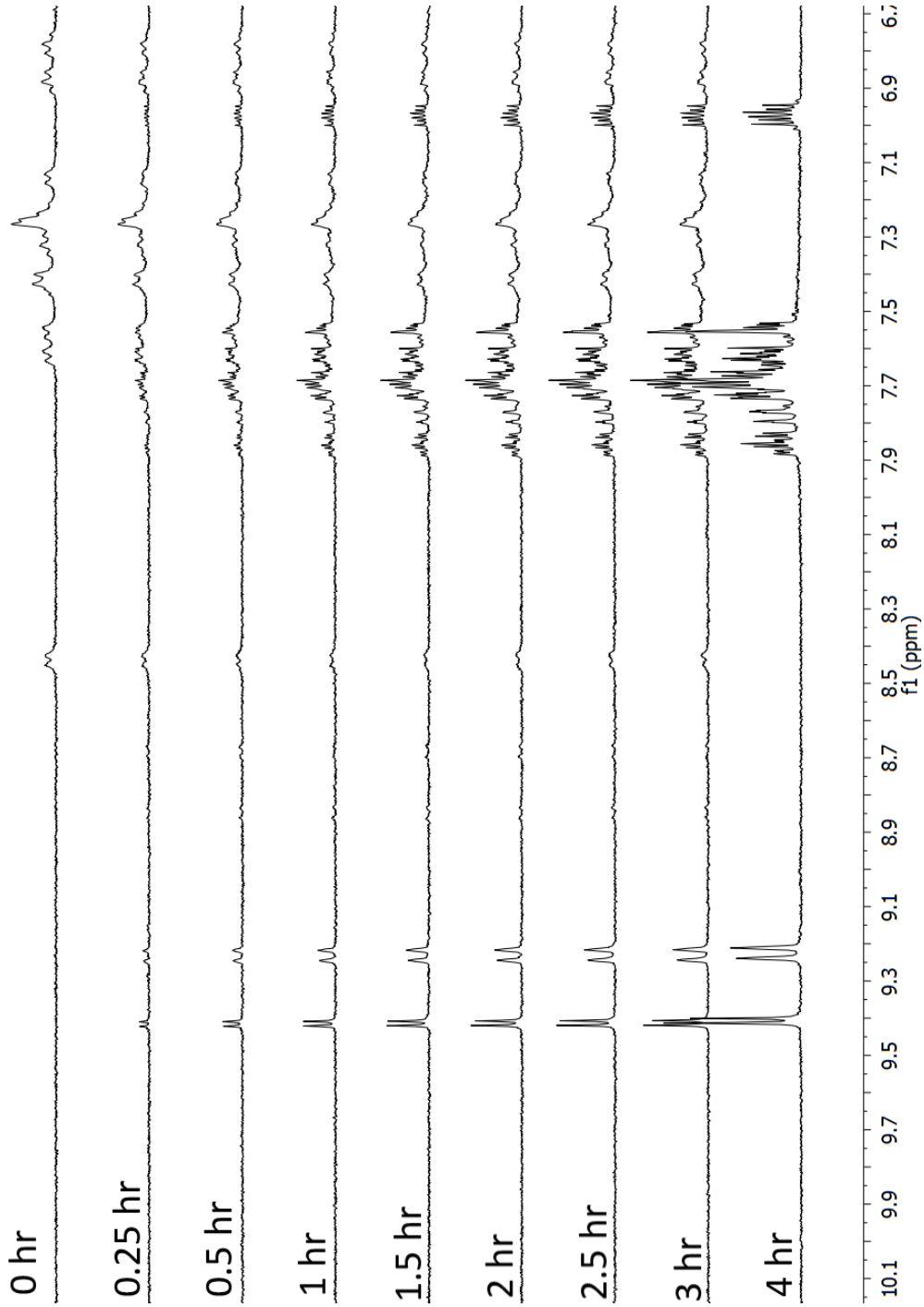

Figure 19: ^{1}H NMR (300 MHz, acetone-d6) monitoring the PCDHC of compound **99** in the presence of K_2CO_3 at various reaction times.

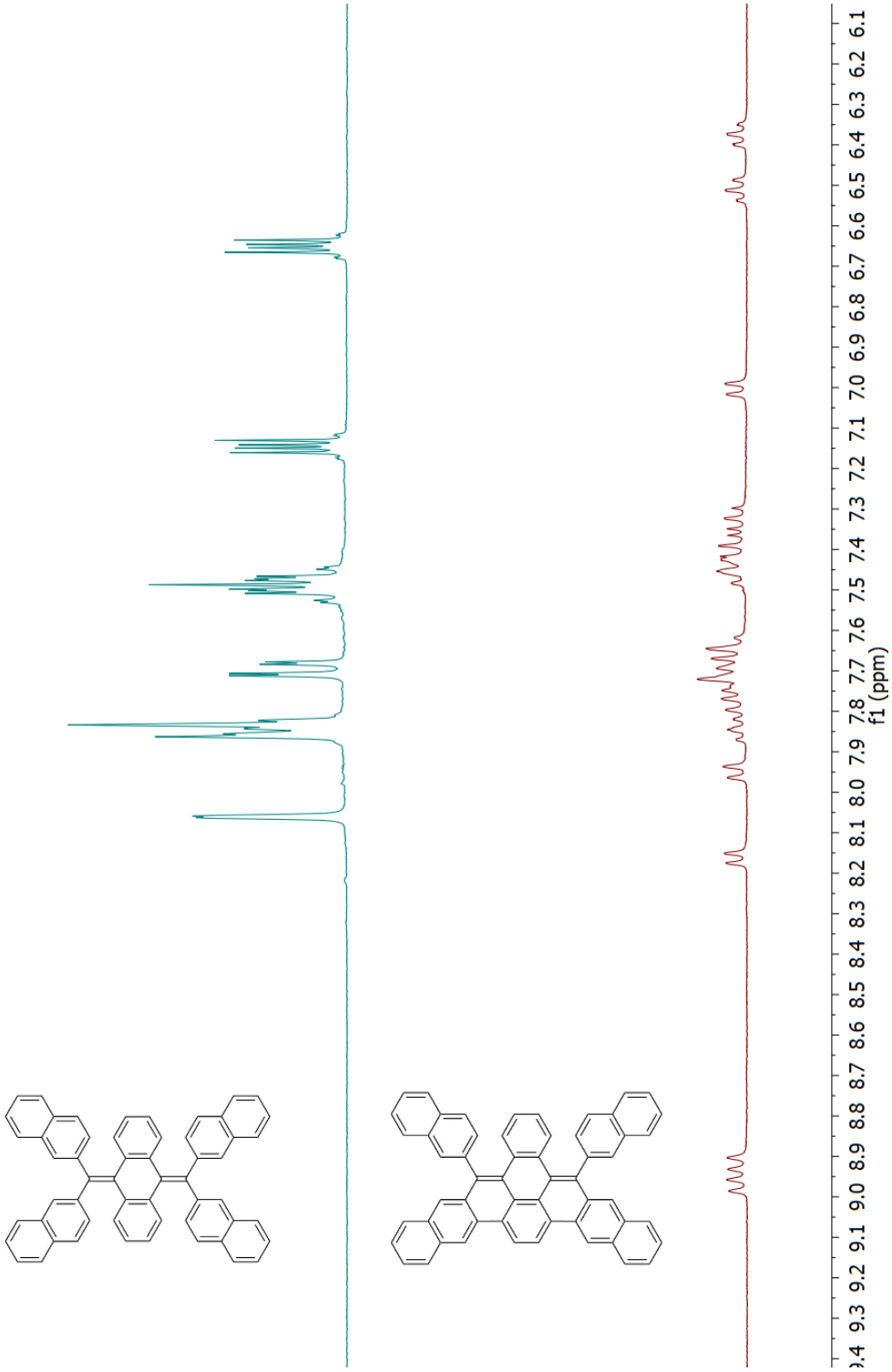

Figure 20: ^{1}H NMR (300 MHz, CD_2Cl_2) spectrum shows the photocyclodehydrogenation of compound **93** to obtain compound **109**.